Physical scale modelling of urban flood systems

Research student: *Matteo Rubinato*

Supervisors: *Dr J.Shucksmith*

Prof. A.J.Saul

Department of Civil and Structural Engineering

University of Sheffield

Thesis Submitted in Partial Fulfilment of the Requirements for the Degree of Doctor of Philosophy

Date: June 2015

ACKNOWLEDGEMENTS

The author would sincerely like to acknowledge the following individuals for their professional support and friendship during the course of this PhD study and throughout the author's career at the University of Sheffield.

Professor Adrian Saul, for introducing me to the academic career through the PhD, much valued advice and support that you have shown me throughout my career at the University of Sheffield.

Lecturer Dr. James Shucksmith, for his admirable supervision and help through all the process of the research undertaken.

Head of the Department Harm Askes, for his excellent care during critical moments due to the lack of funding.

Finally to my family, Leonardo, Maria Grazia, Lara e Dario, thanks for believing I could do it, thanks for accepting my decision to be far from home during these years to reach this essential degree for my future career. You have been and you will always be the most important people in my life, always there to support and help me when things are both negative and positive. And thanks to my girlfriend Amandine, which has always been there to give me positive support and advices.

ABSTRACT

Urban flooding is defined as ‘an overflowing or irruption of water over urban pathways which are not usually submerged’. Current economic, climatic and social trends suggest that the frequency, magnitude and cost of flooding are likely to increase in the future. Hydraulic models are commonly used by engineers in order to predict and mitigate flood risk. However full scale calibration and validation datasets for these modelling tools are scarce.

The main research objective of this thesis was to design and construct a physical model in order to provide datasets useful to verify, calibrate and validate computer model results in terms of energy losses in manholes.

To address these issues, an experimental facility has been constructed to enable the investigation of energy losses under steady and unsteady flow conditions in a scaled sewer system. Originally the model was composed of six manholes and three main pipes and then it was modified into a single pipe linked to an urban surface through a single manhole.

Experiments involved the measurement of flow rates, velocity, pressure and water depth within the physical models under different hydraulic scenarios.

Steady flow tests were conducted to quantify energy losses though manhole structures with different inlet/outlet configurations under a range of hydraulic conditions. Unsteady flow tests were conducted to examine the performance of different computational hydraulic models. These tests have shown that the performance of the SWMM hydraulic model could be improved by including local losses in the calibration process.

After modification the model was used to quantify sewer to surface and surface to sewer flow exchange through a single manhole during pluvial flooding. The work has demonstrated the feasibility of using weir and orifice equations within modelling tools to quantify this exchange under steady conditions. The model was used to empirically quantify discharge coefficients for energy loss equations which describe flow exchange for the first time.

CONTENTS

List of Figures

List of Tables

Notation list

The notation and symbols used in this thesis are listed with their interpretation.

$\Delta H = head\ loss$

ΔH_{i-j} = *the head loss between cross-sections i and j of the drainage structure*

ΔH_{1-2} = *head loss through the street inlet*

ΔH_{2-3} = *head loss at the drainage tube entrance or exit*

ΔH_{3-4} = *friction loss through the drainage tube*

ΔH_{4-5} = *the head loss at the junction between the main pipe and the drainage tube for combining flows (drainage case) or dividing flows (overflows case)*

$\lambda = friction\ factor$

$\lambda_l = length\ scale$

$\lambda_{Fr,l} = Froude\ length\ scale$

$\lambda_{Fr,Q} = Froude\ flow\ scale$

$\lambda_{Fr,t} = Froude\ time\ scale$

$\lambda_{Fr,v} = Froude\ velocity\ scale$

$\lambda_{Re,l} = Reynolds\ length\ scale$

$\lambda_{Re,Q} = Reynolds\ flow\ scale$

$\lambda_{Re,t} = Reynolds\ time\ scale$

$\lambda_{Re,v} = Reynolds\ velocity\ scale$

a,c = coefficients to be determined for K_{13} *and* K_{23}

α_{V1-2} *and* α_{V2-1} *= coefficients to pass from the tube flow velocity to the flow velocity approaching the street inlet grid*

A = cross-sectional area

A_1*=cross-sectional area main pipe*

A_2*=cross-sectional area lateral pipe*

A_3*=cross-sectional area outlet pipe*

A_{mh} *= Area manhole*

A_t *= cross-sectional area drainage tube*

B (Surface Width) = width of the channel, measured in cross section, at the free surface

C_f *= correction factor*

$\overline{C_f}$ *= average correction factor*

C_c *= Coefficient of contraction*

C_d*= Coefficient of discharge*

C_i *= Discharge coefficient for submerged orifice equation*

c_o = *Orifice coefficient*

C_v = *Coefficient of velocity*

C_{va} = *Coeff. to account for exclusion of approach velocity head*

Cw = weir coefficient

D = hydraulic diameter of the pipe

D_1=*diameter main pipe*

D_2=*diameter lateral pipe*

D_3=*diameter outlet pipe*

D_d = *downstream pipe diameter*

D_h = *equivalent diameter* = $4R_h$

D_l= *lateral pipe diameter*

D_m = *diameter manhole*

D_o= *diameter outlet pipe*

d_q= *discharge through a given slice of area*

D_t = *diameter drainage tube*

D_u= *diameter upstream pipe*

E_u = *(Euler number) shows the proportion of the ration of inertial force to pressure force*

F_r = *(Froude number) characterizes the ratio of the inertial force to gravity force*

Fr_m = *Froude number of the physical model*

Fr_o = *Froude number of the real system*

g = acceleration of gravity

H = Hydraulic head

H_1=*Hydraulic head main pipe*

H_2=*Hydraulic head lateral pipe*

H_3=*Hydraulic head outlet*

H_d = *Hydraulic Head downstream*

hf = Head Loss due to friction

h_L = *Head Loss (change of pressure)-hf*

$Hdown,p$ = *Hydraulic head in pipe downstream the manhole*

$Hdown,s$ = *hydraulic head on the surface downstream the manhole*

H_{mh} = *Hydraulic Head manhole*

H_{up} = *Hydraulic Head upstream*

Hup,p = *hydraulic head in pipe upstream the manhole*

Hup,s = *hydraulic head on the surface upstream the manhole*

j= junction manhole

K = head loss coefficient

K_{i-j} = *head loss coefficient associated to the local head loss* ΔH_{i-j}

K_{el} = *energy loss coefficient for the lateral pipe*

K_{eu} = *energy loss coefficient for the main straight-through pipe*

Ks = roughness

L = Characteristic length

L_t = *length drainage tube*

M_a = *(Sarrau-Mach number) characterizes the ratio of inertial force to elasticity force*

m_t = *value measured in the physical model*

n = the total number of samples in data set

P = Pressure head

p_t = *value obtained from the computer model*

$P_{down,p}$ = *pressure downstream manhole in pipe*

$P_{up,p}$ = *pressure upstream manhole in pipe*

$P_{up,s}$ = *pressure downstream stream manhole on urban surface*

$P_{up,s}$ = *pressure upstream manhole on urban surface*

Q = volumetric flow-rate

Q_1 = *Flow inlet main pipe*

Q_2 = *Flow inlet lateral pipe*

Q_3 = *Flow outlet*

Q_4 = *Flow out surface*

Q_d = *Flow downstream pipe*

Q_e = *Flow exchange*

Q_i =*Infoworks Scaled flow*

Q_l = *Flow lateral pipe*

Q_m = *Measured flow*

Rt = correlation coefficient

Re = Reynolds number, characterizes the ratio of inertial force to viscous force

Re_m = *Reynolds number of the physical model*

Re_o = *Reynolds number of the real system*

S_l= *drop between the lateral pipe and the downstream pipe*

S_u= *drop between the main upstream and the downstream pipe*

v = kinematics viscosity

V = velocity

V_3 = *Outlet velocity*

V_o= *velocity orifice*

V_d=*Downstream velocity*

V_m= *velocity physical model Froude similitude*

V_o= *velocity real system Froude similitude*

V_u=*Upstream velocity*

$V_{down,p}$ = *velocity downstream manhole in the pipe*

$V_{down,s}$ = *velocity upstream manhole on the urban surface*

$V_{up,p}$ = *velocity upstream manhole in the pipe*

$V_{up,s}$ = *velocity downstream manhole on the urban surface*

y =h/D = filling ratio

y_m=*water depth physical model Froude similitude*

y_o= *water depth real system Froude similitude*

w=circonference manhole

We = Weber number is proportional to the ratio of the inertial force to capillarity force

z = height above datum

z_{crest} = *datum level*

ϑ = *junction angle*

β = *diameter ratio*

ρ = *density*

μ = *dynamic viscosity*

ε = *shape factor*

1. INTRODUCTION

During the last 10 years, the frequency of flooding and the associated damage caused by urban flood events have increased worldwide. In the United Kingdom, major examples of recent flood events include the 2005 flood in Carlisle (Neal et al., 2009) (Figure 1), the June 2007 flood in South Yorkshire (Environment Agency, 2010), the September 2008 event in Morpeth (Parkin, 2010) and the November 2009 flood in Cumbria (Met Office, 2013).

Internationally recent examples include the floods in Rio de Janeiro, Brazil, (Flood risk in Brazil, 2013), the September 2000 flood in Tokai, Japan, where the Central Nagoya was inundated and the urban infrastructure paralyzed (Tominaga, 2007), the flooding in Queensland, Australia, (Carpenter, 2013), and Dakar, Senegal, which since 2005 has been affected by urban flooding (Schmidt, 2011).

Figure 1 - Carlisle, England, 2005 (Image source: Wikimedia Commons)

Generally a flood occurs when water overflows or inundates land or areas that are normally dry. This phenomenon can happen in a multitude of ways: water can arrive from rivers or streams that overflow their banks due to excessive rain, a ruptured dam or rapid ice melting in the mountains. Floods can occur on the coasts where they can be generated by large storm or tsunami which causes the sea to surge inland. In contrast, urban (also termed pluvial or surface water) floods can be defined as "flooding of streets, underpasses, basements and other low-lying urban areas" (Environmental Engineering Dictionary, Mehdi Ahmadi, 2008). This phenomenon is frequently caused by heavy rainfall events which overwhelm the limited capacity of drainage systems with the consequent exchange of flow from sewers to the urban surface via manholes and gullies. Factors such us an increase in urbanization, climate change and the deterioration

of sewer networks, are expected to contribute to an increase in the number of urban flood events in the future. For example it is predicted that by 2030, 61% of the world's population will be living in urban areas (by that time expected to be approaching 5 billion - Cohen, 2006). In the United Kingdom, the urban population is expected to increase by 0.73 per cent per year from 2015 until 2020 (World Population Prospect, 2012). The resulting industrial and urban developments cover permeable grounds and increase the amount of rainwater that runs off the surface into drains and sewers with a limited capacity. Simultaneously, the effect of climate change (IPCC 2014, Summary for Policymakers) may increase flood risk as the predicted increased occurrence of intense rainfall events will place further stress on urban drainage systems (Ashley et al., 2005).

Finally, many sewerage and drainage networks are operating past their design life. As these systems deteriorate, there is the potential for urban flood risk to increase due to the increased occurrence of asset failure such as sewer collapse and blockage, e.g. Columbo, Sri Lankan capital (WaterWorld, 2012). This particular aspect is not affecting just the United Kingdom (Defra, 2007) but many other countries and cities around the world, e.g. Canada (Kerr Wood Leidal Associates LTD, Consulting Engineers, 2008), San Francisco (City and County of San Francisco, 2030 Sewer System Master Plan), Delhi (Singh, United Nations University).

It is generally recognized that urban flooding is the most difficult type of flooding to predict, model and defend against (The Pitt Review, 2008). This is due to the nature of intense rainfall events (convective, intensive rainfall events which are highly uncertain and difficult to forecast), the hydraulics of linked sewer and surface flow being complex and because it is harder to construct cost effective flood defences in urban areas.

Thus, there is a need to provide better modelling capabilities to predict flooding and to manage flood routes in urban areas. Engineers commonly assess the hydraulic performance of existing sewer systems using computer models. Whilst these models are reliable in terms of assessing the below ground system composed of pipes and manholes, when replicating the phenomenon of flooding into streets they are very difficult to calibrate and validate due to the paucity of data in real flood conditions. In particular the uncertainties caused by complex 3D flow fields at the interface between surface and sub-surface flows are recognized as an important uncertainty within urban flood models (Djordjević et al., 2005). Current validation datasets in fact often comprise approximated depth data from CCTV images with poor spatial and temporal resolution.

Other desirable datasets such as velocity field and flow exchange are not currently available. This thesis describes the design and the construction of a new physical model capable of providing high-resolution experimental datasets in order to calibrate and validate computational modelling tools. By completing the construction and conducting initial testing using the physical model, this research provides new understanding of the hydraulic characteristics of urban flood events.

1.1. Aims of thesis

The aim of this thesis is to develop and test an experimental facility to provide novel experimental datasets which describe complex sewer and flood flow phenomena such as above/below ground exchange events.

1.2. Thesis structure

This thesis is organised according to the following structure:

- Introduction to the concepts of energy losses and urban flooding, a review of previous work utilising physical models to describe flows in urban drainage systems and identification of key research questions to be addressed in this work (Chapter 2).
- A description of the physical models used to answer the research questions identified, as well as the experimental procedure (Chapter 3).
- A presentation and discussion of the results arising from the experimental program (Chapters 4-5).
- A review of the performance of existing hydraulic models when tested against the experimental data (Chapter 4).
- A presentation of the main conclusions of the thesis as well as recommendations for future work (Chapters 6-7).

2 BACKGROUND – LITERATURE REVIEW

The aim of this chapter is to describe the current 'state of the art' in terms of urban flood modelling and the use of physical models as well as defining the knowledge gaps to be addressed by this thesis.

2.1 Urban flooding

The European Community directive EN 752 defines urban flooding as a "*condition where wastewater and/or surface water escapes from or cannot enter a drain or sewer system and either remains on the surface or enters buildings*" and surcharge as "*a condition in which wastewater and/or surface water is held under pressure within a gravity drain or sewer system, but does not escape to surface to cause flooding*".

An urban flood is a complex, unsteady hydraulic process, involving interaction between sewer systems (i.e. pipe network hydraulics) and an urban surface (i.e. free surface hydraulics, Figure 2). The below ground system (termed the "minor system") includes hydraulic structures such as gully systems, manholes as well as pipes which comprise the conventional urban drainage infrastructure. The above ground system (termed the "major system") is made up of different surface flood pathways, which includes roads, paths, car parks and playing fields.

Figure 2 – Examples of system surcharge and exceedance flow generation. Left) Central Texas, Herald/TJ MAXWELL, Right) Waynesville, Aug. 9, 2013 Steve Zumwalt/FEMA

The impact of urban flooding (Figure 3) is felt worldwide and it is highly significant as affected areas are often densely populated and contain vital infrastructure.

In addition, due to the flow exchange from the sewer network to the urban surface, land and property can be flooded with contaminated water (Jha et al, 2011). This is a special issue for combined sewer systems, which carry foul flow.

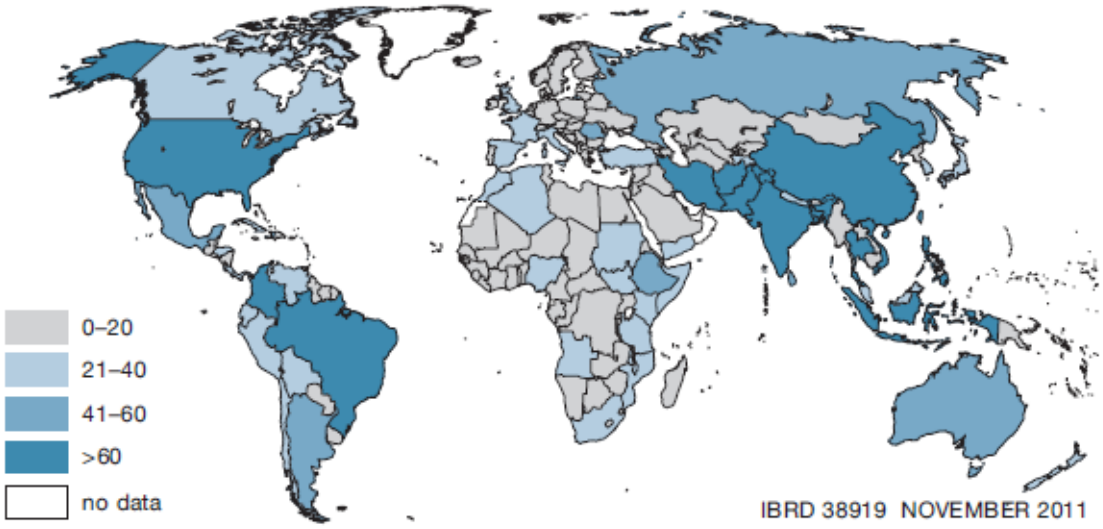

Figure 3 – General Urban Flood Events, 1970-2011. Source: EM-DAT: The OFDA/CRED International Disaster Database www.emdat.be – Universite' Catholique de Louvain – Brussels, Belgium (Jha et al, 2011).

Each flood can generate different kinds of damage, which may include (Mark. et al., 2004):

- Direct damage, typically material damage caused by water or flowing water;
- Indirect damage, such as traffic disruption or production losses;
- Social consequences, such as psychological problems for inhabitants as well as effects on health due to contact with flood water.

ten Veldhuis (2011), created two basic metrics to estimate damage due to flooding. "Tangible damages", which include all damages to buildings and infrastructure, and "intangible damages", which include damage which is more problematic to calculate, such as anxiety, trauma and inconvenience.

To achieve a complete quantification of the total damage due to flooding is essential to incorporate both tangible and intangible damages (Defra, 2004, Ohl and Tapsell, 2000, Fewtrell and Kay 2008).

To estimate potential damage and quantify risk it is important to understand how water moves through the urban environment, hence an understanding of the hydraulics of urban flood flows is critical in order to understand and mitigate risk.

2.1.1 Overview of urban flood modelling

Urban flood models utilise the St Venant equations to describe the motion of fluids in pipes and open channel networks.

Within the minor system the primary direction of flow is defined by the pipe network, hence a 1D form of the equations can be used. Sewer network hydraulic structures are commonly represented using empirical minor head loss relationships. Surface flows are often less constrained, in some floods; flows may follow surface flow paths defined by street profiles. However, it is also possible that flows may be highly two dimensional at urban street scales. In which case it is often more desirable to use 2D form of the Saint Venant equations (at higher computational cost). Models which describe pipe and surface flows in 1D are termed 1D-1D models. 1D-1D models can provide an adequate representation of surface flooding as long as flows stay within the street (i.e. 1D channel) profile (Djordjevic et al., 1999, Mark et al., 2004). Models which describe the surface flow in 2D are commonly referred to as 1D-2D models. 1D-2D models must also include coupling of 1D pipe flow models with 2D surface flow models.

The category of 1D-2D models are considered to give the most accurate representation of urban surface flooding currently available but to achieve this accuracy data and high computational time are required (Bamford et al., 2008).

Although computational models which describe water flows in pipe and open channels are generally considered reliable, it is still seen as important to undertake experimental studies to provide additional results for the calibration and validation of computer models. Such experimental studies are considered especially valuable when they provide information of phenomena for which there is a significant lack of calibration data for modelling results, and the potential accuracy of equations applied is unknown (Dottori et al., 2013, Notaro et al., 2010, Hunter et al., 2007). Specific examples relevant to flood modelling include the quantification of head losses within urban drainage hydraulic structures (such as manholes) with varying geometries, and the interaction of surface and sewer flows at interaction points such as manholes and gullies.

Section 2.2 defines the hydraulic principles that need to be considered when analysing head losses due to manhole structure. Sections 2.3 to 2.5 describe previous experimental research quantifying losses in manholes and sections 2.6 to 2.9 describe how the

interaction of surface and sewer flows is described within current modelling tools and previous experimental research examining such interactions.

2.2 Conservation of energy and head losses

The total energy of a fluid can be considered to comprise:

- Pressure energy;
- Kinetic-energy due to velocity;
- Gravitational Potential, due to elevation above a given datum.

The energy of a fluid is commonly considered as 'head' (with units of length) and expressed as:

$$pressure\ head = \frac{P}{\rho g} \qquad velocity\ head = \frac{V^2}{2g} \qquad potential\ head = z$$

Combining these three components it is possible to obtain the total head (H), which is given by "the Bernoulli equation":

$$H = \frac{P}{\rho g} + \frac{V^2}{2g} + z \qquad \text{Equation 1}$$

Head loss is the reduction in the total head or pressure (sum of pressure head, velocity head and elevation head) of a fluid as it moves through a system.

It is impossible to avoid head loss in real fluids. Its presence is due to the friction between the fluid and the walls of the system where the fluid runs, the friction between fluid particles as they move relative to another one and the turbulence caused whenever the flow is redirected or affected in any way, for example as in flow reducers or pumps. When a liquid is moving from one point to another (1-2) the head losses (h_L) can be expressed as:

$$h_L = \left(\frac{P_1 - P_2}{\rho g}\right) + \left(\frac{V_1^2 - V_2^2}{2g}\right) + (z_1 - z_2) \qquad \text{Equation 2}$$

The complex flow pattern in manholes (which includes effect of retardation, acceleration, rotation in different planes and flow interference) makes it very difficult to formulate a general theory for energy losses for such structures. One approach to quantify the energy loss attributed to a manhole is to interpolate the energy grade line within the pipes on both sides of the manhole (Figure 4). The energy grade lines are extrapolated to the middle of the manhole and one can then measure the energy loss as the difference between the lines at the middle of the manhole.

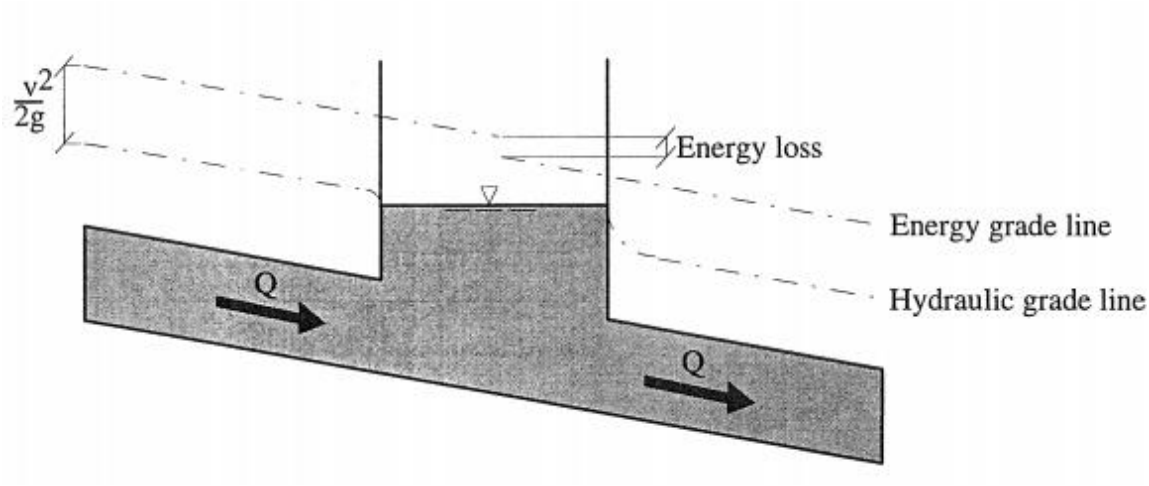

Figure 4 – Pressurized flow with associated energy grade lines and hydraulic grade lines (Asztely, 1995).

Energy loss coefficient (K) for manhole structures are commonly (Marsalek, 1984; Johnston, 1990; Wang, 1998; Zhao et al., 2006; Ramamurthy, 2007; Mrowiec, 2007; Phang, 2011; Arao, 2012; Stovin et al., 2013; Pfister, 2014;) defined as:

$$K = \Delta H \frac{2g}{{V_d}^2} \qquad \text{Equation 3}$$

Studies have pointed out the very complex matter of energy losses in manholes. Some of the parameters which have found to affect the head losses include:

- Depth ratio between the upstream branches and the downstream channel (Taylor 1944; Hsu et al., 1998; Gurram & Karki 2000);
- Upstream and Downstream hydraulic conditions (i.e. subcritical or supercritical, Hager 1989, Del Giudice et al., 2000; Del Giudice & Hager 2001, Gargano & Hager 2002, Gisonni & Hager 2002, Zhao et al., 2004, 2006, 2008);
- Effect of bed discordance on the channel junction flow (Biron et al., 1996)
- Different flow rates for main pipe and combined lateral pipe (Zhao et al., 2006, (Ramamurthy & Zhu 1997);

- Different joining angle between lateral pipe and the main pipe (Pfister & Gisonni 2014);
- Different ratio between water depth in the manhole and pipe diameter (Ramamurthy & Zhu 1997);
- Different ratio between pipe diameter and manhole diameter (Ramamurthy & Zhu 1997);
- Existence of sump inside the manhole and benching effects (Arao et al., 2012);

2.3 Head Losses within In line Manholes

"In line" manholes are commonly defined as manholes with a single inlet and a single outlet, orientated such that the pipe outlet is directly opposite the pipe inlet. The hydraulic behaviour and energy losses of "in line" manholes have been investigated by many researchers.

Studies have been completed investigating behaviour in part-full and pressurized pipes, manholes of different sizes and geometries and over a range of hydraulic conditions. A range of studies and main parameters investigated are summarized in table 1. Manhole 'types' are commonly defined based on inflow/outflow pipe configuration, as presented in figure 5.

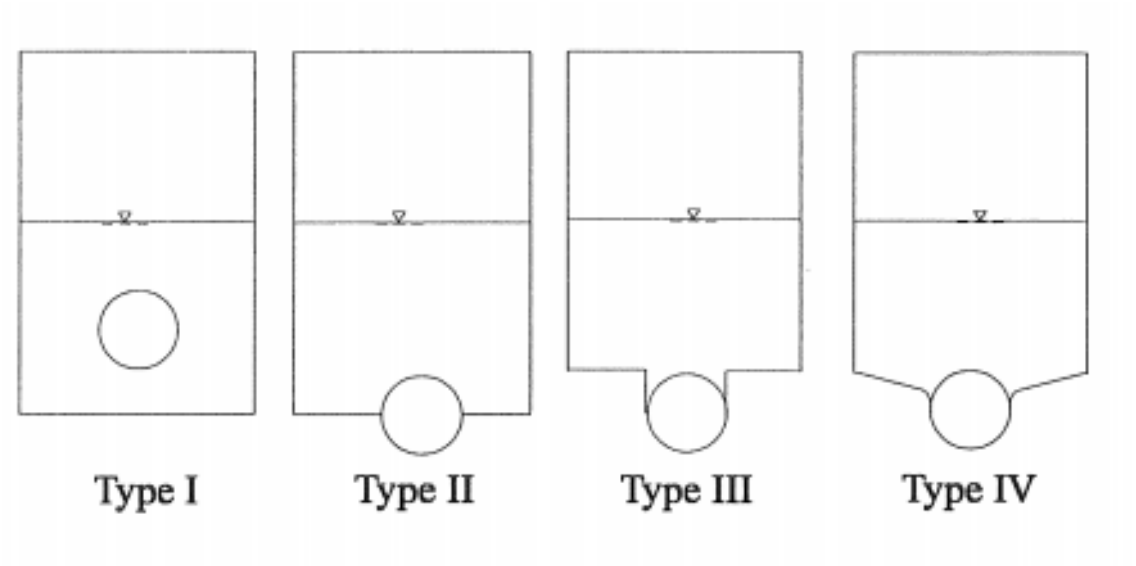

Figure 5 – Elevations of typical manholes (surcharged condition) - Asztely (1995).

Table 1 – Summary of previous studies on in line manholes.

Examined parameter	Sangster et al., 1958	Ackers 1959	Yeyevich and Barnes 1970	Liebmann 1970	Prints and Towsend 1976	Archer Bettes and Colyer 1978	Hare 1984	Howarth and Saul 1984	Marsalek 1981	Marsalek 1984	Marsalek 1987	Jonston and Volker 1984	Lindvall 1984	Lindvall 1986	Lindvall 1987	Lindvall 1993	Mark 1989	Pedersen and Mark 1990	Mugdal and Pani 1995
Type of Manhole	I	IV	II	IV	II,III	IV	I	IV	I, II, III	I, II, III	I, II, III	I,IV	II,III	II,III	II,III	II	I, IV	I	I
Part-Full pipes	-	X	X	X	X	-	-	-	X	-	-	-	-	-	-	-	-	-	-
Totally filled pipes	X	X	-	X	-	X	X	X	X	X	X	X	X	X	X	X	X	X	X
Straight-through flow	X	X	-	X	-	X	X	X	X	X	-	X	X	X	X	X	X	X	X
Varying Diameter of pipe	X	-	-	-	-	-	-	-	-	-	-	-	-	-	-	X	-	-	-
Varying diameter of manhole	X	-	-	-	-	-	-	-	X	X	-	-	X	X	X	-	X	X	X
Rectangular manhole	X	X	X	-	X	X	X	X	X	X	X	X	-	-	-	-	-	-	-
Circular manhole	X	-	-	X		X	-	X	X	X	-	-	X	X	X	X	X	X	X
Varying drop in manhole	X	-	-	-	X	-	-	-	-	-	-	-	-	-	-	-	-	-	X
Varying water depth in manhole	X	X	-	X	X	X	-	X	X	X	-	X	X	X	X	X	X	X	X

2.3.1 Detail of Selected Previous Studies on In-line Manholes

Sangster et al., (1958) conducted experimental tests on in line manholes (type I) and pressurized pipes without changes in pipe size and found that the range of energy loss coefficient K was 0.1-0.2.

Marsalek (1984) reported head loss (K) coefficients observed in a scale model inline manhole of types I, II and III under both free surface and fully pressurized inflow conditions with equal inflow and outflow pipes. Energy losses were found to be approximately proportional to velocity head as predicted by equation 3. K values were found in the range 0.102 to 0.344 in square shaped manholes, and 0.124 to 0.221 in circular manholes. K values were found to decrease with decreasing manhole width. The type of manhole was also found to influence reported K values, with losses for type I, approximately double that of type III manholes.

Pedersen and Mark (1990) completed experimental tests on in line manholes with fully submerged inlet and outlet pipes (of equal diameters). Empirical results were used to define a shape factor (ε_i) adjustment parameter for different manhole types (table 2), which quantifies the relative impact of the different geometries on the observed K values.

Table 2 – Shape factor estimated from measurement with Dm/D up to 4.

Shape	Type I	Type II	Type III
ε_i	0.24	0.07	0.025

These tests demonstrated the importance of geometry and shape as governing parameters for the quantification of head losses.

Mrowiec (2007) studied head losses within in line circular type I manholes in drainage systems under surcharge conditions. The manhole had a 290 mm diameter. Inlet and outlet pipes were connected to the manhole at the same height and have the same internal diameter (70 mm). Mrowiec (2007) found that the head loss coefficient for depths h_s/d_o between 1-3 increases linearly while for $H_{mh}/D_m > 3$ had almost a constant value K=0.45.

Pang and O'Loughlin (2011) measured energy losses within flows passing through a box-shaped pit (200 mm X 200 mm) without benching, with varying geometric conditions and flow ranges in both free inflow and submerged conditions. Observed K values were within the range 0.1-0.4, the authors attempted to relate K values to pit sizes and pipe diameters, however considerable scatter was observed in trends.

Despite numerous studies already completed on energy losses in manholes, due to the complexity of existing sewer systems, results achieved need to be verified while considering more variables at the same time (for example benching effects, upstream and downstream conditions etc.). Computer models rely on these parameters and if local authorities and governments request the publication of flood hazard maps, which are very useful for inhabitants, it is crucial to calculate energy loss at manholes including all variables of structural elements of the pipes and of the manhole which has not been accomplished yet (Arao et al., 2012).

2.4 Junction Manholes

A "manhole junction" is defined as a manhole which features two or more inflow pipes. This can cause more complex variations in the flow structures within the manhole; hence energy losses may be significantly different to those within in line manholes.

Zhao et al., (2006) and Pfister et al., (2014) utilized a common framework for defining energy loss coefficients at junction manholes, based on the principles of conservation of mass, energy and momentum.

The local energy losses ΔH_i induced by multiple inlets may be expressed through the energy equation, can be written as follow (Zhao et al., (2006) and Pfister et al., (2014)):

$$Q_1 H_1 + Q_2 H_2 - Q_3 H_3 = Q_3 \Delta H_i \qquad \text{Equation 4}$$

By considering two pipes entering a manhole (1), and (2) and outlet pipe (3) (as in Figure 6) the head losses coefficients for the possible flow "pathways" $K_{1,3}$ and $K_{2,3}$ are conventionally defined as:

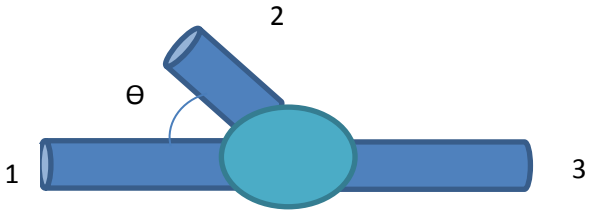

Figure 6– Head losses for a multiple inlet manhole.

$$K_{1,3} = \frac{H_1 - H_3}{{V_3}^2 / 2g} \qquad \text{Equation 5}$$

$$K_{2,3} = \frac{H_2 - H_3}{{V_3}^2/2g}$$ Equation 6

The global head loss coefficient for the manhole can be expressed as:

$$K = \frac{Q_1}{Q_3} K_{1,3} + \frac{Q_2}{Q_3} K_{2,3}$$ Equation 7

A method for determining K values was also produced based on momentum conservation. Zhao et al., (2006) utilized the conservation of momentum to relate pressure, flow and inlet orientation, providing the flowing equation:

$$\rho(Q_1 V_1 + Q_2 V_2 \cos\theta - Q_3 V_3) = \sum P_x$$ Equation 8

Where θ is the junction angle and P_x are the components of the pressure forces along the main flow direction. The exchanges of momentum can result in net energy transfer from the main stream to the merging stream. It is thus possible that due to the changing plane through which the flow passes, the merging flow may appear leave the junction manhole with energy content larger than it had upstream. This circumstance implies the possibility of having an apparent 'negative' loss coefficient. However such reported negative losses (such as in Zhao et al. 2006) are due to the fact that the full system (total flow in vs total flow out) is not considered and that measurements are taken at a cross-section where the assumption of straight, parallel streamlines perpendicular to the cross-section is not met, which is essential for the Bernoulli equation to be valid.

For combining flows, in the case of surcharged manholes, with both inlet pipes and the outlet pipe pressurized, assuming that the piezometric heads of the approach flows are equal to the water level in the manhole (i.e. hydrostatic pressure distribution), Zhao et al., 2006 defined the terms in equation 9 and 10 to propose a definition for K values as follows:

$$K_{1,3} = \left[1 - 2\frac{A_3}{A_1}\left(\frac{Q_1}{Q_3}\right)^2 - 2\frac{A_3}{A_2}\left(\frac{Q_2}{Q_3}\right)^2 \cos\theta + \left(\frac{A_3}{A_1}\right)^2 \left(\frac{Q_1}{Q_3}\right)^2\right]$$ Equation 9

$$K_{2,3} = \left[1 - 2\frac{A_3}{A_1}\left(\frac{Q_1}{Q_3}\right)^2 - 2\frac{A_3}{A_2}\left(\frac{Q_2}{Q_3}\right)^2 \cos\theta + \left(\frac{A_3}{A_2}\right)^2 \left(\frac{Q_2}{Q_3}\right)^2\right]$$ Equation 10

2.4.1 Detail of selected experimental studies in junction manholes

A number of experimental studies have also been conducted to quantify energy losses in junction manholes under different geometric combinations or hydraulic conditions.
Sangster et al., (1958) completed tests at the University of Missouri in order to inform the hydraulic design of stormwater drainage structures. However only a limited range of manhole geometries was considered. Observed K values for the range of geometries and conditions tested are displayed in table 3.

Table 3 – Typical values of K for junctions tested by Sangster et al., (1958).

Junction geometry and flow conditions	Observed K values
Upstream pipe in line with outlet pipe and 90 degrees lateral flow (from the lateral one, 20% of total flow)	0.5
Two opposed laterals, one-third the flow from the lateral with the higher velocity	0.7
Two offset opposed laterals, two-third of the flow from the lateral nearest the outlet pipe	1.5-1.9
90 degrees angle, without change in size. No lateral flow	1.6
Upstream pipe in line with outlet, plus 90 degrees lateral. Flow equally divided between the upstream pipes	1.2

Archer et al., (1978) worked on junction head losses involving rectangular and circular structures to determine the magnitude of energy losses occurring at surcharged sewer manholes. The tests were limited to deflection angles of 0, 30 and 90 degrees (where deflection angle is defined as the angle between the lateral inflow pipe and the main flow direction) with no lateral inflow and with a constant pipe diameter ratio D_u/D_o of unity (D_u = diameter upstream pipe, D_o=diameter outlet pipe).
The authors concluded that the magnitude of the loss coefficient was independent of the discharge, the degree of submergence and the extent of the air entrainment. The change in alignment and the manhole shape were the main factors influencing the loss of head. Observed K values found are listed in table 4:

Table 4 – Magnitude of K values as determined by Archer et al., (1978)

Type of Manhole	0 ° deflection	30 ° deflection	90 ° deflection
Rectangular	0.1	0.4	0.85
Circular	0.15	0.5	0.95

Ramamurthy et al., (1997) analyzed combining flows at 90^{o} junctions within rectangular closed conduits. Energy loss coefficients were found to vary with the ratio of flows within the inlet pipes, and the varying size of the size of the lateral inflow pipe. Observed energy losses coefficients for K_{12} decreased with increasing of A_2/A_3 at fixed Q_2/Q_3 for rectangular conduits. For high discharge ratios ($Q_2/Q_3 > 0.8$) and low values of area ratios ($A_2/A_1 = 0.22$) authors found a considerable discrepancy between the experimental results presented related to K_{23} for rectangular conduits and existing results for circular conduits (Serre et al., 1994). This can be explained by the large difference in the flow structure of combining flows in rectangular conduits and circular conduits.

Wang et al., (1998) designed an experimental facility (scale 1:6) to determine head losses at sewer pipe junctions (Manholes) under surcharged conditions. The manholes studied were type I and tests were conducted for various flow rates, pipe sizes and for flow configurations including a T-junction, cross and a 90 degrees bend.

Head loss coefficients were in the range K = 0-1.2 and head-loss coefficients were found to be strongly dependent on the relative inlet flow rate and the change of pipe diameter within the pipelines, Additionally, head losses become more significant in the presence of significant lateral inflow or the junction forces a change in flow direction. It was also found that as the lateral flows become more unequally distributed, the lateral loss coefficients increase dramatically.

Zhao et al., (2006) and Pfister et al., (2014) compared observed K values within junction manholes with those predicted by equation 9 and 10. Zhao et al., (2006) utilized 90° (Figure 7) and 25.8° Edworthy junction (a bespoke junction designed by Zhao et al., 2006, to replace the problematic T-shaped junction of the Edworthy storm trunk in the city of Calgary, Alberta, Canada – Figure 8).

The junction chamber was a 3D * 2D rectangular box without benching as shown in figure 7. The inverts of two inlet pipes connected 5 cm above the bottom of the chamber and the downstream pipe invert connected 4 cm above.

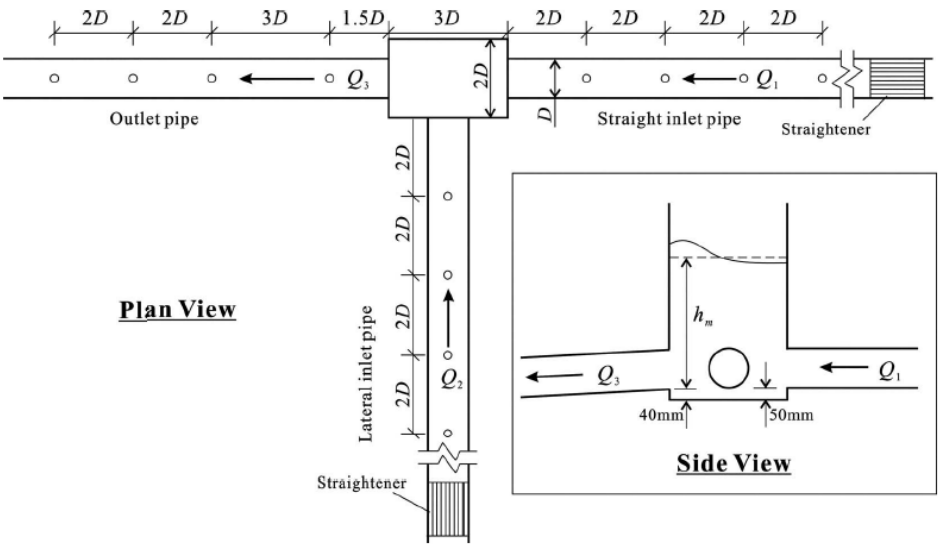

Figure 7 - Experimental setup of a 90° sewer junction (Zhao et al., 2006).

Figure 9 and Figure 10 present the observed relationship between the energy loss coefficients and relative inlet flow in the Edworthy junction and the 90° junction, respectively. Zhao et al. stated that "*for the 25.8° Edworthy junction, the energy loss coefficient of the straight-through stream, K_{13}, or of the lateral stream, K_{23}, can attain negative values at Q_2/Q_3 approaching 1 or 0 respectively*".

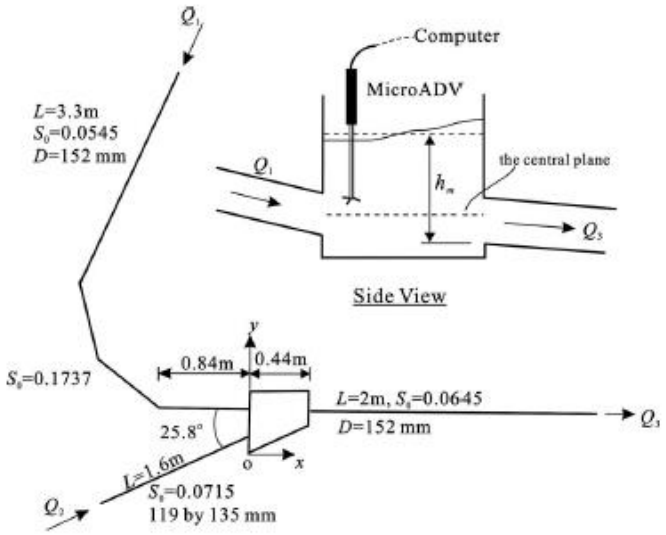

Figure 8 – Plan view of the 25.8 Edworthy model junction (Zhao et al., 2006).

Zhao et al. stated that "*in the 90° junction the lateral flow can gain energy from the main flow. The energy loss in 90° junctions is more significant than that in the 25.8° junction (the coefficient K is approximately twice of that in the 25.8° junction)*". Together with these measurements, another four experimental data sets from previous studies are plotted: Marsalek's (1985) data without benching and with half-benching;

Wang et al. (1998) data for a junction with half-benching. Both studies were conducted in 90° model junctions with three connecting pipes of equal diameters. In Figure 10 (Zhao et al., 2006), K_{23} and K in this study compare well with data of all the other studies, but discrepancies in K_{13} are noticeable. Note the difference in the manhole geometry: Marsalek (1985) conducted the experiments in round manholes of 2.3D in size; Wang et al.'s 1998 data were from a round manhole of 2D in size; and the Zhao et al., 2006, investigation was for a 3D-2D rectangular chamber with a sump at the bottom. The sump obviously had a significant impact on the results.

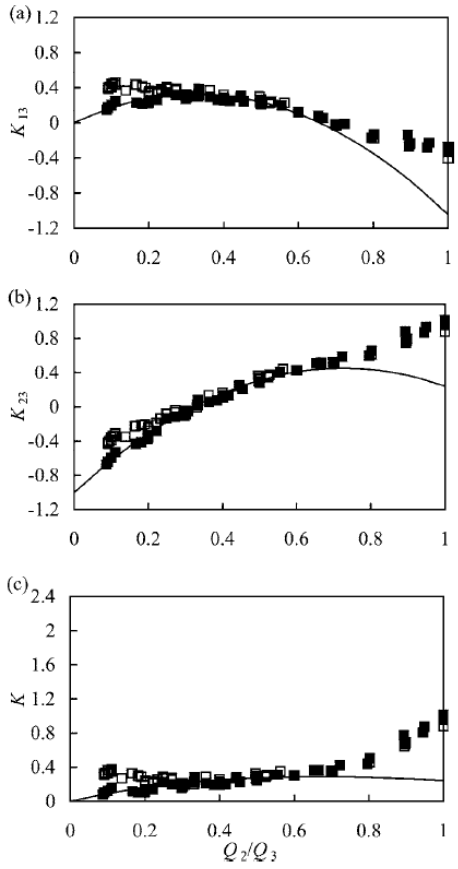

Figure 9 – Energy loss coefficients for pressurized flow pipe in the 25.8 degrees Edworthy junction of a) K_{13}; b) K_{23}; and c) K measurements with half benching (filled square), without benching (empty square) and predictions of Equation 9 and 10 (straight line) [Zhao et al., (2006)].

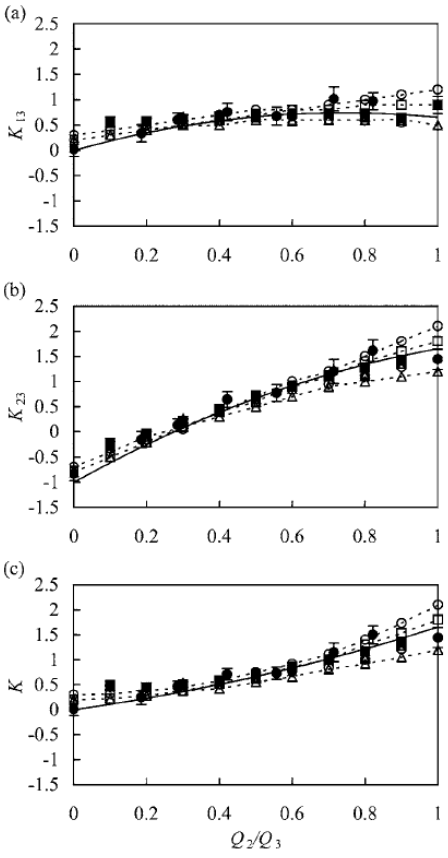

Figure 10 - Energy loss coefficients for pressurized flow pipe in the 90 degrees junction of a) K_{13}; b) K_{23}; and c) K measurements Zhao et al., (2006) Q_3 = 0.90 (empty triangle), Q_3=1.35 (cross) and Q_3=1.79 (empty circle) with So=0 and Q_3 =1.79 (filled square) with So=0.061. Results of Wang et al (1998) (filled circle), Marsalek (1985), no benching (dash line with empty circle), half benching (dash line with empty square), full benching (dash line with empty triangle) and predictions of Equation 9 and 10 (straight line) [Zhao et al., (2006)].

Zhao et al. (2006) stated that "*it is expected that the sump affects the straight-through stream more than the lateral one because the discrepancies in the comparisons is significant in K_{13} and in K at small Q_2/Q_3. The effect of the sump on K vanishes when the lateral flow become significant. In all of the junctions, good correlations between the energy loss coefficients and the flow ratio Q_2/Q_3 are clear*" (results from Zhao et al., 2006 are plotted in Figure 9 and Figure 10).

Zhao et al. (2006) showed that for the 25.8° Edworthy junction, Equation 9 and 10 describe the variation of the coefficients tolerably well for Q_2/Q_3 ratios smaller than 0.7-0.8.

In the 90° junction, Equation 9 and 10 predict K_{23} well in all junctions tested and the K_{13} of Zhao et al., (2006) datasets with the exception of tests with a small Q_2/Q_3 ratio (as shown in Figure 10, Zhao et al., 2006). The equation was judge to accurately predict K at larger Q_2/Q_3 ratios (when K_2 is the largest contributor to overall head loss). However Equation 9 and 10 omit any effect of benching design in a junction manholes. However, the authors suggest that the half-benching has little influence on the head loss in the surcharged flow with the discrepancies at small Q_2/Q_3 caused by the sump in the chamber without benching; in 90° junctions, the effects of the benching in Marsalek (1985) and Wang et al. (1998) are negligible when inflows are comparable, and only a fairly small influence on the head loss observed when the lateral flow is dominant. Therefore, in surcharged flows, common benching designs for sewer junctions with straight channels and comparable discharges Q_1 and Q_2 exhibit no significant contribution to reducing the energy loss. Based on the discussions above, Equation 9 and 10 are expected to provide a good estimate for energy losses for pressurized flow in 90° sewer junctions.

Arao et al., (2012), proposed equations for quantifying energy losses at three-way circular drop manholes under surcharged conditions which take the influence of the ratio of the diameter between inflow pipes and outflow pipe and drop gaps between those pipes into consideration. The outline of the experimental facility developed by Arao et al. (2012) is illustrated in figure 11.

For this research, Arao et al., (2012) used manhole models with the diameters of 0.15 m and 0.6 m. As shown in figure 11, the total energy head at inflow and outflow pipes was calculated at distances of 0.3, 0.5 and 0.7 m from the manhole in terms of equation 1. The energy loss at a manhole was defined according to equation 3.

The increase of energy loss due to the drop gaps (term S_u in figure 11) between the main upstream pipe and the downstream pipe was proposed based on the observed datasets (equations 11 and 12) and applied for the estimation of energy loss coefficients, K_{13} and K_{23}.

$$C_{Su} = 1.3\left(\frac{S_u+D_u-D_d}{D_u}\right)\left(\frac{D_d}{D_u}\right)^3\left(1-\frac{Q_l}{Q_d}\right)^3 \; if \; 0.2 \le \frac{S_u+D_u-D_d}{D_u} \; and \; \frac{S_u}{D_d} \le 1.2 \qquad \text{Equation 11}$$

$$C_{Su} = 1.3\left(\frac{0.2D_d+D_u}{D_u}-0.2\right)\left(\frac{D_d}{D_u}\right)^3\left(1-\frac{Q_l}{Q_d}\right)^3 \; if \; 0.2 \le \frac{S_u+D_u-D_d}{D_u} \; and \; \frac{S_u}{D_d} > 1.2 \qquad \text{Equation 12}$$

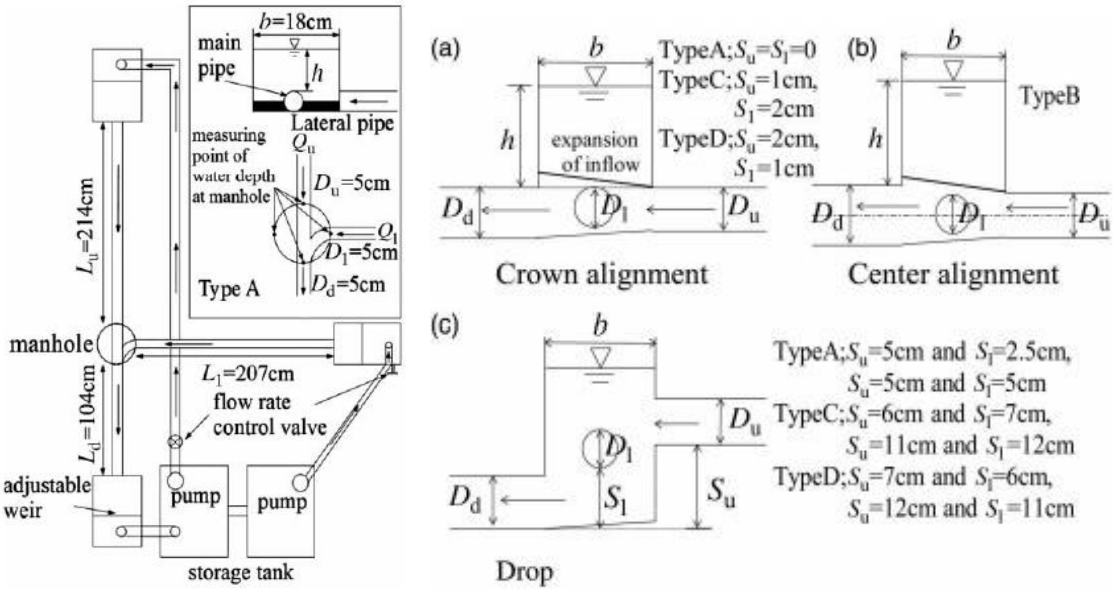

Figure 11 – Experimental apparatus (on the right), crown alignment (a), center alignment (b) and perpendicular connection between inflow and outflow pipes (c) (Arao et al., 2012).

The increase of energy loss due to the drop gaps between the lateral pipe and the downstream pipe is proposed in equations 13 and 14, which are applied for the estimation of energy loss coefficient K_{23}.

$$C_{Sl} = 0.35\left(\frac{S_l+D_l-D_d}{D_l}\right)\left(\frac{D_d}{D_l}\right)^3\left(\frac{Q_l}{Q_d}\right)^3 \; if \; 0 \le \frac{S_l+D_l-D_d}{D_l} \; and \; \frac{S_l}{D_d} \le 1 \qquad \text{Equation 13}$$

$$C_{Sl} = 0.35\left(\frac{D_d}{D_l}\right)^3\left(\frac{Q_l}{Q_d}\right)^3 \; if \; \frac{S_l}{D_d} > 1 \qquad \text{Equation 14}$$

The effect of the drop gaps between the lateral pipe and the downstream pipe was found to be smaller than the effect of the presence of lateral inflow itself. Arao et al., (2012) concluded that the energy loss at three-way manhole varies considerably with the ratio of the diameter between inflow pipes and an outflow pipe, the ratio of flow rate between those pipes, the water depth in a manhole and the drop gaps between the pipes.

A similar approach has been utilized by Saldarriaga et al., 2012, who constructed a physical scale model (Figure 12) at the University of Los Andes.

As for other studies measuring hydraulic behaviour, all elements utilized were constructed of acrylic crystal in order to facilitate the visualization of the hydraulic conditions inside the structures, in this case pipes and a manhole. Saldarriaga et al., 2012, investigated supercritical flows inside junction manholes.

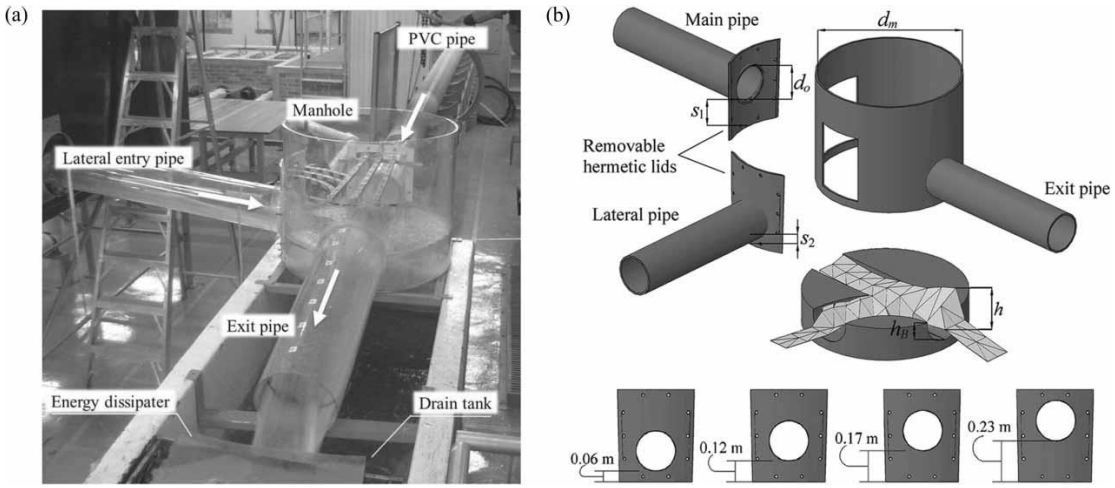

Figure 12 – The model of the junction with the correspondent possible variations of the model itself (Saldarriaga et al., 2012).

The physical model developed by the authors was composed of a main entry pipe and a lateral of 90° junction angle (Figure 12). Due to the geometry of the system, the study reproduced three different flow scenarios:

- Manhole entry flow through main pipeline only, called direct flow;
- Manhole entry flow through lateral pipeline only;
- Manhole entry flow through both entry and lateral pipe (junction flow).

To analyze these different flow conditions and obtain governing equations, a statistical analysis was been completed to develop empirical equations for head loss.

Two regressions were utilized to combine the effect of Froude number, pipe drop (height above base of manhole) and water depth inside the pipe.

The authors found that the effect of Froude number is small and that the water depths in the main pipe and the lateral pipe have higher impact on the head loss coefficient.

Pfister and Gisonni (2014) developed an experimental tool at the Ecole Polytechnique Federale de Lausanne composed of 45 and 90 degrees junctions combining varying diameters conduits. The outlet pipe diameter was fixed as D_3=0.240 m and the approach pipe diameters D_1 and D_2 were varied (0.123, 0.190 and 0.240 m) (Figure 13). Empirical expressions to estimate the value of the head loss coefficient were provided based on more than 600 tests (equations 15-16).

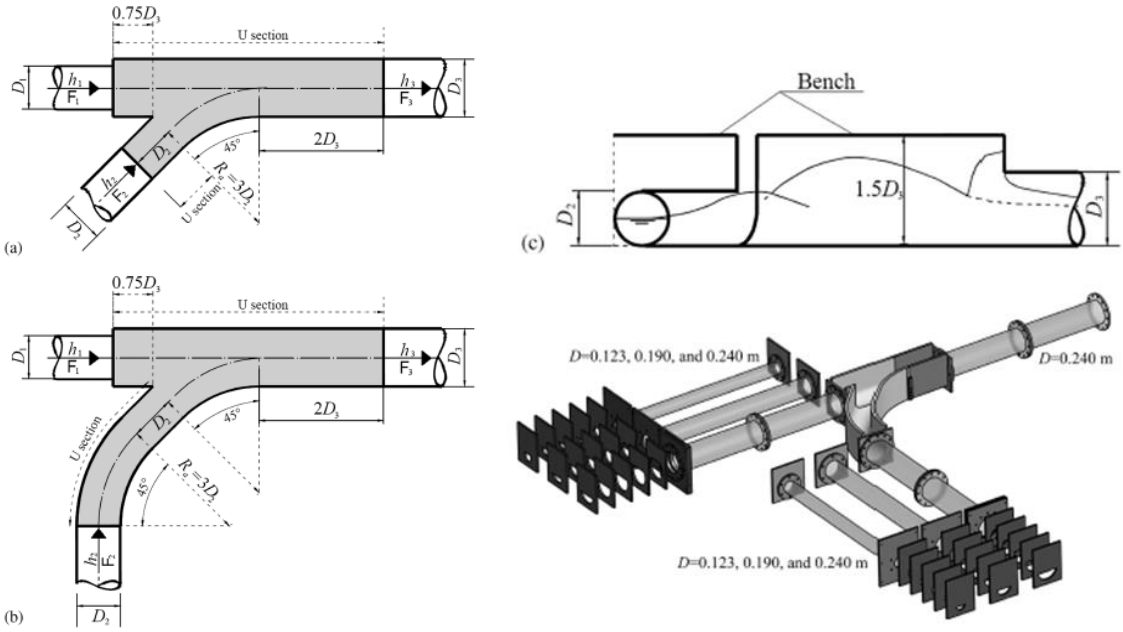

Figure 13 – Scheme of the junction manhole: (a) plan view for 45 º, (b) plan view for 90 º (c) section and overview of the model including jet boxes, conduits and junction, (Pfister and Gisonni, 2014).

$$K_{1,3} = c_{1,3} + a_{1,3}\left[1 - 2\frac{{Fr_1}^2 {y_1}^{2.5} {\beta_1}^3 + {Fr_2}^2 {y_2}^{2.5} {\beta_2}^3 \cos\vartheta}{{Fr_3}^2 {y_3}^{2.5}} + \beta_1 \frac{{Fr_1}^2 y_1}{{Fr_3}^2 y_3}\right] \quad \text{Equation 15}$$

$$K_{2,3} = c_{1,3} + a_{1,3}\left[1 - 2\frac{{Fr_1}^2 {y_1}^{2.5} {\beta_1}^3 + {Fr_2}^2 {y_2}^{2.5} {\beta_2}^3 \cos\vartheta}{{Fr_3}^2 {y_3}^{2.5}} + \beta_1 \frac{{Fr_1}^2 y_1}{{F_3}^2 y_3}\right] \quad \text{Equation 16}$$

Observed paramters for equations 15-16 are presented in table 5 for the different junction angles and flow regimes tested.

Table 5 - Coefficients for equation 15-16 (Pfister et al., 2014)

Junction Angle	$a_{1,3}$	$c_{1,3}$	$a_{2,3}$	$c_{2,3}$
45°				
Supercritical Flow	0.72	0.27	0.83	0.16
Subcritical Flow	0.91	-0.30	0.75	-0.16
90°				
Supercritical Flow	0.70	0.15	0.68	0.16
Subcritical Flow	0.80	-0.13	0.54	-0.08

2.5 Summary

It can be seen from the reviewed literature that a considerable amount of work has been conducted to define energy losses through urban drainage hydraulic structures using physical models. Extensive experimental data are available to estimate local head losses in free-surface and pressurized flow for "in line" manholes, Flows in angulated junctions present more complicated patterns, such as waves, mixing, separation, turbulence, and the transition between (or coexistence of) open channel flow and full pipe flow and these complex configurations are as important as "in line" manholes. However for manhole junctions with multiple inlets, existing experimental studies are largely limited to lateral pipe orientated 90degrees to the inflow and outlet pipes. More studies would therefore be beneficial using different geometric configurations (for example 45° degrees lateral junctions) and different hydraulic conditions (i.e. under high/surcharge flow events (Lopes et al., 2013).

2.6 Interaction of below/above ground flows and flow over the surface

Flood models must also describe the linkages (i.e. flow exchange) between the major and minor system. An accurate determination of the exchange rates between major and minor systems is one of the most challenging aspects of urban flood modelling (Mark et al., 2004). Flood flows through hydraulic structures such as manholes are highly 3D and unsteady; however within existing models these linkages are most commonly simplified and expressed using 1D weir and orifice equations, which are obtained by applying the principles of Bernoulli.

Weir and orifices are hydraulic structures commonly used for measuring and controlling the flow. *A weir* is an overflow structure built perpendicular to an open channel axis. The weirs are generally classified as rectangular, trapezoidal, triangular etc. In the case of sharp weirs, the triangular one is also called a V-notch weir. One kind of trapezoidal weir is the *Cipoletti* weir. Different kinds of sharp-crested weirs are illustrated in figure 14.

Figure 14 – Examples of rectangular (left) and Cipoletti (right) weirs.

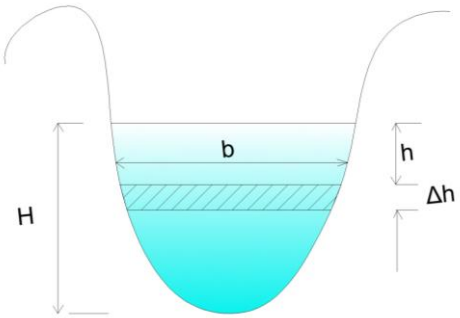

Figure 15 – General any shape notch.

The discharge passing through a given slice of area within a notch of any shape (Figure 15) can be quantified as:

Discharge through strip = dq = C_d ** Area of the strip * Theoretical velocity*

$$dq = C_d L dh \sqrt{2gh} \qquad \text{Equation 17}$$

Integrating from h = 0 at the free surface to h = H at the bottom of the notch, the total theoretical discharge (Q) becomes:

$$Q = \int_0^H bh^{1/2}\, dh\, \sqrt{2g} \qquad \text{Equation 18}$$

$$Q = C_d L \sqrt{2g} \int_0^H h^{1/2} dh$$ Equation 19

$$Q = \frac{2}{3} C_d L \sqrt{2g} H^{\frac{3}{2}}$$ Equation 20

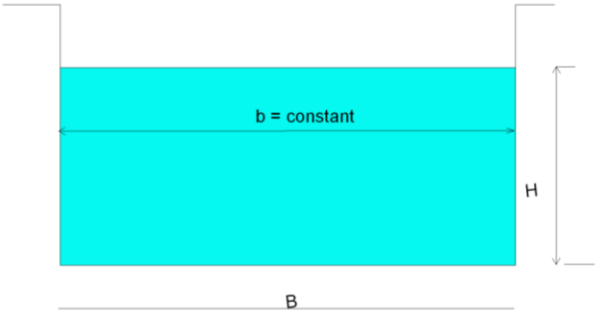

Figure 16 – Rectangular weir scheme.

For a rectangular notch (Figure 16), b = B hence the discharge can be calculated as follows:

$$Q = B\sqrt{2g} \int_0^H h^{1/2}\, dh = \frac{2}{3} B H^{3/2} \sqrt{2g}$$ Equation 21

In addition to the weirs, there is another category of measuring devices which can be defined as *orifices* (Figure 17 – Bottom discharge and side discharge.). Generally, they are sharp-edged opening in a wall or bulkhead through which flow occurs. The discharge through an orifice can be quantified as follows:

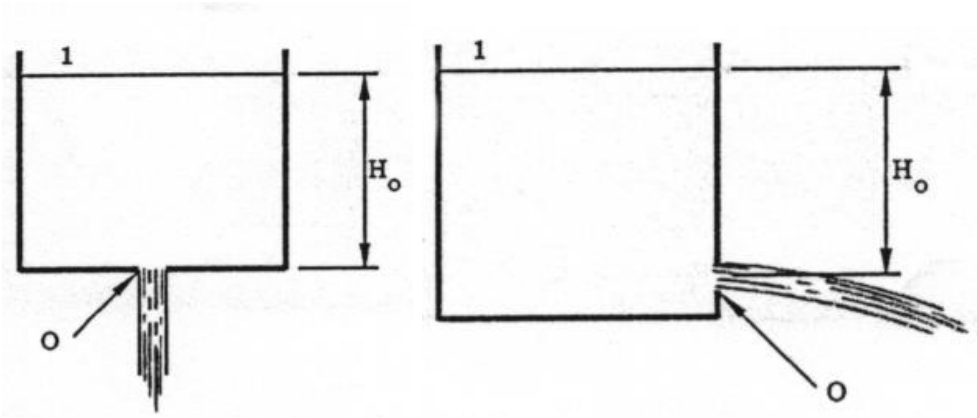

Figure 17 – Bottom discharge and side discharge.

Considering hydraulic head at the water surface (1) and at the orifice (o):

$$Z_1 + \frac{P_1}{\rho g} + \frac{V^2{}_1}{2g} = Z_o + \frac{P_0}{\rho g} + \frac{V^2{}_0}{2g}$$ Equation 22

Considering the pressure at (1) and (0) is equal to the atmospheric pressure (P_1=P_0),

V_1=0 and $Z_1 - Z_0 = H_0$ gives

$$H_0 = \frac{V^2{}_0}{2g} \quad \text{Equation 23}$$

The velocity of the water passing through the orifice is therefore given by:

$$V_0 = \sqrt{2gH_0} \quad \text{Equation 24}$$

This can be used to quantify the water being discharged through the orifice:

$$Q = aV_0 = a\sqrt{2gH_0} \quad \text{Equation 25}$$

In practice the discharge is always less than this theoretical amount due to the viscosity of the fluid, to surface tension and due to resistance of the air. The disparity between the theoretical discharge velocity and the actual discharge velocity is accounted for by introducing a factor C_v known as the **Coefficient of Velocity** so that:

$$V_{actual} = C_v\sqrt{2gH_0} \quad \text{Equation 26}$$

If the discharge from a sharp edged orifice is examined closely it will be observed that the minimum diameter of the jet of water discharging from the orifice is smaller than the orifice diameter. The plane at which this occurs is known as the **Vena Contracta**, which is the plane where stream lines first become parallel. Applying the discharge equation at the vena contracta,

$$Q = a_c C_v\sqrt{2gH_0} \quad \text{Equation 27}$$

This can be written as

$$Q = a\, C_c C_v\sqrt{2gH_0} \quad \text{Equation 28}$$

Where $C_c = a_c/a$ = Coefficient of Contraction

Or more simply as

$$Q = aC_d\sqrt{2gH_o} \qquad \text{Equation 29}$$

Where $C_d = C_cC_v = Coefficient\ of\ Discharge$ Equation 30

Typical values of C_d range from 0.6 to 0.65 (Massey and Ward-Smith, *Mechanics of Fluids, Seventh Edition, Volume 1*). The actual value of the coefficient of discharge for any orifice may be determined by measuring the quantity of water discharged over a period of time as well as the head difference upstream and downstream of the orifice.

$$Q = C_cC_{vf}C_{va}\,A\,\sqrt{2g(h_1 - h_2)} \qquad \text{Equation 31}$$

Weir and orifice coefficients depend on the effects of viscosity, the velocity distribution in the approach section and the capillarity, but they are most commonly determined by empirical methods (Rouse, 1950).

2.7 Application of exchange equations within urban flood models

Within coupled urban flood models (e.g. Djordjevic et al. 2005, Seyoum et al 2012) surface to sewer exchange is commonly quantified using equations originally derived for flow over a weir or through an orifice.

To quantify the exchange discharge between major and minor systems, Chen et al., (2007) defined a framework based on hydraulic head in the major and minor systems and applied the weir and orifice equations.

Three scenarios were defined, with head in each case referenced to a datum point (z_{crest}), representing the street level. The discharge $Q_{exchange}$ is positive when water runs from the sewer into the surface and negative when it runs from the overland area into the sewer.

1. *Surface to sewer flow exchange (figure 18) when head in sewer is lower than* Z_{crest}

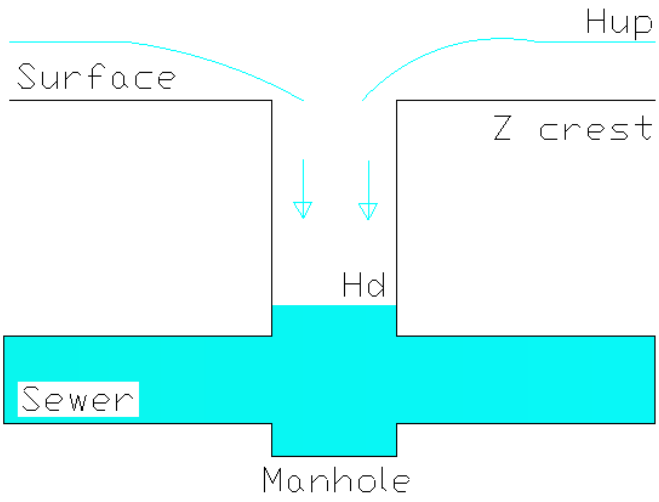

Figure 18 – Free weir linkages.

In this case, the formulation that is commonly used is based on the shape crested weir equation:

$$Q_{exchange} = C_w w \sqrt{2g} \left(H_{up} - z_{crest}\right)^{3/2} \qquad \text{Equation 32}$$

Within reviewed existing flood models, the 'free weir scenario' is considered applicable for surface to sewer exchange in all cases when the $H_d < z_{crest}$, although in Djordjevic et

al., (2005), it is noted that a 'somewhat reduced capacity' should be considered at high flow rates when the manhole becomes submerged by the surface flow.

In all reviewed cases, when $H_d < z_{crest}$ flow in the pipe network is not considered to have any influence on flow exchange.

This is despite more detailed experimental studies of flows over sharp crested weirs (e.g. Wu and Rajaratnam, 1996) which have shown the existence of different flow (and discharge) regimes as a function of flow depth both upstream and downstream of the weir crest, even when the downstream water level is below the level of the weir crest.

2. *Sewer to surface exchange (figure 19) with head above the manhole between water level on the surface and Z_{crest}.*

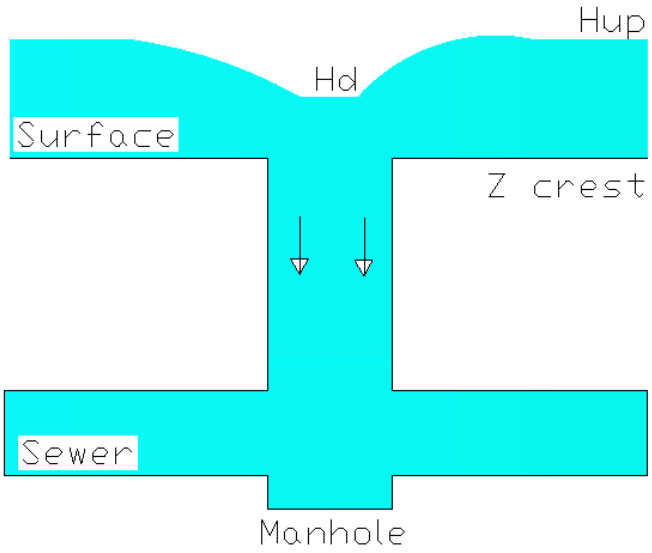

Figure 19 – Submerged weir linkage.

In this case:

$$Q_{exchange} = C_w w \sqrt{2g}\left(H_{up} - z_{crest}\right)\left(H_{up} - H_d\right)^{1/2} \quad \text{Equation 33}$$

This linkage is considered applicable when $H_d > Z_{crest}$ and $H_{up} < A_{mh}/\pi D_m$. If $H_{up} > A_{mh}/\pi D_m$ the link is considered 'fully submerged' and the submerged orifice formula is judged a more suitable description of the interface.

The submerged orifice equation can be expressed to provide flow exchange as

$$Q_e = C_i A_{mh} \sqrt{2g}\left(H_{up} - H_d\right)^{\frac{1}{2}} \quad \text{Equation 34}$$

In this case, the discharge coefficient, C_i accounts for energy losses due to flow through the orifice, the continued contraction of the jet as it passes through the restriction (*vena contracta*), and the assumption of negligible velocity head in the upstream (i.e. surface) flow.

It is currently unclear from the literature how the transition point between submerged weir and orifice behaviour has been evaluated or defined.

3. *Sewer to surface exchange (figure 20) when water lever above the manhole is higher than water level in the surface.*

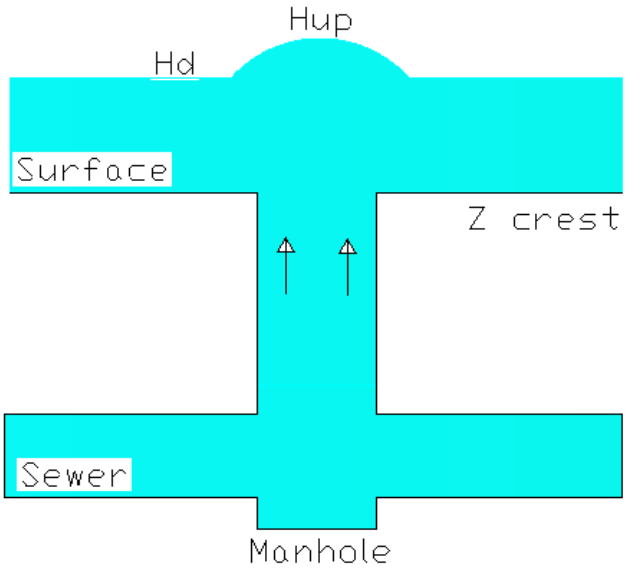

Figure 20 – Orifice linkage.

In this case:

$$Q_{exchange} = c_o A_{mh} \sqrt{2g} \left(H_{up} - H_d\right)^{1/2} \qquad \text{Equation 35}$$

For sewer to surface exchange to occur, hydraulic head in the pipe network must be greater than the depth of the surface flow. Within flood models, flow exchange from sewer to surface flow is commonly (Djordjevic et al. 2005) evaluated by considering the interface point to act as an orifice.

In the case that the flow on the surface is negligible, the flow exchange is dependent on the head in the pipe network relative to Z_{crest}.

The weir and orifice equations used in this framework are derived using the principles of energy conservation and hence contain assumptions such as steady 1D flow, with energy losses due to turbulence taken into account via a constant discharge coefficient. While energy losses in manholes and junctions have been estimated as described by

different studies, surface/subsurface flow exchange and correlated energy losses at links such as manholes and gully structures is one area that is currently poorly understood.
A lack of understanding of surface/subsurface flow exchange and quantification of energy losses is seen as a cause of significant uncertainty in pluvial flood modelling (Djordjević et al, 2005).

2.8 Experimental quantification of flow exchange

Djordjević et al., 2013 examined the performance of urban drainage structures during street to sewer flow conditions. A full-scale gulley structure connecting a surface area (which is 4270 mm by 1830 mm) with a pipe (Figure 21) was used to produce experimental results to validate a three-dimensional CFD (Computational Fluid Dynamics) model which has been set up to investigate the hydraulic performance of this type of gulley during interactions between surface flood flow and surcharged pipe flow.

Figure 21 – Experimental setup used for this study (Djordjevic et al., 2013).

Recently Bazin et al. (2014) used a physical model of a drainage pipe linked to a street surface by a series of drainage tubes and 'street inlets' (similar to gullies) to quantify and model flow exchange between below and above ground systems (Figure 22).
The 'street' was 10 m long, 0.5 m wide and had zero slope. The 'pavements' were 15 cm wide and 2 cm high. The street inlets were located every 1 meter, with a total of 20 street inlets (10 on each side). The drainage pipe had a diameter of 5 cm and a slope of 1/900. Due to the geometry of the model, authors had to maintain the water depth in the street above 1 cm to avoid significant capillarity effects that would influence the street flow and its interaction with the exchange structures.

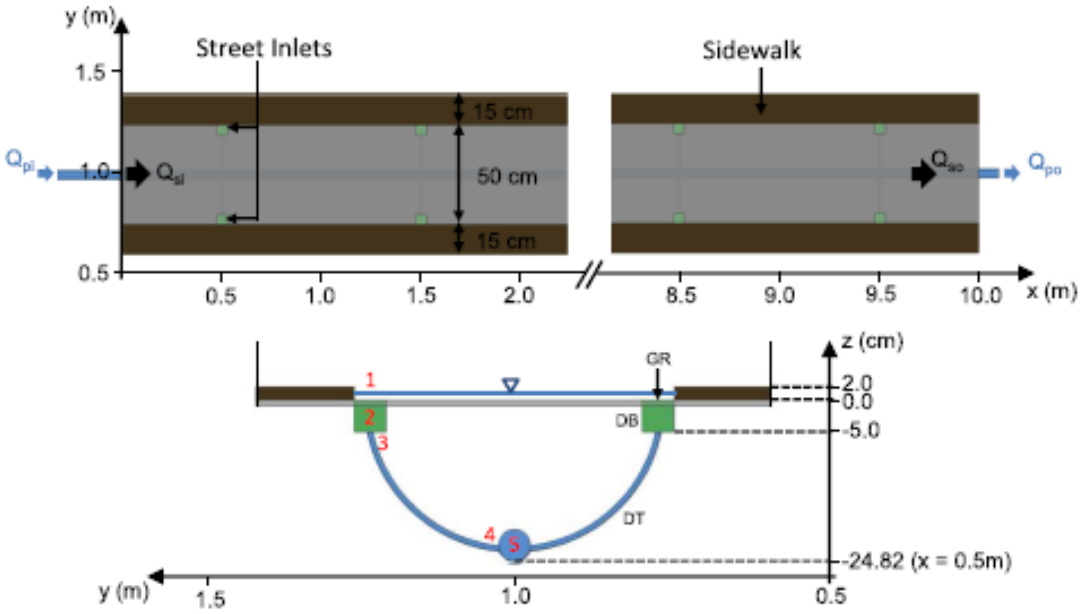

Figure 22 – Top view and cross section view of the experimental facility developed by Bazin et al., 2014. GR corresponds to the street inlet grid, DB is the drainage box, DT the drainage tube and DP the drainage pipe.

Additionally, considering that air bubbles can enter the drainage structure and the pipe, complicating measurements and analysis, only pressurized flows through the drainage structures and through the drainage pipes were considered.

The authors defined the total head losses over the street model as:

$$\Delta H_{1-5} = \Delta H_{1-2} + \Delta H_{2-3} + \Delta H_{3-4} + \Delta H_{4-5} \quad \text{Equation 36}$$

All these terms have been expressed as a function of the exchange discharge Q_e in the drainage tube:

$$\Delta H_{1-5} = \left(K_{1-2} * {\alpha_{V1-2}}^2 + K_{2-3} + f_t * \frac{L_t}{D_t} + K_{4-5}\right) * \frac{{Q_e}^2}{{A_t}^2 * 2g} \quad \text{Equation 37}$$

$$\Delta H_{1-5} = -\left(K_{2-1} * {\alpha_{V2-1}}^2 + K_{3-2} + f_t * \frac{L_t}{D_t} + K_{5-4}\right) * \frac{{Q_e}^2}{{A_t}^2 * 2g} \quad \text{Equation 38}$$

However tests were limited to scenarios with pressurized pipe conditions only and the scale of the model limited the range of flow Reynolds numbers tested.

The examples of previous work described illustrate the importance of experimental data from physical models to calibrate and validate models and determine accurate values of

C_w and C_o. Large uncertainties exist in field datasets due to uncertainties in urban hydrology and the presence of multiple exchange points.

The suitability of orifice and weir equations and the impacts of assumptions (i.e. applicability in unsteady flow) on predictive uncertainty have not been explored and little guidance exists on appropriate discharge coefficients for use within these equations.

2.9 Existing limitations and gaps in flood modelling tools

Hydraulic flood models rely on parameters to represent flow conditions such as pipe roughness, energy losses and surcharge. In most cases, during normal operational conditions in sewer, parameters (such as pipe roughness) can be calibrated with confidence to the availability of flow data from existing in pipe monitoring.

In contrast, during surcharge and flood events there is a lack of field data suitable for model calibration and validation (Hunter et al., 2008, Prodanovic et al. 1998). This is due to two main reasons:

1. High resolution data is expensive and difficult to obtain for long periods of time;
2. Flood events happen relatively infrequently, and thus measurement devices are highly unlikely to be in the correct place to record data.

Fully instrumented physical models that can reproduce urban flooding events are therefore very valuable to better understand complex hydraulic processes associated with urban floods.

Parameters which are highly desirable for the calibration of computer modeling results but are often difficult to obtain in real scale systems under high or infrequent flow conditions include:

- Energy losses through manhole structures of differing geometries and inlet conditions.
- The flow exchange between minor and major systems during flood events and energy losses during such interaction events.
- Flood wave behavior and velocity fields in shallow urban flood flows.

Existing urban drainage models may use empirical datasets to obtain local head loss values. However these head loss values may be obtained from observations conducted in scenarios different to the modelled situation. The variation of head loss values for typical hydraulic structures such as manholes is currently unclear. In addition the

implications for urban drainage models of inaccurate head loss values have not currently been adequately defined.

Considering the linkage between major and minor system, one significant potential limitation of flood models concerns the use of weir and orifice equations to represent exchange rates through manhole structures. Currently there is a significant lack of calibration data for modelling results, and the potential accuracy of these equations is unknown, given that they are representing a complex 3D unsteady flow condition using a constant coefficient to represent energy losses.

2.10 Thesis objectives

The overall aim of this research is to develop a physical urban flood model able to provide datasets to improve urban pluvial flood models and provide a more accurate understanding of the hydraulic characteristics of flood flows. By achieving this, the work will seek to meet the following specific objectives:

1. To verify existing energy head losses for “in line” manholes and providing new datasets for 45º manhole junctions, using a physical scale model under a range of high flow (i.e.surcharged conditions);
2. Evaluate the accuracy of existing computer modelling approaches for describing flows in urban drainage systems via comparison with a physical model and quantify the importance of identifying local head losses in computational models;
3. Assess the suitability of weir and orifice equations for representing the exchange of flow between major and minor systems during flood flows.
4. Determine appropriate energy loss coefficients for use within weir and orifice equations when representing flow exchange events.

3 METHODOLOGY

This chapter describes the equipment and methodology used to collect and process the data required to fulfil the aims and objectives described in chapter 2.

This physical modelling can be subdivided into two parts due to the different configurations that have been developed and used. The first configuration was constructed to meet research objectives 1 and 2, and comprised a sewer network scale model featuring six manholes which are connected to each other by five circular pipes of two different sizes. This configuration was operational from October 2010 to June 2012.

In order to meet research objectives 3 and 4 the second configuration was then constructed, this comprised a simplified physical model of the sewer network (one manhole, one pipe) linked to an overhead shallow flow flume, which represented an urban surface. This configuration was constructed from July 2012 to July 2013 and used from August 2013 until June 2014.

3.1 Scaling factors and similitudes

When working with a physical experimental model to investigate hydraulic mechanisms, scaling factors are used to define the geometrical ratio between the real system and the model. In order that the models faithfully reproduce hydraulic conditions in the real system, the flows must display a similitude to the real system. In a physical model, the flow conditions are said to be similar to those in the prototype if the model displays similarity of form (*geometric similarity*), similarity of motion (*kinematic similarity*) and similarity of forces (*dynamic similarity*) (Chanson, 1999). Similarity of these aspects can be determined by a dimensional analysis.

When completing a dimensional analysis for physical models a range of fundamental parameters need to be considered:

- Fluid properties (such as density of water, kg/m^3 – dynamic viscosity of water, Ns/m^2);
- Channel or flow geometry (characteristics lengths are requested);
- Flow properties (such as velocity, m/s).

Considering all these parameters it is possible to complete a dimensional analysis:

$F_1\ (\rho, \mu, , \sigma, E_b, g, L, V, \Delta P)$

If mass (M), length (L) and time (T) are chosen as fundamental units, then the Buckingham Π-theorem (Buckingham 1915) implies that the quantities can be grouped into five (5=8-3) independent dimensionless parameters.

$$F_1\left(\frac{V}{\sqrt{gL}};\ \frac{\rho V^2}{\Delta P};\ \frac{\rho VL}{\mu};\ \frac{V}{\sqrt{\frac{\sigma}{\rho L}}};\ \frac{V}{\sqrt{\frac{E_b}{\rho}}}\right)$$

$$F_2\ (F_r, E_u, R_e, W_e, M_a)$$

- F_r number (Froude number) characterizes the ratio of the inertial force to gravity force;
- E_u number (Euler number) shows the proportion of the ration of inertial force to pressure force;
- R_e number (Reynolds number) characterizes the ratio of inertial force to viscous force;
- W_e number (Weber number) is proportional to the ratio of the inertial force to capillarity force;
- M_a number (Sarrau-Mach number) characterizes the ratio of inertial force to elasticity force.

When reproducing scaled flows in physical models of urban drainage systems two similitudes are often used: the Reynolds No. (i.e. ratio between inertial/viscous forces) or the Froude No. (i.e. ratio between inertial/gravitational forces). The similitude number should be identical in the physical model and at full scale if the hydraulic phenomena are to be replicated accurately. Reynolds No. is given by:

$$Re = \frac{V \times D_h \times \rho}{\mu} \qquad \text{Equation 39}$$

Where:

$\boldsymbol{V}$ = average water velocity (m/s)

$\boldsymbol{\rho}$ = water density (= 1000 kg/m^3)

$\boldsymbol{\mu}$ = dynamic viscosity (= 10^{-3} kg/sm)

$\mathbf{D_h}$ = equivalent diameter (= $4R_h$, m)

And hence Reynolds similitude is satisfied when:

$$Re_o = Re_m \quad \text{Equation 40}$$

Where:

Re_m = Reynolds number of the physical model

Re_o = Reynolds number of the real system

By applying this similitude the Reynolds Law Ratio of velocity, discharge and time can be derived as follows:

$$\lambda_{Re,v} = \frac{1}{\lambda_l} \quad \text{Equation 41}$$

$$\lambda_{Re,Q} = \lambda_v * \lambda_l^2 = \frac{1}{\lambda_l} * \lambda_l^2 = \lambda_l \quad \text{Equation 42}$$

$$\lambda_{Re,t} = \lambda_l/\lambda_v = \lambda_l^2 \quad \text{Equation 43}$$

If gravitational forces are prevailing (because for example tests are completed in partially filled pipes), the Froude no. becomes the dominant scale. Froude similitude is satisfied when:

$$Fr_0 = Fr_m = \frac{V_o}{\sqrt{g*y_0}} = \frac{V_m}{\sqrt{g*y_m}} \quad \text{Equation 44}$$

If λ_l is the length scale, the corresponding velocity, the volume-flow, time ratios can be established, using equations 45, 46, 47:

$$\lambda_{Fr,v} = \frac{V_o}{V_m} = \sqrt{\frac{y_o}{y_m}} = \lambda_l^{1/2} \quad \text{Equation 45}$$

$$\lambda_{Fr,Q} = \lambda_v * \lambda_l^2 = \lambda_l^{5/2} \quad \text{Equation 46}$$

$$\lambda_{Fr,t} = \lambda_l/\lambda_v = \lambda_l^{1/2} \quad \text{Equation 47}$$

3.2 Experimental facility (configuration 1)

Prior to the commencement of the PhD project, a physical model of an urban drainage was constructed by Darren Unwin (PhD Thesis, 2008 - *Development of control algorithms: to describe flow discharge reduction and energy loss at a manhole junction*). This model was made available for this project.

The model was constructed to represent an equivalent 'real system' at 1/6 geometrical scale. The model consisted of:

- Header tank of dimensions 6 m (L) 2.4 m (W) 1.2 m (H);
- 75 mm (internal) diameter pipework for the main model sections (figure 23a) (simulating a 450 mm pipe at full scale);
- 100 mm (internal) diameter pipework for the model outlets (simulating a 600 mm pipe at full scale);
- 240 mm (internal) diameter pipe utilised as the manhole structures (figure 23b) (simulating a 1440 mm manhole at full scale).

In addition the laboratory prototype was permanently fitted with the following instrumentation:

- Electro-magnetic (MAG) flow meters (x 3 in the inlet, 2 in the outlet) of 75 mm internal diameter;
- Flow control valves (x 3) of 75 mm internal diameter, butterfly operation fitted downstream of the flow meters;
- Pressure (vertical) sensors, Gems series 5000 (x 21 on the below ground system, x 6 on the urban surface), 1 on each upstream of the manhole structure, 1 below each manhole and 1 just downstream from each manhole.

Figure 23 - Examples of scaled pipes on the left (a) and junction manhole on the right (b).

The pipes and manholes were constructed from acrylic due to its ease of workability (i.e. for when retro-fitting of instrumentation fixtures may be necessary) and its

transparent properties (beneficial when visualising experimental testing). The manhole was circular in cross section with an internal diameter of 240 mm and a height of 500 mm.

A scheme diagram of the physical model is presented in figure 24:

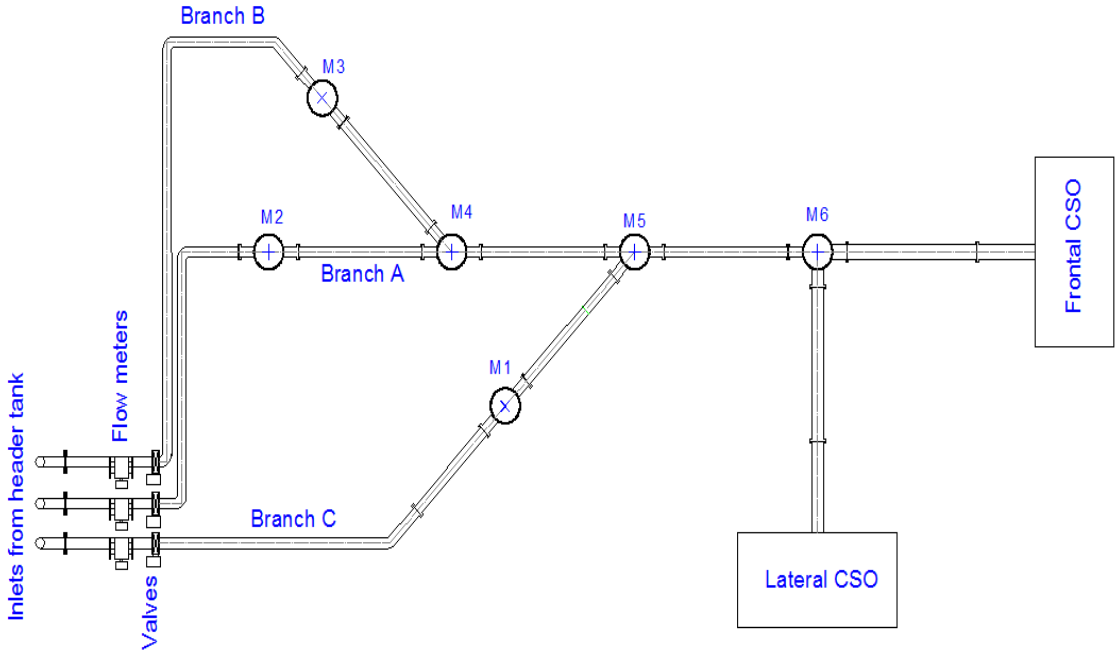

Figure 24 - Scheme of system inherited from D. Unwin with manhole labels (M_x).

The subsequent pictures elucidate details of the below ground sewer system. Figure 25 displays the first manhole of the central pipe (M2). Every manhole located along the system was situated on a wooden support fixed to the main structure.

Figure 25 - Main pipe (branch A) First manhole (downstream view)

Figure 26 shows the junction between branch A and the pipe joining from the right with an angle of 45°, (branch C).

Figure 26 - Main pipe (branch A) Third manhole (downstream view)

Figures 27 display a view of branch C and Figure 28 the overview of the facility.

Figure 27 - Branch "C" (upstream view)

Figure 28 - Birdseye view of the whole system prior the construction of the urban surface (from "upstream").

In the original, inherited model the water re-circulation system was composed of two tanks which received the flow from the outlets of the pipe system (Figure 29, Figure 30). A pump (Figure 31, left and right) was used to send the water into three inlet tanks (Figure 32) which fed each inlet pipe separately.

Figure 29 – Tank receiving outlet's flow and combined sewer overflow.

Figure 30 – Downstream view of the two re-circulating water tanks underneath the pipe system.

Figure 31 – Particular detail of the pump (left) used to fill the three feeding tanks (right).

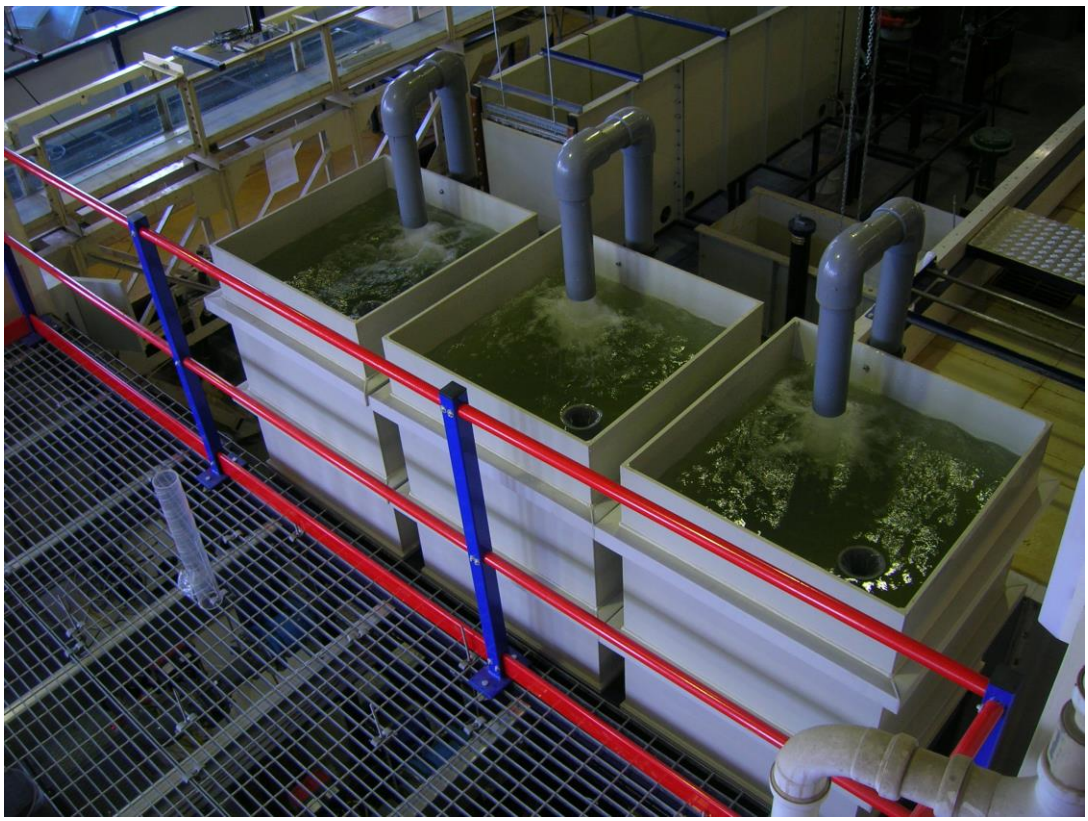

Figure 32 – Particular detail of the three tanks being filled with water.

On initial testing of the system, it was found that the maximum Reynolds number achievable was $3*10^4$ (and only for a short period of time due to the lack of recirculation), i.e. it was not possible to achieve turbulent conditions inside the pipes. In order to obtain results scalable to full systems and meet research objectives 1 and 2 it was therefore necessary to redesign the inlet system such that higher flow rates could be achieved. Due to practical considerations it was decided that the most straightforward option to achieve this was to connect the system directly to the main laboratory header tank (Figure 33 and Figure 34). The tank sits 3.30 m above the physical model hence can provide a constant head sufficient to achieve much higher flows.

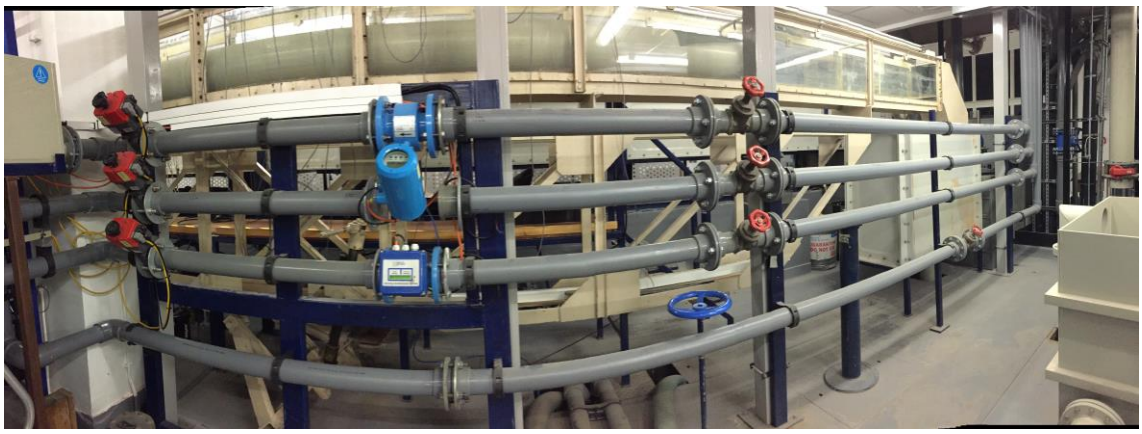

Figure 33 – Full view of the new inlet system.

Figure 34– Connection between header tank and the three inlet pipes plus the inlet of the urban surface.

It was evaluated that (after modifying the inlet conditions) this experimental setup would be sufficient to meet research objectives 1 and 2. Hence phase 1 of this research has been utilized to provide additional datasets by using this unique physical model (3 pipes and 6 manholes included). To achieve this, a set of steady conditions from 0 to a maximum of 8 l/s (maximum capacity) has been run through the system. By using these hydraulic characteristics, it has been possible to investigate hydraulic behaviours with a range of 9000-140000 Reynolds Number and velocities between 0.11-1.85 m/s.

3.3 Facility testing phase 2

To meet objectives 3 and 4, the experimental system required significant modification such that pluvial flooding conditions could be replicated, and both surface/sewer interaction and hydraulic head in sewer and surface systems could be quantified over a range of flow conditions. The second part of the research required the construction of a linked urban surface (slope 1:1000) above the pipe network. The urban surface is 8.2 m long, 4 m wide and has side walls of 0.015 m height. The below ground pipe network was significantly simplified so that the surface is connected to the below system through a single manhole, located on the central pipe.

The decision to utilise only a single manhole has been made for the following reasons:

- The aim was to investigate the flow interactions between an urban surface and the sewer network. Considering the complexity of the phenomena, it has been necessary to select only a single manhole because by selecting more than one, would have been more difficult to quantify to exact flow exchange.
- After preliminary tests, results have shown that this manhole exceeds its capacity at the lowest flow rate due to its position. Therefore, this manhole will be able to simulate more extreme flooding than others.

The entire urban surface was constructed in PVC. This material has been selected for the following reasons:

- This material is easy to cut and modify, considering the limited working space in the water lab;
- Its pale colour is suitable for the implementation of a PIV system expected to be used in future research.

Prior to the construction of the flume bed (i.e. the urban surface), the metallic support system was surveyed and adjusted such that the new surface facility would have a regular sloping surface. To do this, the metallic grid was divided into 28 points on a 1 m x 1 m and 4 points on a 1 m x 0.3 m grid. The level of each point on the grid was identified using an optical theodolite. The theodolite was fixed on top of a tripod downstream of the model and maintained in a constant position. The levels of each point above the given datum are presented in figure 35:

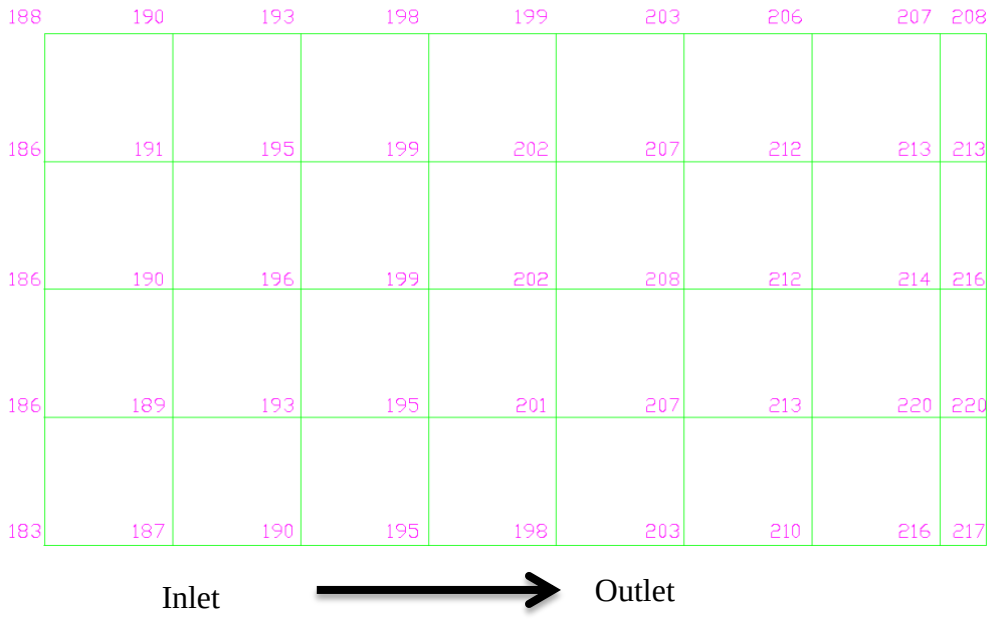

Figure 35 – Initial elevation above datum (in mm) of the system divided in a grid 1 m x 1 m

The maximum range between inlet and outlet was originally 37 mm, with considerable variation in the lateral dimension. To rectify the grid system in order to obtain the correct slope for the overlaying flume bed, thin metallic washers were added to the metallic structure in appropriate points. After modification and further verification, a shallow flow flume was constructed over the top of the metallic grid, with additional pressure transducers located around the manhole (Figure 37 and Figure 38).

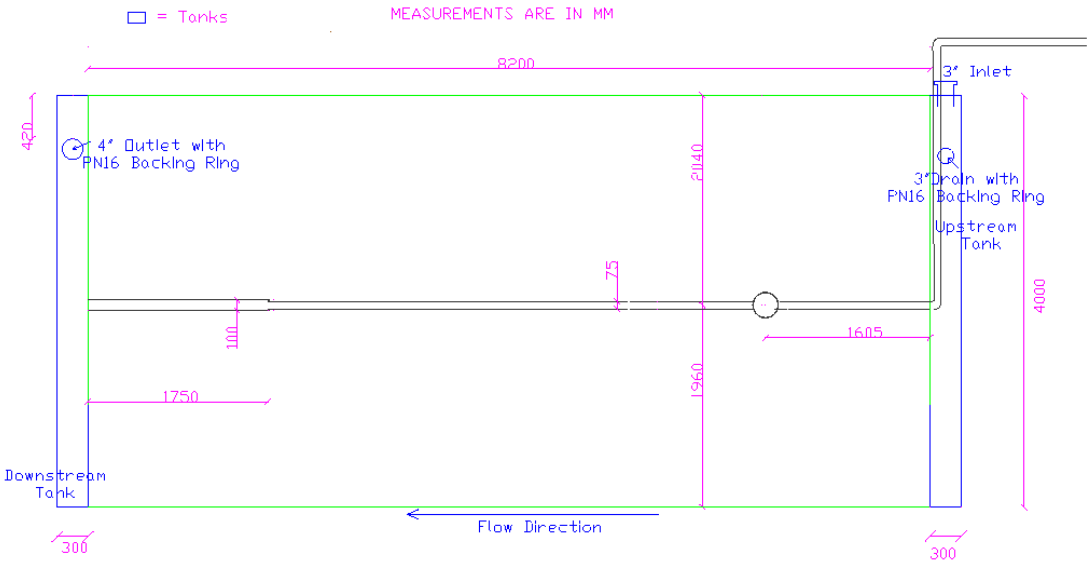

Figure 36 – Plan view of the urban surface.

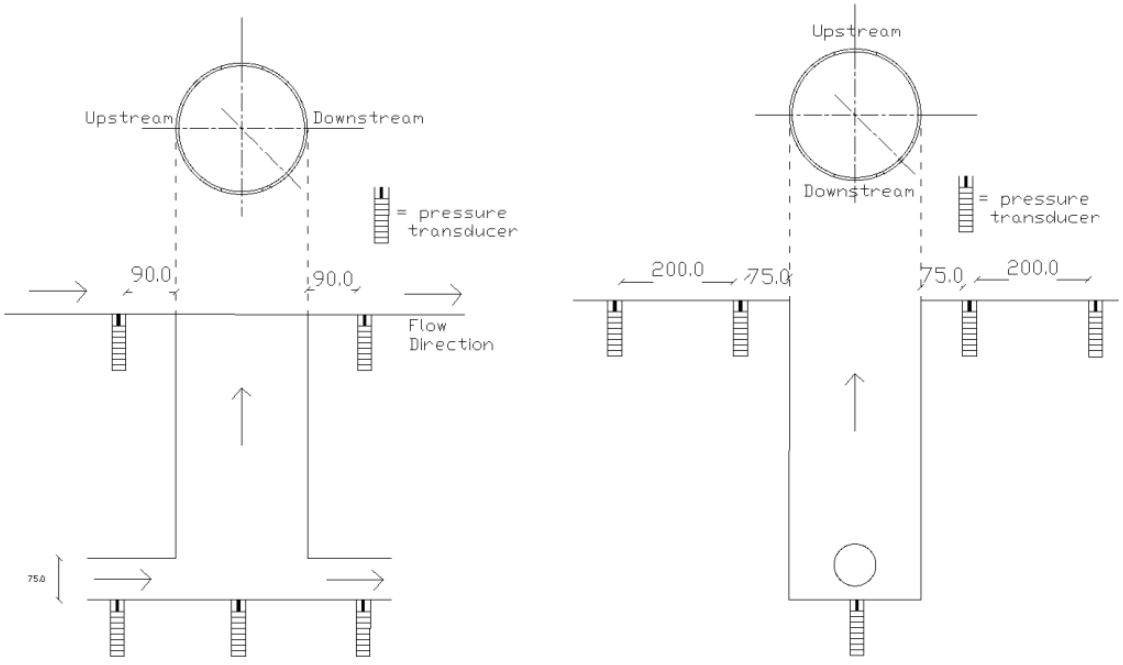

Figure 37 –Location of the pressure measurement points (distances in mm) on the urban surface around the manhole.

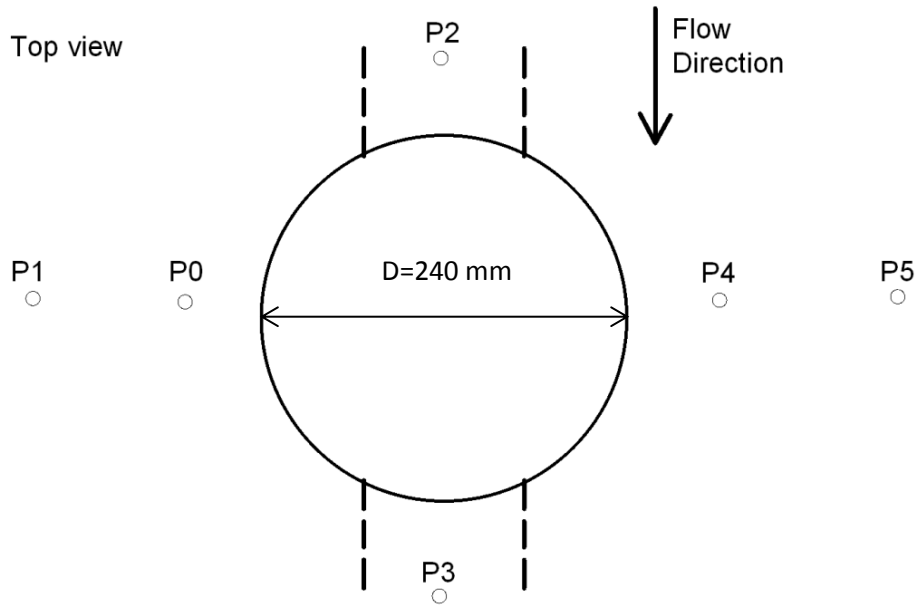

Figure 38 –Plan view of the pressure measurement points (P_x) on the urban surface around the manhole.

Inlet and outlet tanks were constructed upstream and downstream of the urban surface model (Figure 36).

The inlet tank (dimensions L= 4 m, W= 0.3 m, H= 0.35 m) receives water from a 75 mm pipe connected to the main laboratory header tank.

Inflow rates are controlled by an in line valve (on the inflow pipe) which can be regulated both manually and by the command of LabVIEW software (section 3.4). In addition, the pipe is fitted with a mag flow meter connected to LABVIEW (section 3.4) such that inflow rates can be monitored in real time.

Inflow and outflow weirs were also constructed to ensure a regular inflow and outflow over the entire width of the model. The downstream (outlet) weir is manually adjustable to allow a greater degree of control of flow depth on the model urban surface. The inlet tank has been filled with baffle material so that flow disturbances around the inflow pipe do not caused uneven flow over the inflow weir (Figure 39). The inlet tank also contains a 75 mm internal diameter drain for emergency in case of a failure of the system (e.g. electrical blackout during the simulation, inability to close the valves with LabVIEW software).

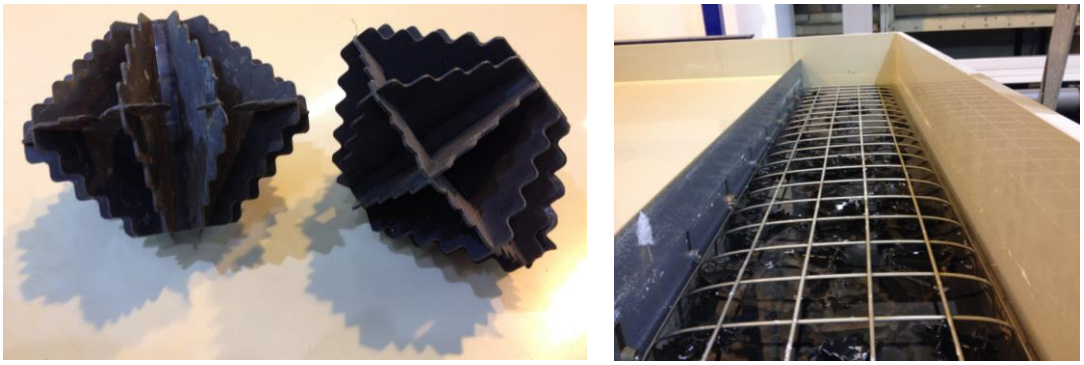

Figure 39 –Material inserted in the inlet tank (Left). Inlet Weir (Right).

The outlet tank has the same dimensions of the inlet (L= 4 m, W= 0.3 m, H= 0.35 m). Flows are discharged via a 100 mm pipe that returns flow to the laboratory sump. This pipe is also fitted with a magflow meter as described above.

Figure 40 illustrates the longitudinal profile of the model including the urban surface (which is illustrated in figure 41):

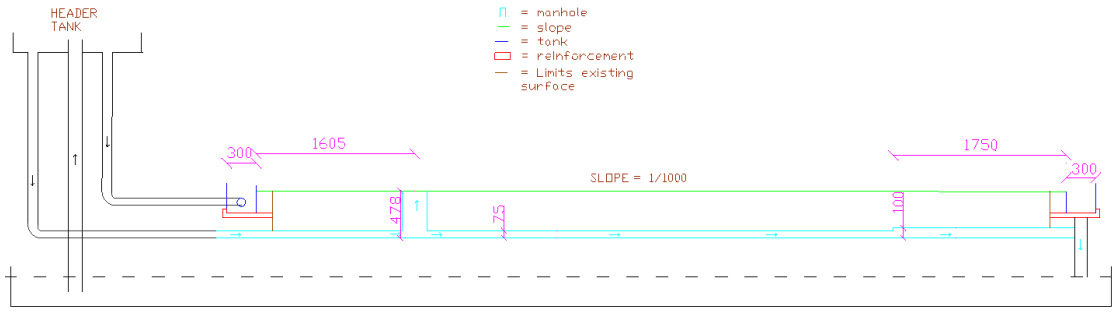

Figure 40 – Longitudinal profile of the physical model used in phase 2.

For Phase 2 simulations the flow was configured to run on both the surface and in the pipes. The maximum flow rate for both surface and sewer systems is 11 l/s. By applying the principles previously described in section 3.1, this flow rate corresponds to ≈70 l/s in a real pipe system (by using the Reynolds Similitude, up to a max Reynolds Number of 190000) and ≈850 l/s in a urban surface (by using the Froude Similitude, with values of Fr always less than 1 to maintain subcritical flow).

Velocities on the linked urban surface were expected to be between 0.1-0.25 m/s corresponds to a real scale velocity field of 0.245-0.625 m/s. This is between the range that may be expected for a shallow water running over a shallow urban surface during a flood event, and is similar to the range used by (Djordjevic et al., (2013) for the physical modelling of gully performance during flood events (range of full scale velocities tested was 0.05-0.5 m/s).

Figure 41- Urban surface: on the left view from the upstream, on the right view from the downstream.

3.4 Managing and controlling the model (testing phase 1 and 2)

The physical model is instrumented to provide the following outputs which are directly collected by a LabVIEW interface:

- flow at each inlet to the model;
- flow at each outlet;
- water depth in the pipes at 27 locations;
- water level in each manhole;
- valves opening ratio.

LabVIEW software is used to control the valve openings and to acquire data in real time.

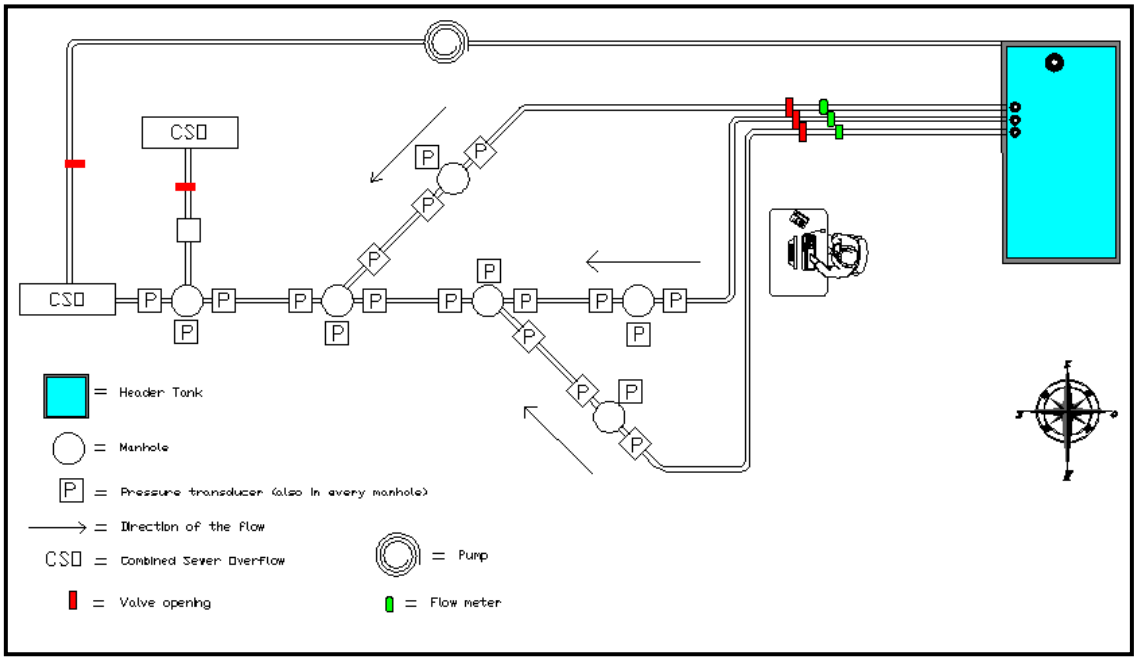

Figure 42 – Instrumentation scheme on the pipe network (phase 1 setup).

LabVIEW works through a double file: one called “Front Panel” where the controllers and indicators of the system can be checked and another one called “Block Diagram” where there is a scheme of the system that must be measured and controlled. This instrumentation can control the range of values in multiple formats (Ampere, Volts, and I/O Boolean). This is a fundamental step because all the output signals from the PAC (Programmable Automation Controllers) hardware are electrical (Boolean, current or voltage) and they must be converted into physical parameters such as water depth.

All the electrical outputs from the instrumentation can be checked through an IP address assigned to each series of data. The internet connection was also used to send input

signals to the hardware and subsequently to the model. In this way, simulations can also be conducted if the operator is not physically present by using internet connection to activate and deactivate all the system control and instrumentation devices.

The VI shown in figure 43 has been used to manage the rig tests. This software enables a good visualization of the data in real time, permitting visualization of the flow through the pipes as well as water depth in the manholes.

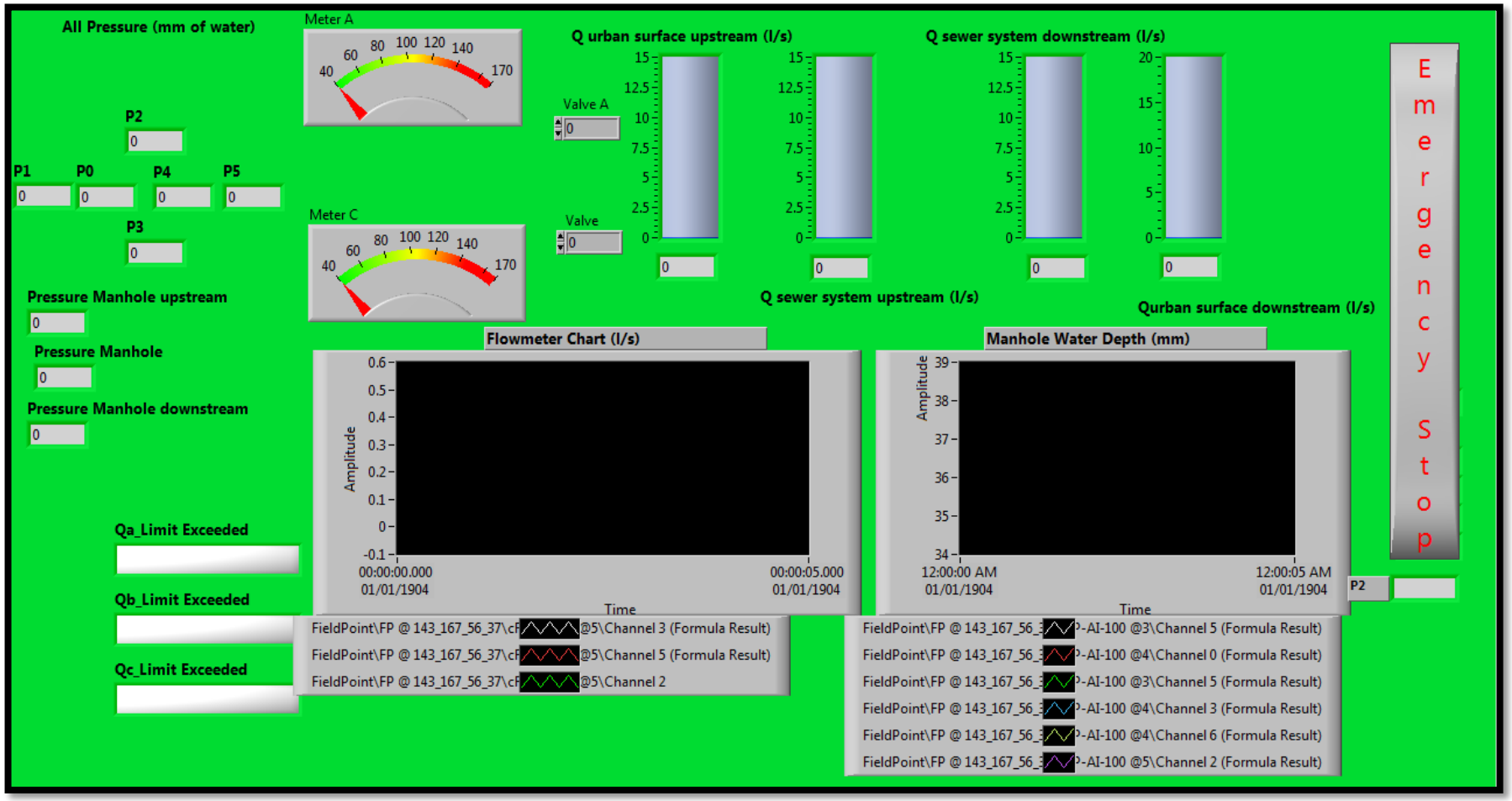

Figure 43– Front panel of the interface developed.

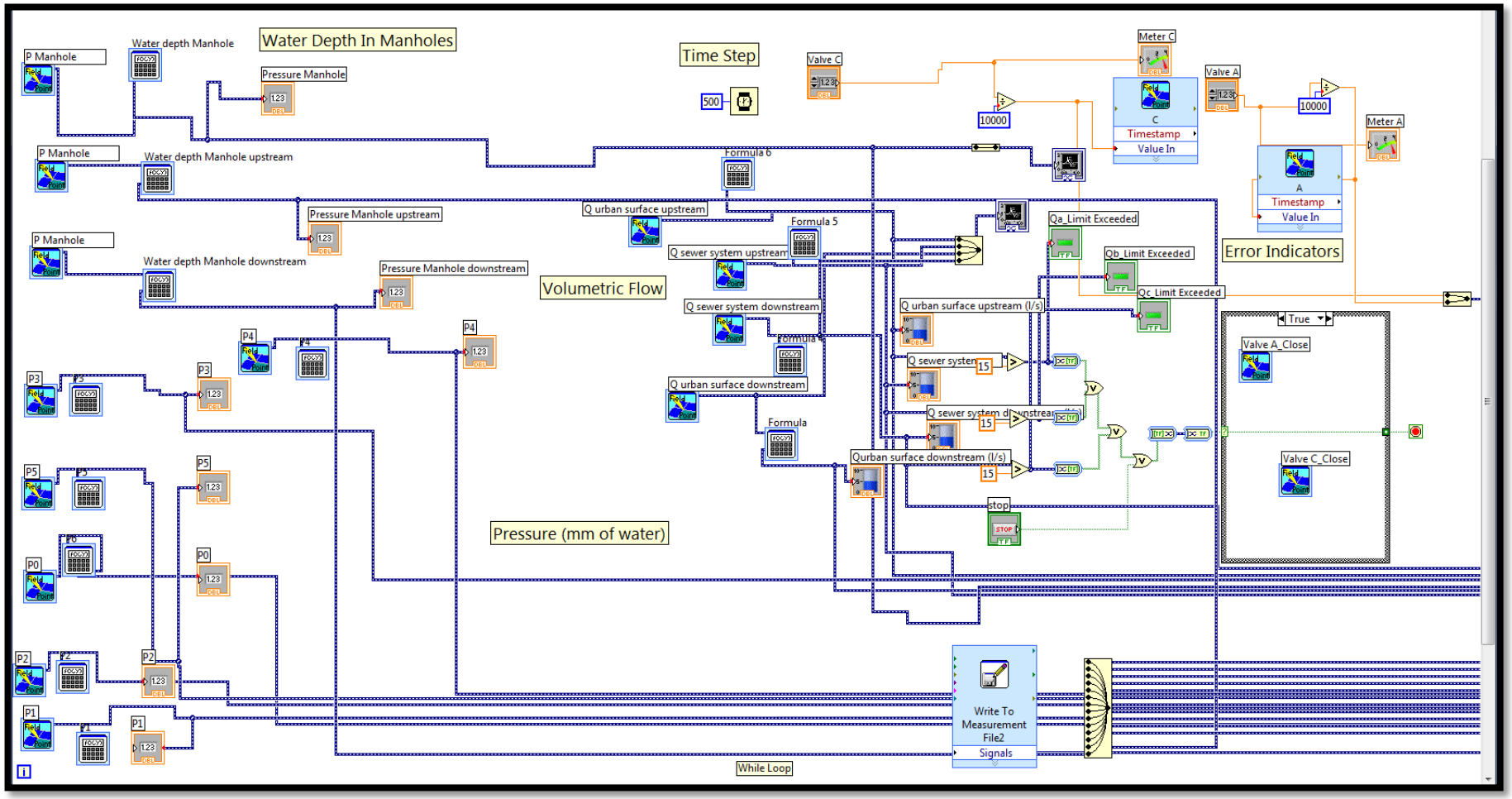

Figure 44- Block diagram of the interface developed.

3.5 Instrumentation

The aim of this section is to explain the instrumentation which has been used to collect the data and how they have been calibrated.

The instrumentation used for the collection of the data includes pressure transducers that are distributed all along the pipes system to measure the water level, flow meters and valve control systems. As previously mentioned, they are all connected to a hardware system that collects the inputs and transmits them to the operator laptop through LabVIEW software.

3.5.1 Valves

The valves selected for this research are of the butterfly operation (Figure 45). Butterfly valves are flow control devices that incorporate a rotational disk to control the flowing media. The disk is rotated to different angles to allow different flow rates through the valve. Even if the disk is always in the passageway, being relatively thin, it offers little resistance to flow. This kind of valve operates with live electricity and is quick and easy to connect. It works with a 4-20 mA range. It can be set manually or automatically turning the specific actuator. The valves are fitted with the Digital Positioning System (DPS). The main advantages are that the system is retro-fittable to the standard on-off actuator, it is self-calibrating, providing an output as signal as standard. There is an internal microprocessor on the DPS circuit board that continuously monitors digitally the analogue input and output signals and compares them to the physical position via an output shaft feedback system, moving the actuator as required to balance the signals. Digital control ensures high sensitivity and receptivity, with all the usual positioner characteristics coming in at under 1% (hysteresis, linearity and precision).

Figure 45 – Valve and DPS.

3.5.2 Flow meters

The flow meters utilised for this research are MagFlow type devices (Figure 46), supplied by Arkon Flow System (UK). The magnetic flow meter, which technically is an *electromagnetic flow meter*, is generally called a *mag meter*.

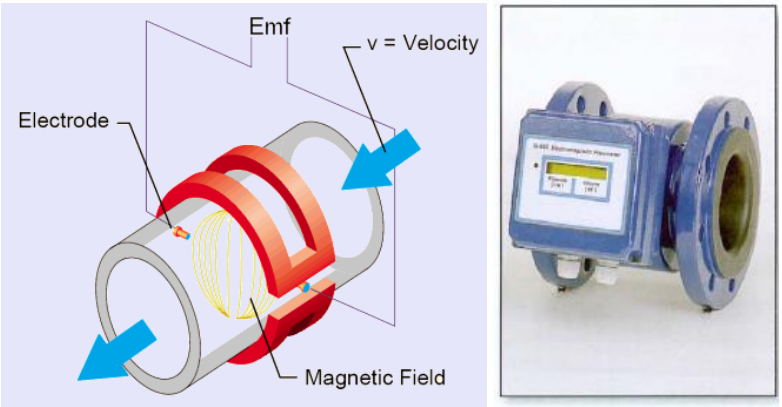

Figure 46- How an Electromagnetic Flow meter MAG 900 works and real example

This equipment is based on a specific physical principle: electromagnetic induction. In effect, a magnetic field is applied to the tube where the flow is measured and this generates a potential difference proportional to the flow velocity perpendicular to the streamlines of the discharge. This method has some key benefits such as wide range of measurement and potential for real time control while having a relatively simple installation procedure, low maintenance requirements and a stated accuracy ± 0.5% (the range of flow-rates tested for each pipe is 1-11 l/s, therefore this is equivalent to maximum error of ± 0.055 l/s at 11 l/s).

Mag flow-meters are often used to perform fluid in line discharge measurements for numerous reasons. The main advantage of this kind of equipment is the lack of moving parts and non-invasive nature; this decreases the risk of possible breakdowns and the frequency of repairs.

Despite these advantages, there are certain complications to consider. If the mag flow meter is located at a point which can be affected by irregular hydrodynamic effects, this can alter the normal flow pattern and consequently disturb the reading. Because of this it is imperative to install in accordance with manufactory instructions as well as calibrate the instruments in-situ. Manufactory instructions recommend the installation of the instrumentation not closer than 10 pipe diameters to a sharp bend or junction.

The flow-meters utilised in this research were 75mm internal diameter. Considering the limitation in terms of space available in the water laboratory, to design the downstream section for the re-circulation of the water a “T” connection has been necessarily utilized for the two downstream flow meters (Figure 47 – Figure 48).

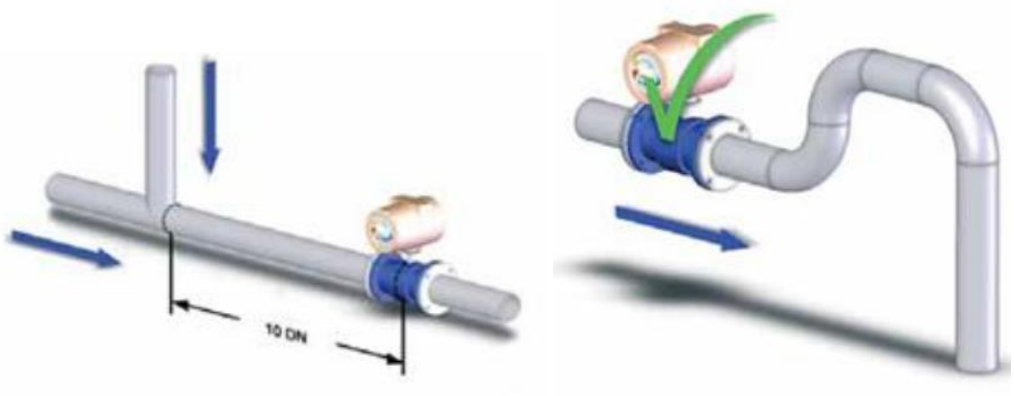

Figure 47 - Suggested location for Mag Flow Meters (MAG Flow Meter, Installation Manual, Ver.2001-1).

Figure 48 - “T” connection utilized for pipe downstream urban surface as well as sewer system.

3.5.3 Pressure transducers

The pressure transducers utilized for this research are the “Series 5000 GEMS sensors” (Figure 49). This kind of transducer converts fluid pressures into a proportional electrical signal.

Figure 49 – Pressure transducers GEMS

These pressure transducers require a specific periodic inspection of the cable and moulding because it is important to constantly guarantee that they do not suffer damage. Every day before each test, the pressure transducers were checked and cleaned with a small amount of water introduced gently with a syringe to avoid the deposit of any material from the previous tests which may cause erroneous results.

3.6 Calibration of Instrumentation

3.6.1 Pressure sensor calibration

Each pressure sensor and valve has been calibrated to determine the relationship between pressure and electrical output signal for each pressure sensor. The specified pressure range of the sensors is 0-70mb, and the specified electrical output ranges between 4-20mA. During calibration pressure is determined by measurement of water depth above the pressure sensor. For the pressure sensors used in phase 1, the calibration has been carried out within the pipe network facility using the following methodology (Figure 50):

- Set the valve opening and record in a spreadsheet the signal sent by the pressure sensor after a stabilization of 300 seconds for each valve opening.
- Record the water depth in the manhole for each valve opening after the stabilization.
- Plot the correlation between the sensor output Amperes and the measured water depth of the manhole (directly related to pressure).

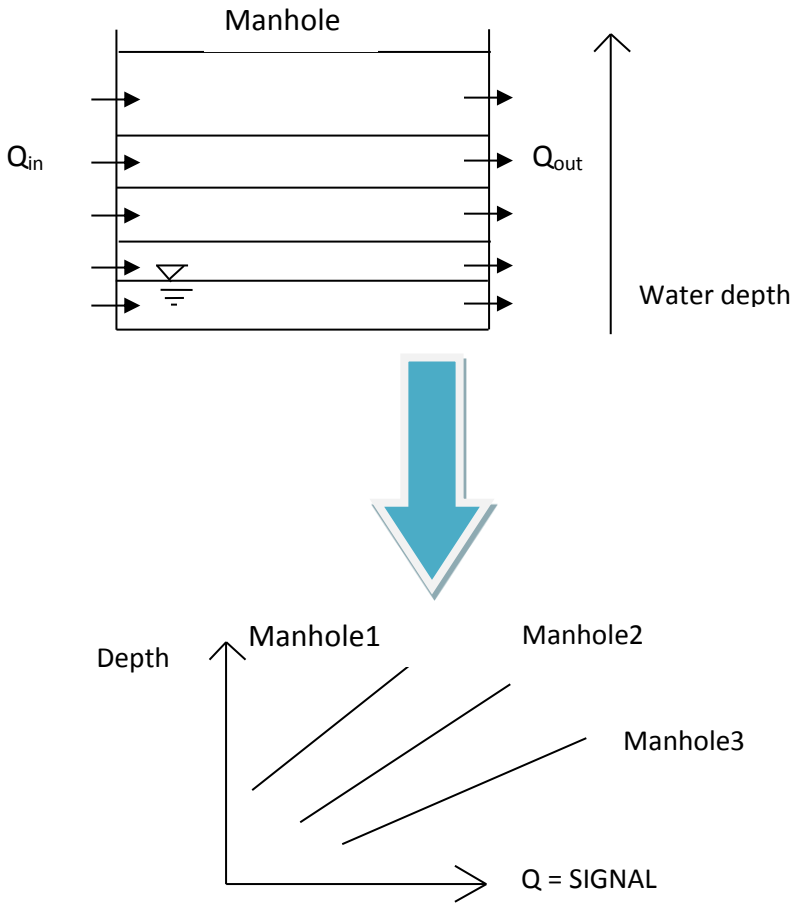

Figure 50 – Description of the process to find the relationship depth of water vs output in Ampere

Every transducer was calibrated and checked at the same time. To calibrate the pressure sensors used for the Phase 1 series of tests the range of water depth considered was 0-350 mm. All calibrations found were linear with a minimum R^2 of 0.999.

Once the calibration relationship was determined a VI interface in LabVIEW was written to convert the electrical output signal into a hydrostatic pressure reading.

Phase 2 has included the construction of the urban surface and during its assembly all the pressure sensors used in Phase 1 have been removed to avoid damage.

Once the surface had been built, nine new pressure sensors were selected to measure the pressure in the below (one located in the manhole, with one upstream and one downstream the manhole) and the surface system (placed around the manhole) and they were re-calibrated.

The six pressure sensors in the urban surface around the manhole were calibrated using innovative small equipment designed prior to the calibration, figure 51 (the water depth range considered was 0-100 mm).

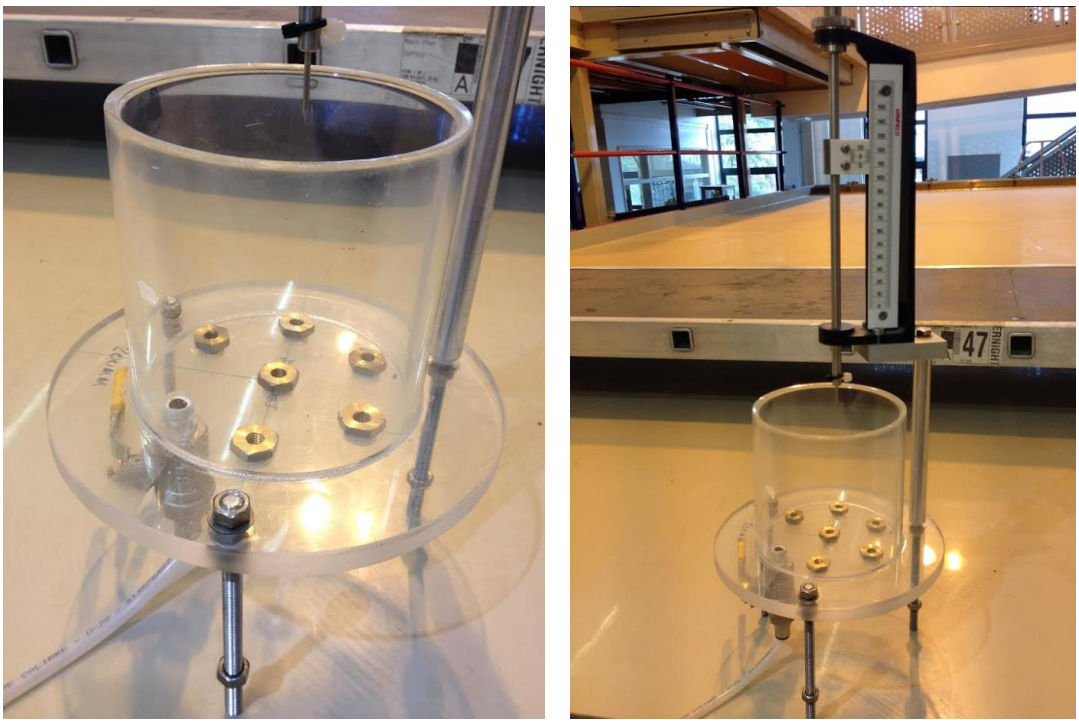

Figure 51 – Equipment for calibration of the pressure sensors for the urban surface.

Example calibration plots relating measured water depth to electrical output signal are displayed in fig. 52, 53, 54 conducted for sensors installed upstream, within and downstream of the interaction manhole (*P Manhole Upstream*, *P Manhole* and P *M Downstream*). For sensors P0, P1, P2, P3, P4, P5, R^2 for each linear calibration relationship was =>0.999 in all cases.

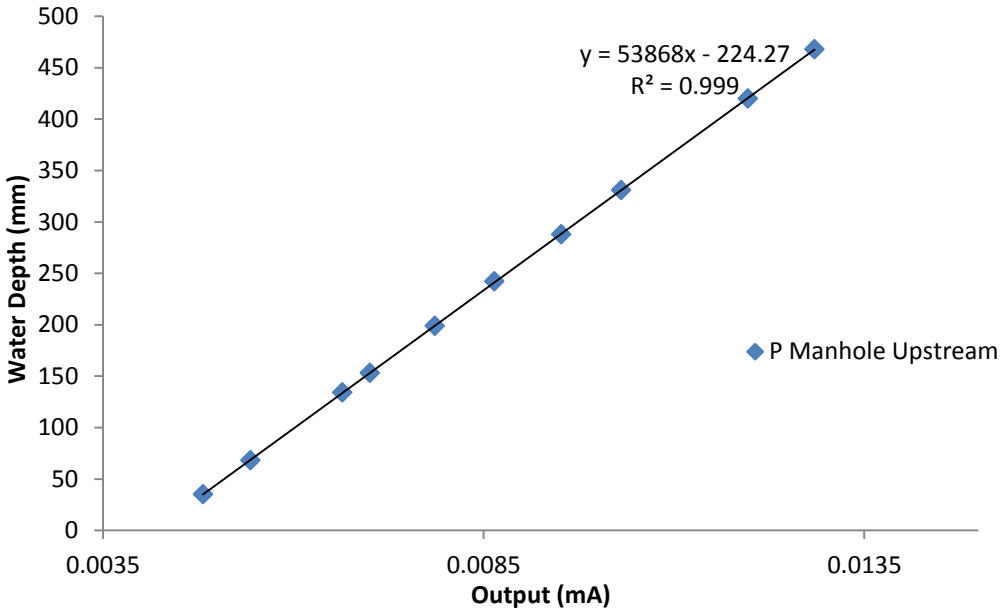

Figure 52 - Calibration pressure sensor P M Up vs water depth (P Manhole Upstream).

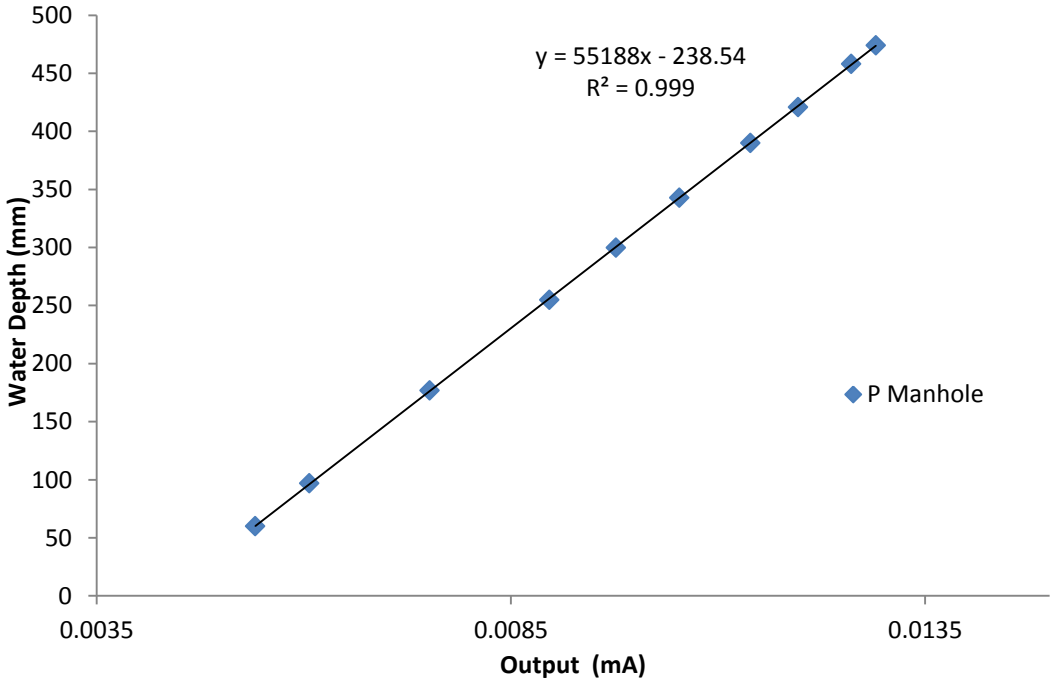

Figure 53 - Calibration pressure sensor P Manhole vs water depth (P Manhole).

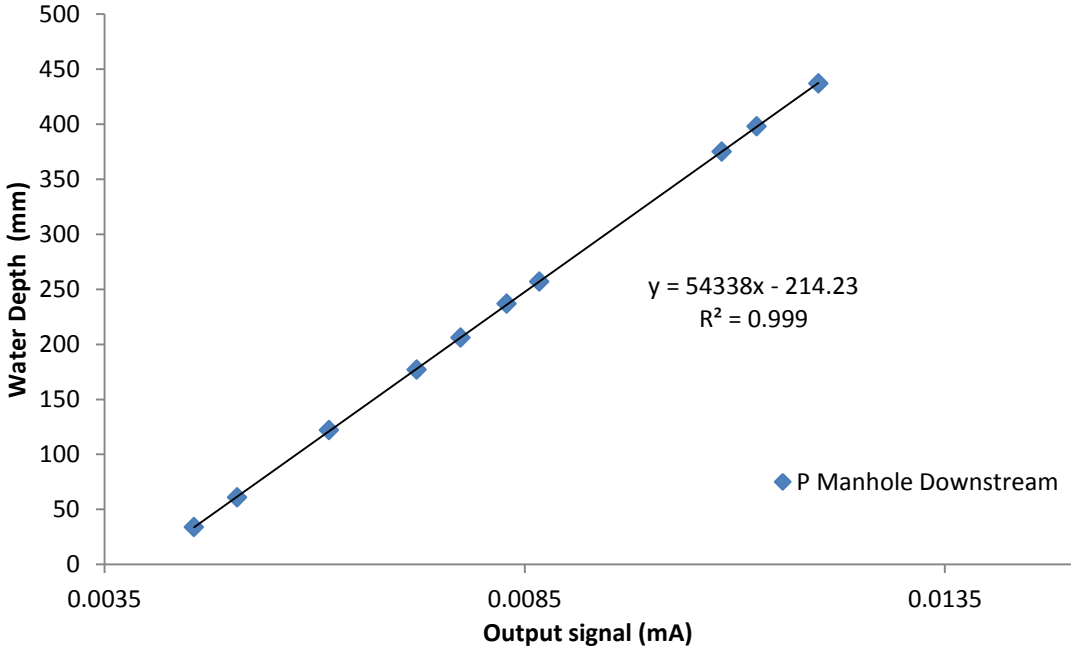

Figure 54 - Calibration of pressure sensor P M Down vs water depth (P Manhole Downstream).

3.6.2 Valve calibration

The purpose of the valve calibration is to determine the relationship between the valve input (mA) set by the operator (which directly controls the valve opening) and the flow rate (l/s) into the system as recorded by the flow meters.

Once this relationship is determined, it is possible to control the flow rate independently via the LABVIEW system and to stipulate time varying flow rates by assigning an opening ratio vs time relationship to the valves using a simple VI in LabVIEW. The methodology for calibration is:

1. Set the valve opening until a flow in the pipe is detected
2. Let the flow stabilize for 5 minutes
3. For the following 5 minutes read the flow rate (m^3/hr) from the flow-meter every 5 seconds and record at the same time the input and output signal of the flow meter (Amps) in a spreadsheet file.
4. Then increase the valve opening signal by 0.1 mA and repeat steps 2 and 3.
5. At the end of the simulation time average the recorded data to obtain a unique value of flow rate (l/s) and input and output signals (Amps) for each valve opening.
6. Plot the correlation between the valve opening (mA) and average flow rate recorded (l/s) and also between the average output signal from the flow meter (Amperes) and average flow rate recorded (l/s).

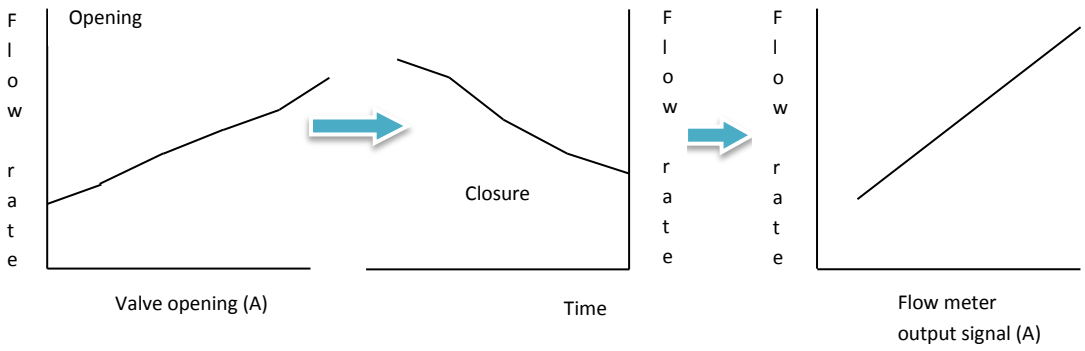

Figure 55 – Process for the calibration of the flow with the opening and the closure of the valves and the final interpolation of the data.

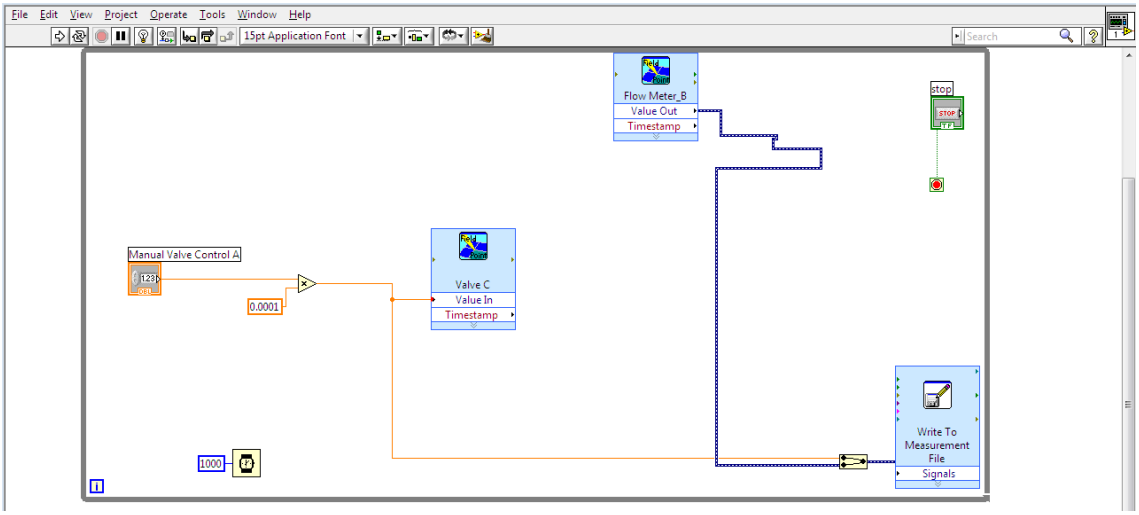

Figure 56 – VI interface designed to calibrate each flow meter.

Figure 57 – Figure 58 display the relationship between the flow rate and the valve electrical outputs. Figure 57 displays the relationship for the original flow meters, while Figure 58 displays the relationship for the additional flowmeters purchased for the Phase 2 experimental setup.

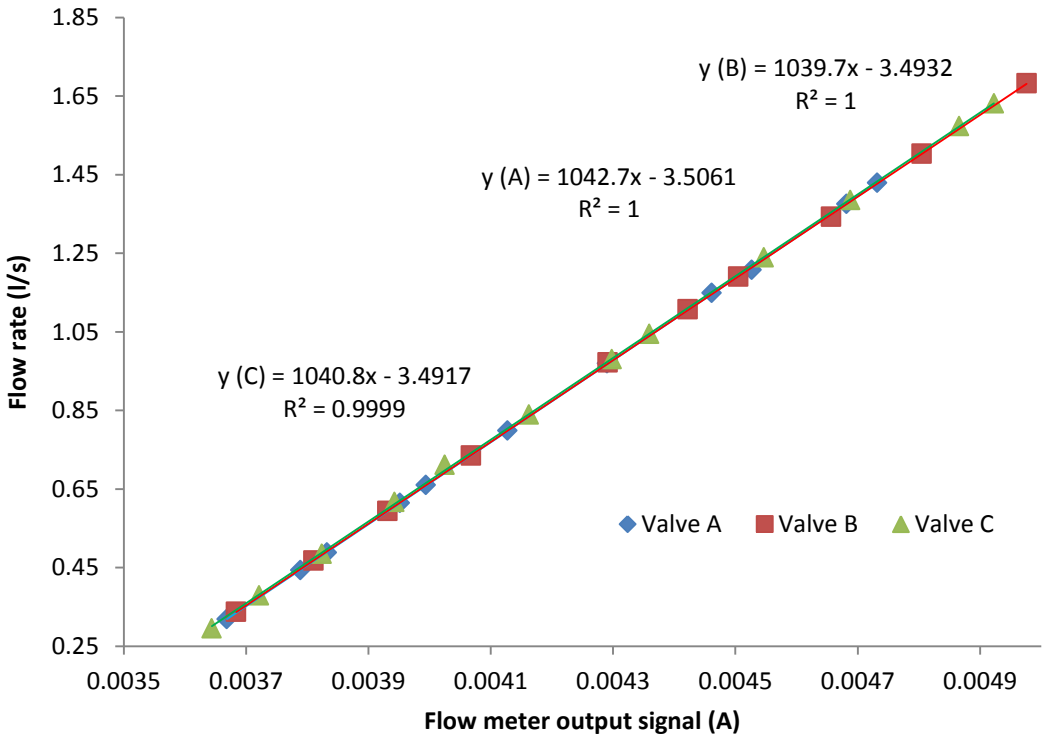

Figure 57 – Interpolation between valve opening and flow rate for valve A, B, C.

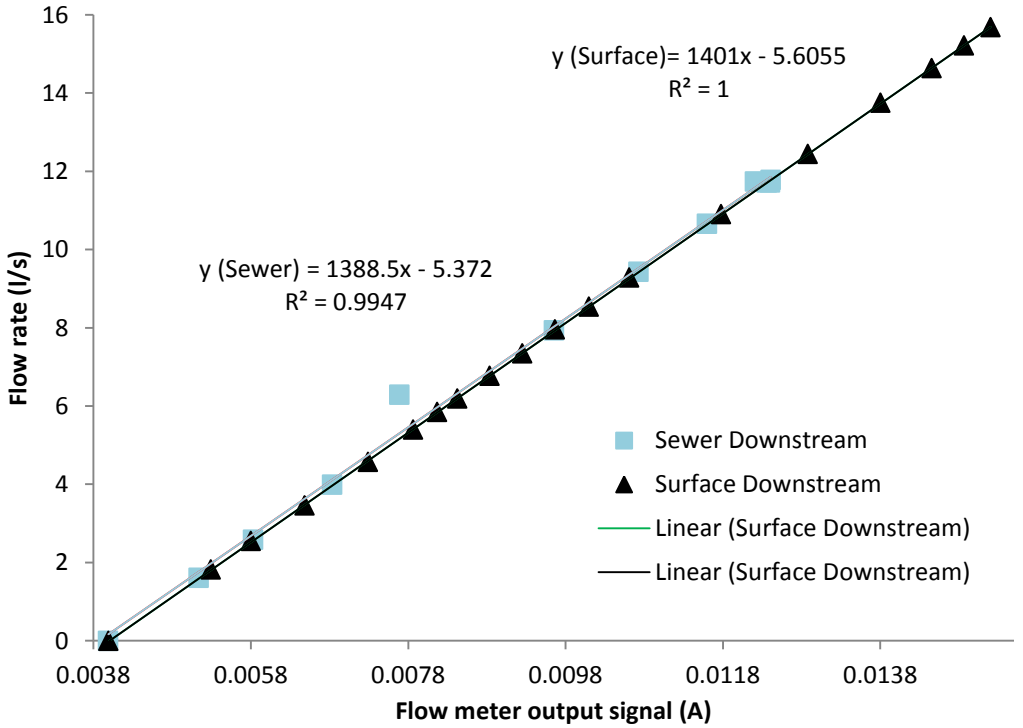

Figure 58 – Interpolation between valve opening and sewer and surface downstream valid for phase 2.

Figure 59 displays the calibration relationship between the observed flow rate and the valve opening input signal for A, B and C.

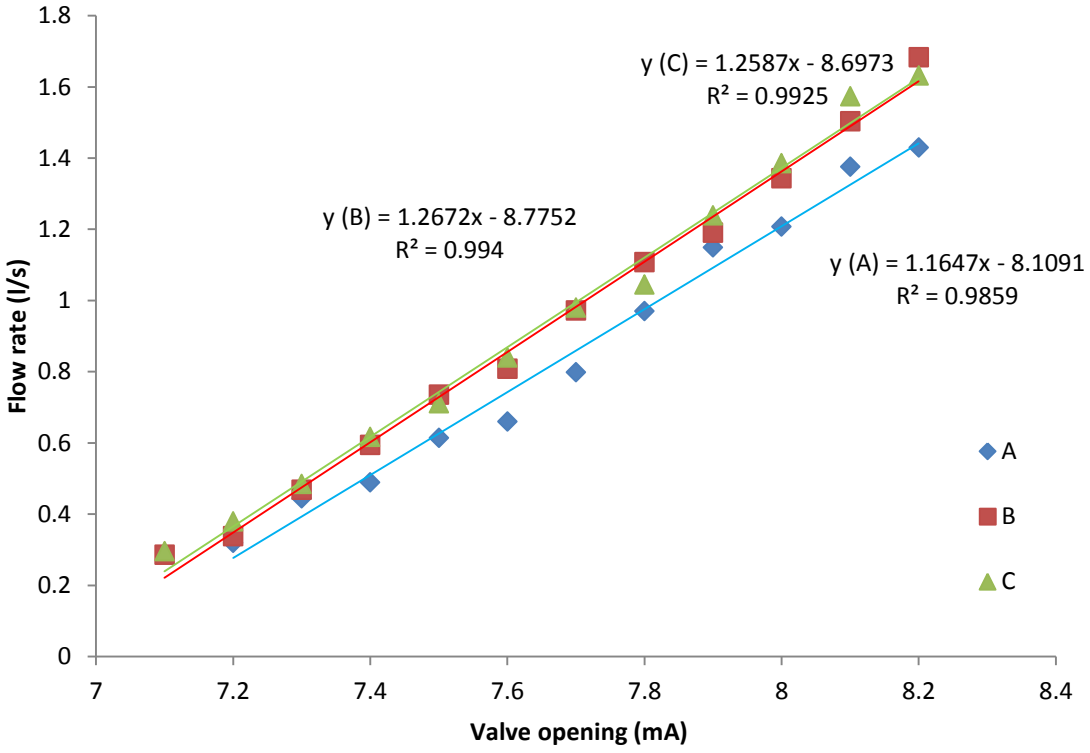

Figure 59 – Valve Opening vs Flow rate for A, B and C.

Once the calibration of the input electrical signals was complete, a verification set of tests have been conducted to compare the flow rate measured by the values against the values provided by the laboratory measurement tank.

These confirmation tests were only conducted during the phase two tests. Two tests were conducted; one using the 'sewer' inflow and outflow meters, and one using the 'surface' inflow and outflow meters (Figure 60 – Figure 61).

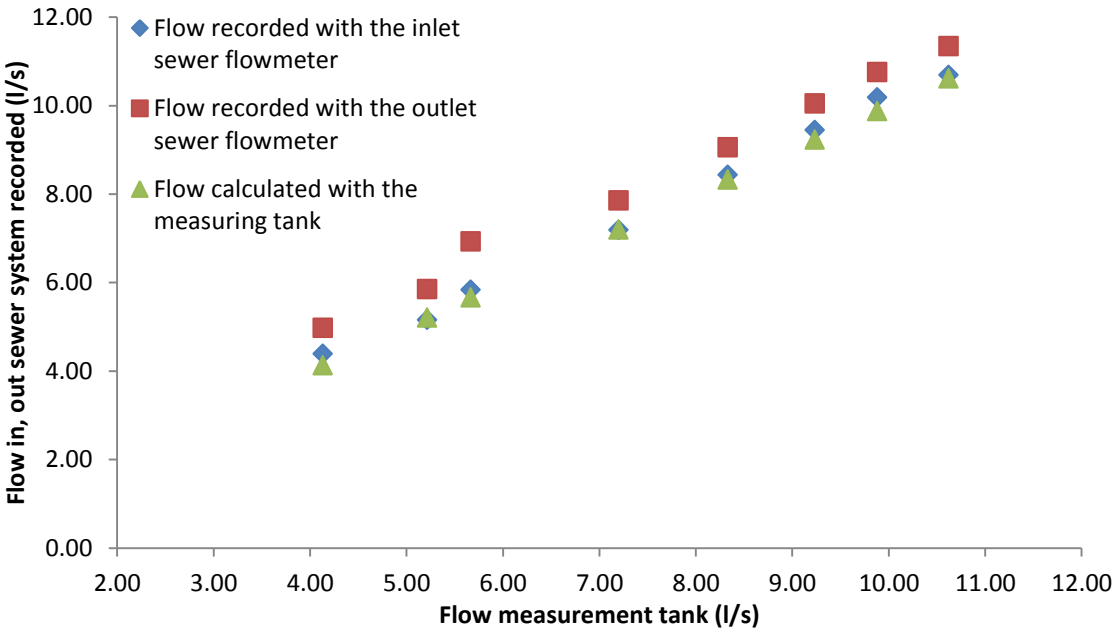

Figure 60 – Calibration tests sewer flow meters vs measurement tank prior to correction factor

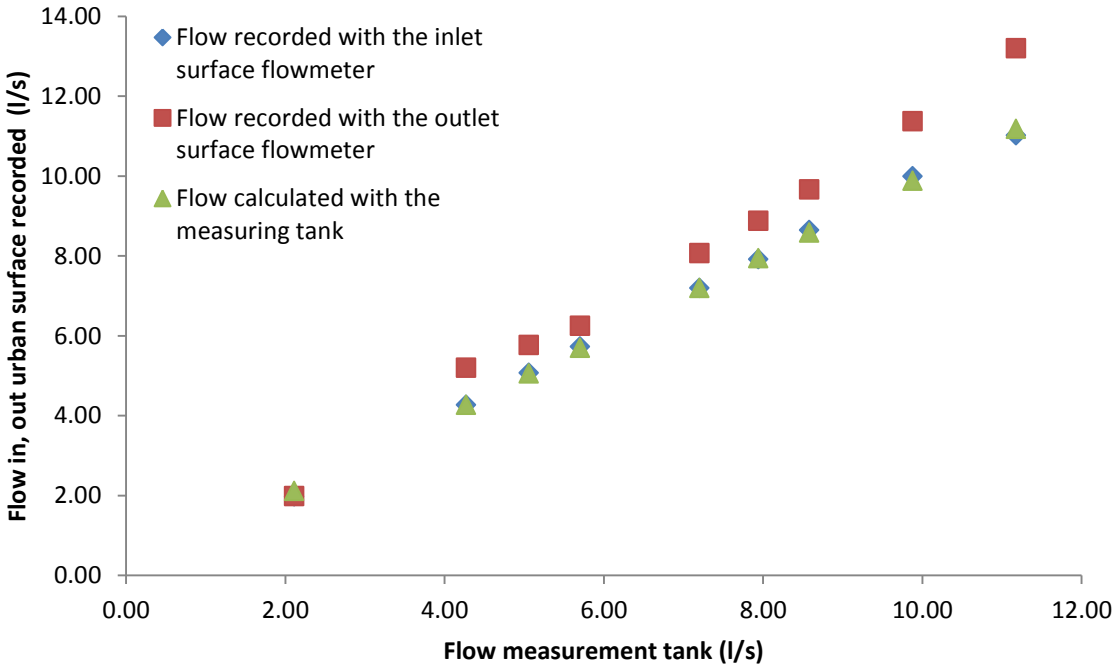

Figure 61 - Calibration tests surface flow meters prior to correction factor.

Inflow meters for both surface and sewer pipes gave accurate readings for all flow conditions (within ±1.75 % for the sewer and within ±0.5 % for the surface). The maximum sewer inflow pipe error over all tests conducted is 0.19 l/s.

By applying the criteria of full pressurized flow and the Reynolds similitude this value corresponds to 1.15 l/s error in a real scale system (assuming full pipe diameter equal to 450 mm). The maximum surface inflow error over all tests conducted is 0.055 l/s. By applying the similitude of Froude for the free surface flow on the urban surface, this value corresponds 4.85 l/s in a real scale system.

As can be seen in figure 60 and figure 61, the outflow meters for both surface and sewer pipes exhibited a fairly constant error over all flow rates. In order to account for these errors a correction factor has been identified for the downstream valves.

The correction factor C_f was calculated by $\frac{Qout\ (sewer\ or\ surface)}{Qtank}$. For surface downstream and sewer outlet the average correction factor ($\overline{C_f}$) calculated were 1.122 for the sewer outlet and 1.121 for the surface outlet flowmeter. Flows have then been re-calculated taking this into account (tables 6 and 7).

Table 6. List of flows related to sewer flow-outlet meters measured before and after the $\overline{C_f}$ vs flow measuring tank.

Recorded flow in outlet pipe out (l/s)	Flow from measurement tank (l/s)	C_f	Outlet flow after $\overline{C_f}$ (l/s)
4.98	4.13	1.206	4.45
5.86	5.21	1.124	5.23
6.93	5.66	1.224	6.19
7.86	7.20	1.092	7.02
9.06	8.33	1.088	8.09
10.05	9.23	1.089	8.97
10.76	9.88	1.089	9.61
11.35	10.62	1.069	10.13

The maximum observed error after application of the correction factor is 0.52 l/s. By applying the criteria of full pressurized flow and the Reynolds similitude this value corresponds to 1.15 l/s error in a real scale system (assuming full pipe diameter equal to 450 mm).

Table 7. List of flows related to surface flow-outlet meters measured before and after the $\overline{C_f}$ vs flow measuring tank.

Flow out (l/s)	Flow tank (l/s)	C_f	Flow out after $\overline{C_f}$ (l/s)
1.99	2.11	0.942	1.77
5.20	4.27	1.218	4.64
5.77	5.06	1.140	5.14
6.25	5.70	1.096	5.57
8.07	7.20	1.121	7.20
8.88	7.94	1.119	7.92
9.67	8.58	1.127	8.62
11.37	9.88	1.151	10.14
13.20	11.18	1.181	11.76

The maximum observed error after application of the correction factor is 0.58 l/s. By applying Froude similitude this value corresponds to 51.15 l/s error in a real scale system.

The significance of these errors in relation to the outputs of the thesis is explored is section 3.6.3.

3.6.3 Error Analysis

In order to determine how the measurement errors defined above impact energy loss and discharge parameters derived from the physical model an error analysis has been conducted. Measurement errors (as defined above) from flow meters and transducers have been propagated through the local energy loss, weir and orifice equations over the expected range of measurement. This allows the expected maximum variability in these parameters to be defined based on the measurement error. Maximum flow measurement errors are based on variations in the correction factors defined in section 3.6.1 for the outflow valves ($1.069 < \overline{C_f} < 1.224$), and the maximum identified error for the inflow valve (1.5% of measured value). Errors from pressure transducers are based on the maximum observed variation between the measured values and the calibration relationships in the calibration dataset (0.72 mm)

These errors have been applied to equations for determining the energy losses coefficient (Equation 3), the weir coefficient (Equation 32) and the orifice coefficients (Equations 33-34-35):

Within these equations, errors in the flow readings impact velocity and flow exchange quantification, whilst errors in pressure transducers affect the accurate of hydraulic head and head loss. Errors in quantifying geometrical parameters (i.e. manhole diameter) are

considered negligible. Applying the errors identified to each equation, the results of the error analysis are presented in table 8. Both the range of errors and the average error over the experimental range are presented.

Error values displayed confirm the accuracy of the energy losses and orifice coefficients determined by the facility. Most existing studies do not report error values due to measurement error, however the error values reported imply a higher accuracy then, for example, Marsalek (1984) who reported 95% confidence limits (K values were found in the range 0.102 to 0.344 in square shaped manholes, and 0.124 to 0.221 in circular manholes) in reported K values. The average error is higher when estimating the weir coefficients (0.13) and this can be explained by the occurrence of a siphon effect when simulating surface to sewer exchange. A siphon effect occurs when the tube or pipe through which a liquid is moving is affected by atmospheric pressure. This can act to force liquid up an outlet due to the weight the liquid in another part of the system. Unfortunately this could not be rectified within the tests conducted in this thesis, but can be eliminated by installation of an additional pipe downstream exposed to atmospheric pressure.

Table 8. Potential error in head loss and exchange equations coefficients over experimental range

Equation	$K_i = \frac{\Delta H_i}{V^2/2g}$	$C_w = \frac{Q_e}{\frac{2}{3} * (2g)^{0.5} * w * (\Delta H_i)^{1.5}}$	$C_o = \frac{Q_e}{A(2g\Delta H_i)^{0.5}}$ **(orifice with no additional flow on surface)**	$C_o = \frac{Q_e}{A(2g\Delta H_i)^{0.5}}$ **(orifice with additional flow on surface)**
Experimental range	4<Q<11.5 (l/s) 0.0035<ΔH_i<0.248 (m)	1.10<Qe<1.71 (l/s) 0.01<ΔH_i<0.013 (m)	0.62 < Qe < 4.67 (l/s) 0.098<ΔH_i<0. 293 (m)	1.26 < Qe < 5.50 (l/s) 0.045<ΔH_i<0.311 (m)
Range of error in coefficient over experimental range	0.0033-0.0051	0.11-0.145	0.00013-0.00015	0.00014-0.00066
Average error over experimental range	0.0045	0.13	0.00014	0.00028

4 Pipe Network Results

The aim of this chapter is to detail the experiments conducted on the pipe network described in section 3 which can be summarized in two categories, steady and unsteady flow conditions. Tests conducted in steady flow conditions were used to define head losses through the system under a range of high flow conditions (hence meeting research objective 1). Tests conducted in unsteady conditions were used to evaluate existing computer modelling tools, and identify the significance of local losses due to manholes (hence meeting research objective 2).

4.1 Steady flow tests in the pipe network system

These tests have been used to characterize the response of the model to steady flow conditions and to provide a complete hydraulic description of the performance of the entire system including head losses through manhole structures.

A range of steady flow tests have been run using specific combinations of inflows controlled via the inflow valves (tables 20-41). Appendix A displays the configuration and the hydraulic conditions for each test, in terms of flow rate for each branch and recorded water depths in Manhole 1, 2, 3, 4 (presented in figure 24).

4.2 Secondary losses

After having assessed the basic hydraulic components within the facility and the frictional losses in the pipes, energy losses at manholes (which depend on flow rate, junction geometry, change in flow direction, change in pipe elevation and the change in pipe diameter between the inflow and outflow lines, Wang et al., 1998) have been calculated under a range of steady flow conditions in order to meet research objective 1.

Pipes were fully pressurized in all tests conducted. The experimental tests conducted are summarized in table 9, full details are provided in appendix A.

Table 9 – Details of the 22 steady state experimental tests.

Test	Flow Range (l/s)	Description of the test
1	Pipe B: 2.26 – 5.38	Only pipe A valve opening with increases of 0.4-0.5 l/s
2	Pipe A: 2.17 – 5.91	Only pipe B valve opening with increases of 0.4-0.5 l/s
3	Pipe C: 2.10 – 6.62	Only pipe C valve opening with increases of 0.4-0.5 l/s
4	Pipe B: 0.29 – 6.07	Only pipe A valve opening with increases of 0.1 l/s
5	Pipe A: 0.30 – 6.86	Only pipe B valve opening with increases of 0.1 l/s
6	Pipe C: 0.22 – 6.56	Only pipe C valve opening with increases of 0.1 l/s
7	Pipe B: 0.73 – 5.95	Only pipe A valve opening with increases of 0.2 l/s
8	Pipe A: 0.85 – 6.79	Only pipe B valve opening with increases of 0.2 l/s
9	Pipe C: 0.89 – 6.52	Only pipe C valve opening with increases of 0.2 l/s
10	Pipe B: 0.69 – 2.84 Pipe A: 0.86 – 3.02 Pipe C: 0.49 – 0.50	Pipe flow C kept constant, Pipe A and B with 0.4-0.5 l/s increases
11	Pipe B: 0.39 – 0.41 Pipe A: 0.84 – 3.51 Pipe C: 0.84 – 3.50	Pipe flow A kept constant, Pipe B and C with 0.4-0.5 l/s increases
12	Pipe B: 0.67 – 3.30 Pipe A: 0.46 – 0.49 Pipe C: 0.85 – 3.40	Pipe flow B kept constant, Pipe A and C with 0.4-0.5 l/s increases
13	Pipe B: 1.31 – 3.89 Pipe A: 1.41 – 1.47 Pipe C: 1.45– 1.49	Pipe flow B and C kept constant, Pipe A with 0.2 l/s increases

14	Pipe B: 1.22 – 1.25 Pipe A: 1.42 – 4.47 Pipe C: 1.40 – 1.45	Pipe flow A and C kept constant, Pipe B with 0.2 l/s increases
15	Pipe B: 1.23 – 1.28 Pipe A: 1.35 – 1.39 Pipe C: 1.42 – 5.23	Pipe flow A and B kept constant, Pipe C with 0.2 l/s increases
16	Pipe B: 1.28 – 3.89 Pipe A: 1.36 – 1.41 Pipe C: 1.45– 1.48	Pipe flow B and C kept constant, Pipe A with 0.4-0.5 l/s increases
17	Pipe B: 1.22 – 1.27 Pipe A: 1.38 – 4.54 Pipe C: 1.44 – 1.42	Pipe flow A and C kept constant, Pipe B with 0.4-0.5 l/s increases
18	Pipe B: 1.20 – 1.24 Pipe A: 1.37 – 1.42 Pipe C: 1.45 – 4.68	Pipe flow A and B kept constant, Pipe C with 0.4-0.5 l/s increases
19	Pipe B: 1.26 – 2.95 Pipe A: 1.39 – 3.08 Pipe C: 0.76 – 0.80	Pipe flow C kept constant, Pipe Aand B with 0.1 l/s increases
20	Pipe B: 0.66 – 0.68 Pipe A: 1.41 – 3.50 Pipe C: 1.39 – 3.49	Pipe flow A kept constant, Pipe B and C with 0.1 l/s increases
21	Pipe B: 1.28 – 3.44 Pipe A: 0.76 – 0.81 Pipe C: 1.45 – 3.44	Pipe flow B kept constant, Pipe A and C with 0.1 l/s increases
22	Pipe B: 0.28 – 2.29 Pipe A: 0.30 – 2.47 Pipe C: 0.33 – 2.50	Pipe A, B and C with 0.1 l/s increases

Three example energy grade line profiles are presented based on different primary flow paths through the network. In configuration A flow enters the system via pipe A. In configuration B, flow enters the system via pipe B and in configuration C, flow enters the system via pipe C.

During tests with a single valve opening, the pipe network was surcharged at all points (I.e. even in inlet ‘legs’ with fully closed upstream valves). In Figures 64, 67, 70 values of pressure head are displayed at each measurement point. In Figures 63, 66, 69 values of total head (pressure plus velocity) are displayed. However in this case kinetic head could not be accurately calculated for measurement points within the manhole chambers as due to the changing cross section, the Bernoulli assumption of parallel streamlines is not met. Hence values of total head within the manholes are not reported.

Figure 62, 65 and 68 display the example configuration A B and C.

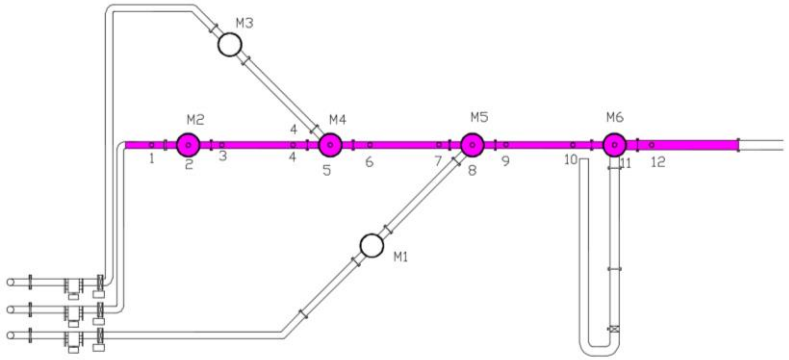

Figure 62 - Configuration A.

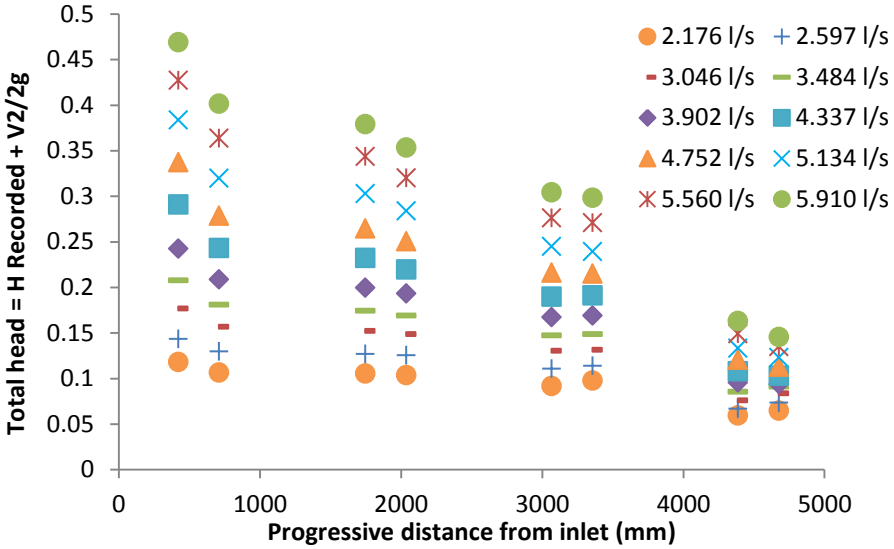

Figure 63 - Longitudinal profile of total head along configuration A for test 2, Appendix A.

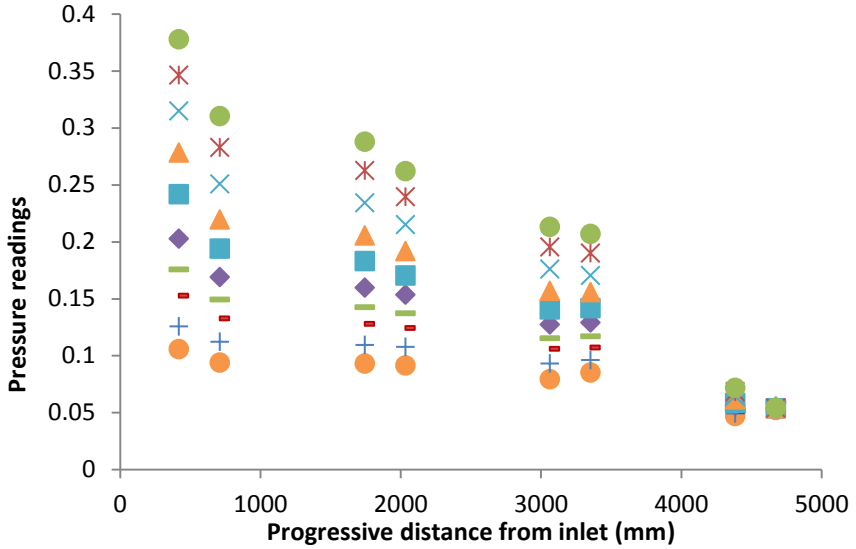

Figure 64 - Longitudinal profile of hydraulic head recorded along configuration A for test 2, Appendix A.

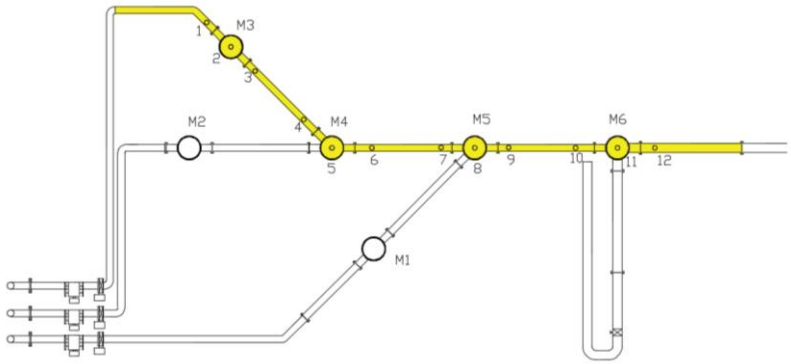

Figure 65 – Configuration B.

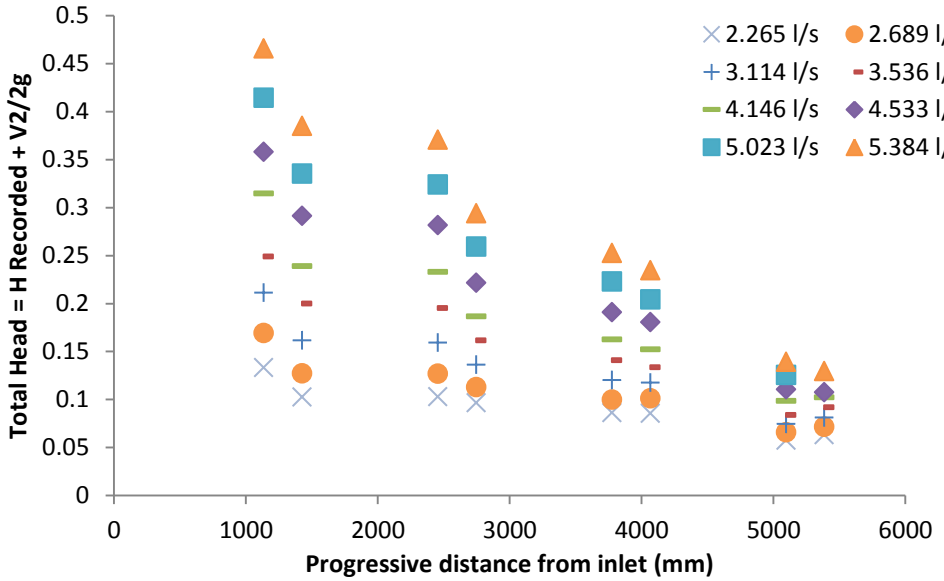

Figure 66 - Longitudinal profile of total head along configuration B for test 1, Appendix A.

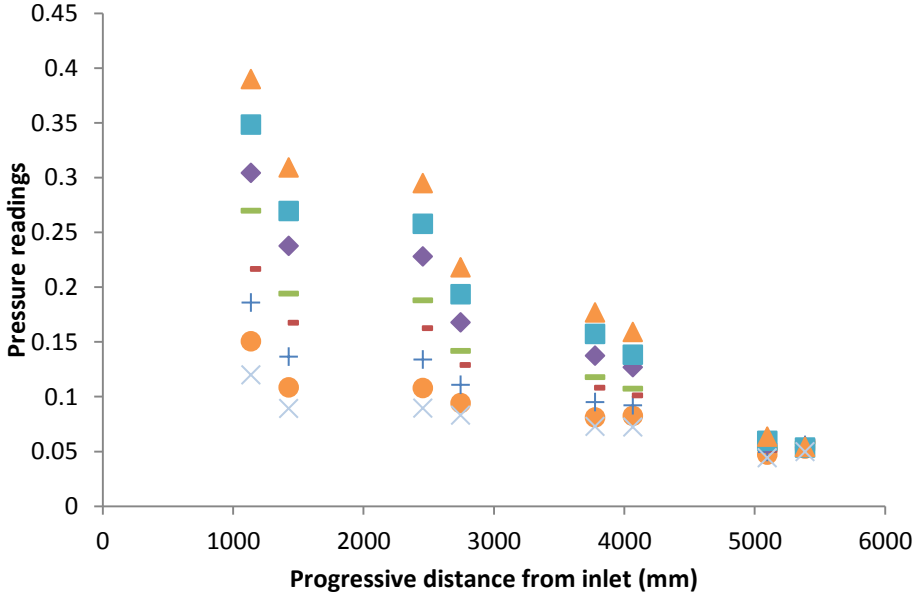

Figure 67 - Longitudinal profile of hydraulic head recorded along configuration B for test 1, Appendix A.

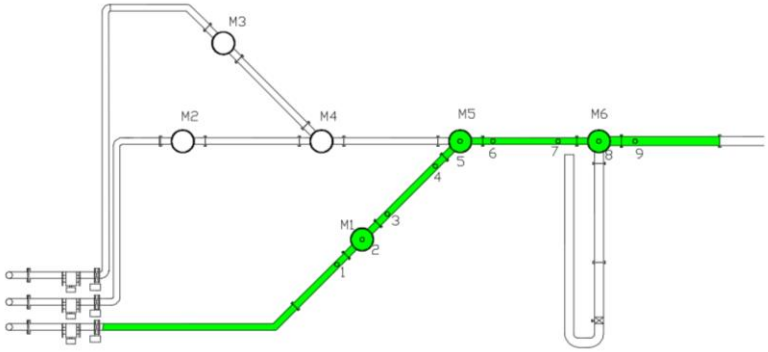

Figure 68 - Configuration C.

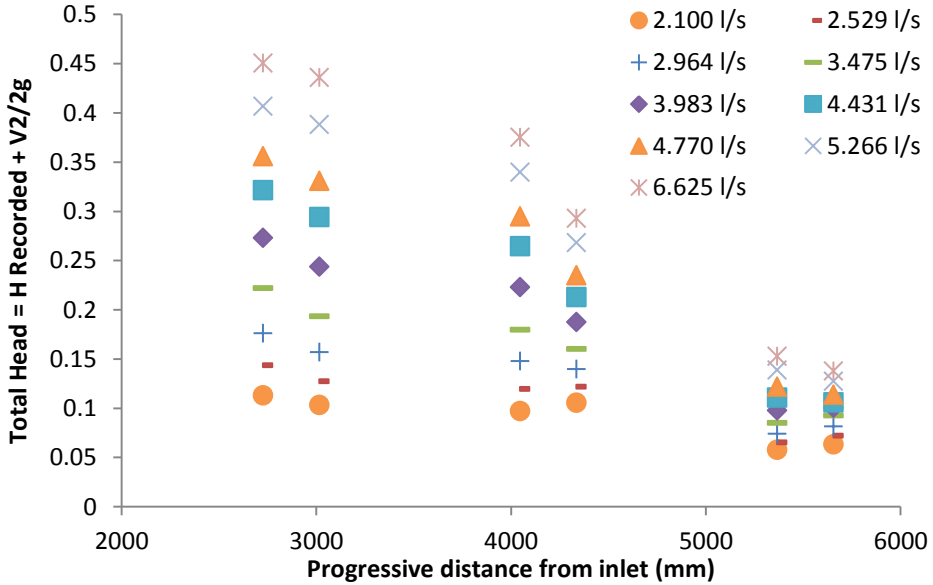

Figure 69 - Longitudinal profile of total head along configuration C for test 3, Appendix A.

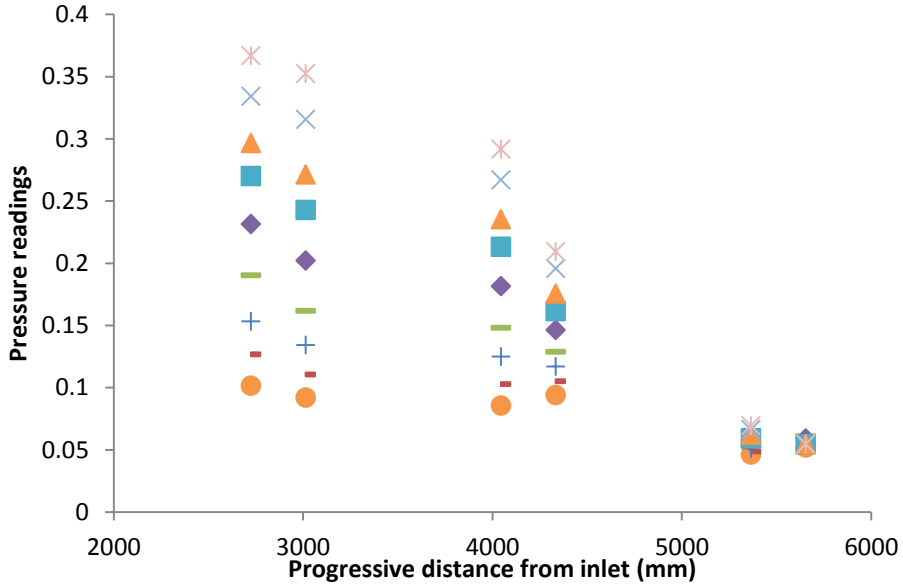

Figure 70 - Longitudinal profile of hydraulic head recorded along configuration C for test 3, Appendix A.

All experimental steady datasets collected (Appendix A) have been used to calculate head losses through the manhole structures over the range of hydraulic conditions. All manholes are either "in line" with a single inlet and outlet (M1, M2, M3 and M6) or feature two inlets and a single outlet (M4, M5).

To calculate frictional losses accountable to manholes based on the framework defined in section, the frictional losses in the pipeline must be determined and used to define the energy grade line.

4.3 Head losses due to friction in pipes

The head loss due to the friction in a pipe is computed as suggested by the Darcy-Weisbach equation, which can be used to relate frictional head losses in pipes, flow velocity and pipe characteristics:

$$h_f = \frac{fLV^2}{2gD}$$ Equation 48

The Moody diagram was developed which relates the Darcy-Weisbach friction factor, Reynolds number and pipe roughness expressed as K_s/D, where K_s is an empirical parameter based solely on pipe material and condition.

$$\frac{Ks}{D}$$ Equation 49

In laminar flow conditions, headloss is independent of pipe roughness and the loss of head is purely a function of the flow regime, as determined by the following function:

$$\lambda = \frac{64}{Re}$$ Equation 50

In "transitional conditions", friction factor is sensitive to both flow and wall properties and the formula of Colebrook White can be used to quantify the friction factor.

$$\frac{1}{\sqrt{\lambda}} = -2\ \log_{10}\left(\frac{2.51}{Re} * \frac{1}{\sqrt{\lambda}} + \frac{Ks}{3.7\ D}\right)$$ Equation 51

For smooth turbulent flow, wall roughness is fully covered by the viscous laminar sublayer hence in that regime roughness does not influence friction losses. Therefore, the friction factor equation becomes:

$$\frac{1}{\sqrt{\lambda}} = -2\ \log_{10}\left(\frac{2.51}{Re} * \frac{1}{\sqrt{\lambda}}\right) \qquad \text{Equation 52}$$

In rough turbulent flow, the full Colebrook White equation applies, however friction factor becomes insensitive to Reynolds number and can be written as:

$$\frac{1}{\sqrt{\lambda}} = -2\ \log_{10}\left(\frac{Ks}{3.7\ D}\right) \qquad \text{Equation 53}$$

Considering the experimental facility developed at the University of Sheffield, to determine frictional losses inside the physical model pipe network, a range of flow tests inside a simple length of pipe downstream of the manhole (Figure 71) were conducted and pressure drop along a single pipe section (between PMDown 1 and PMDown 2) was related to flow Reynolds No.

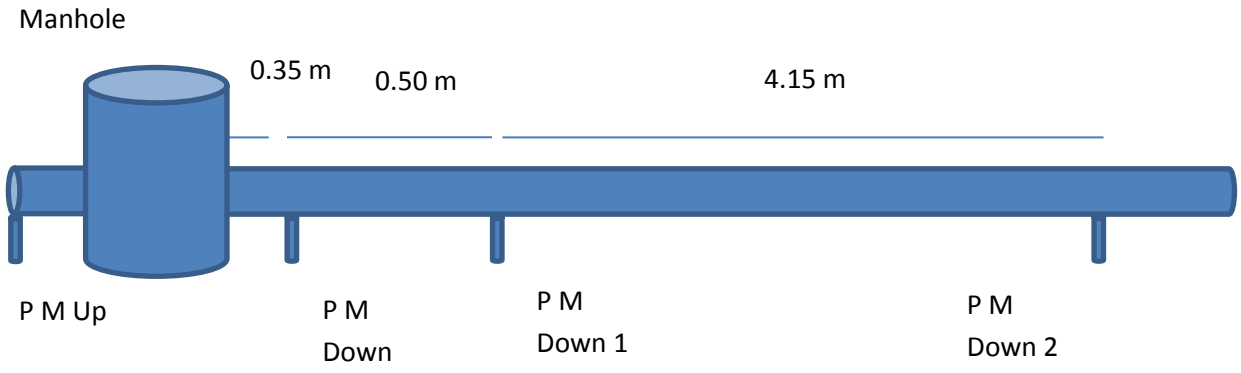

Figure 71 – Scheme of simple length pipe downstream of manhole used to characterize pipe frictional losses.

Table 10 – Hydraulic parameters within the experimental facility.

Test	Flow (l/s)	Pipe Flow Velocity (m/s)	Reynolds No.
1	4.364	0.99	73983
2	7.040	1.59	119335
3	8.213	1.86	139219
4	9.025	2.04	152983
5	9.604	2.17	162797

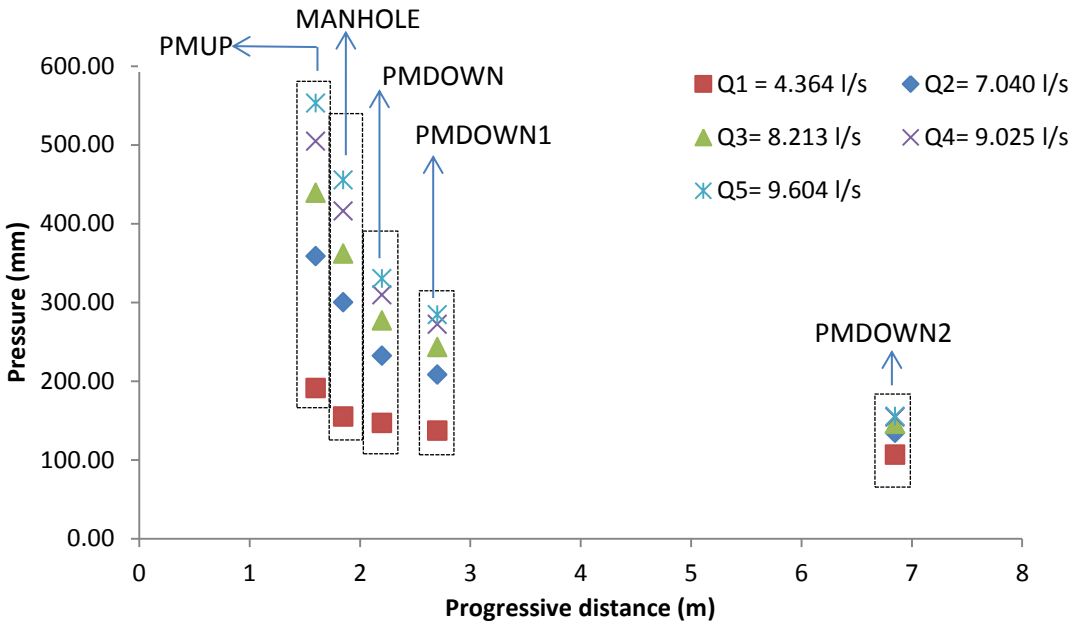

Figure 72– Pressure values recorded for the five tests.

It is possible to determine a relationship for the pipe friction factor based on measured head loss (Down 1 to Down 2) and Reynolds number (Figure 73). These measurement points were chosen to define the pipe friction factor because they are the measurement points furthest away from the manhole chamber, which may have an influence on the turbulent structure in the pipe downstream. Although turbulent effects due to the manhole may not have entirely dissipated between the sections analysed, consideration of figure 72 suggests that the influence of this effect is likely to be relatively small. The head losses due to pipe friction can therefore be identified for a given flow rate and used to define the energy grade line. Friction losses values determined within these experimental tests were similar (± 0.0025 m) to the ones obtained considering the typical roughness of PVC pipe material, where $\frac{e_S}{D} \approx 9.333 \times 10^{-5}$.

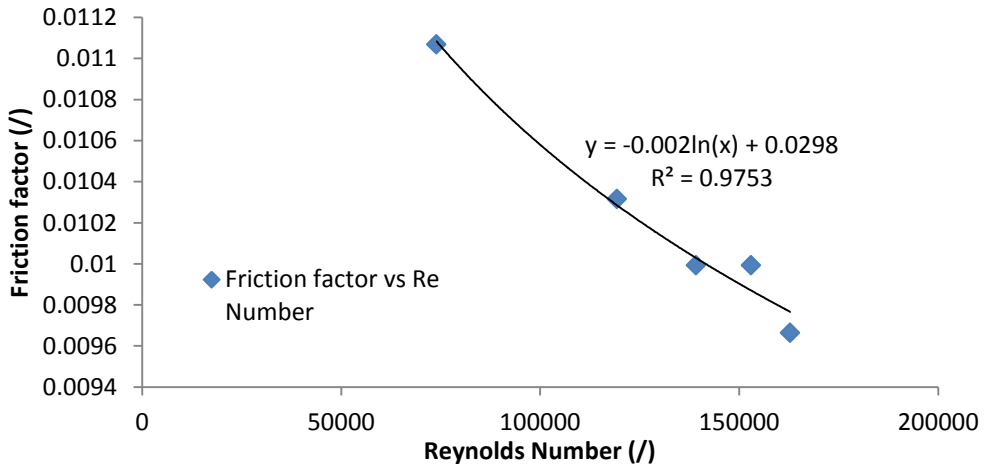

Figure 73– Friction factor vs Reynolds No.

4.4 "In line" manholes

As the slope of the facility is zero, head loss through attributable to each in line manhole is calculated as measured head loss less the expected head loss in a straight pipe of equivalent length due to friction:

$$hL = [(H_{up}) - (H_d)] - \frac{fLV^2}{2gD} \qquad \text{Equation 54}$$

H_{up} and H_d for each manhole can be obtained directly from the pressure readings upstream and downstream of each manhole. In this case, due to constant pipe diameters upstream and downstream of each manhole (and hence constant velocity head), only pressure head is considered in equation 54. Pressure transducers are located 25 cm upstream and 35 cm downstream of the manhole centerline in each case (hence the length, L in equation 54, of the equivalent pipe is taken as 84 cm). Mean pipe velocity for the calculation of frictional losses is obtained by dividing flow rate by pipe cross sectional area. The corresponding head-loss coefficients K for each manhole have then been determined using equation 3. Figure 74 relates calculated head loss (from equation 54) for each 'in line' the manhole to velocity head. The resulting best fit coefficients are presented in table 11.

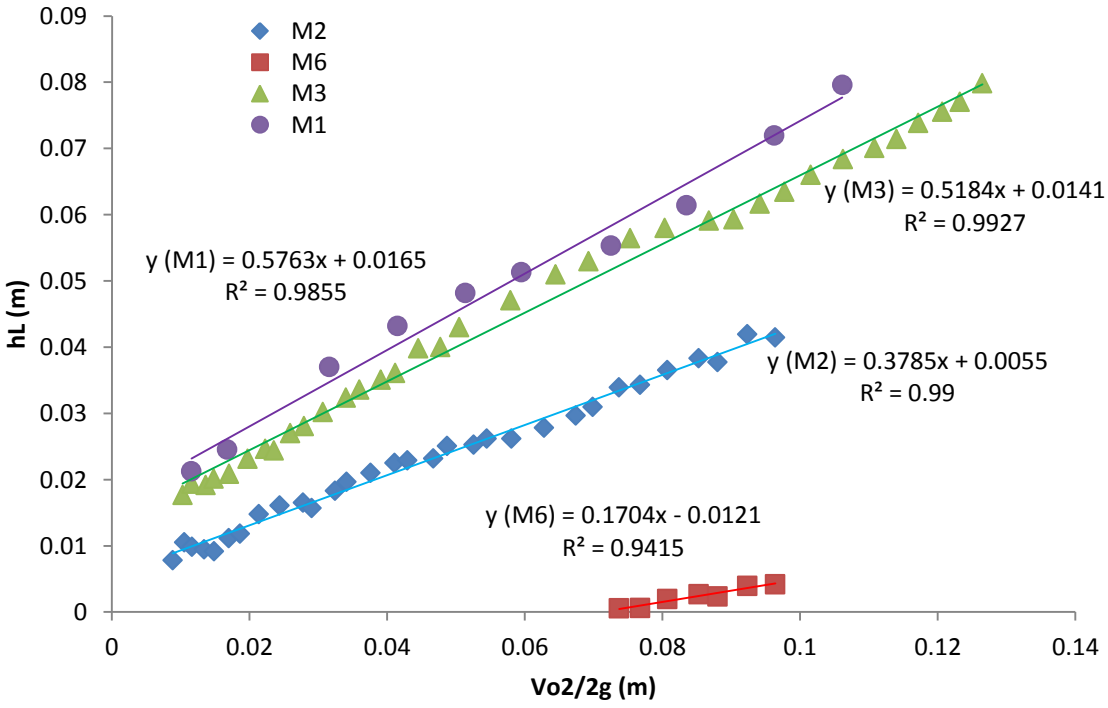

Figure 74– Head losses manhole "in line".

Table 11 – K values for ‘in line manholes’.

Manhole	M1	M2	M3	M6
Coefficient (K)	0.57	0.37	0.51	0.17

The study has confirmed the proportionality of head losses at straight manholes to the velocity head. Head loss coefficients for ‘in line’ manholes M2 and M6 in the central pipe calculated by combining multiple steady flow configurations can be considered close to the range 0.195-0.221 in literature for head loss through a straight manhole (Marsalek, 1984). The value of K may be lower for M6 than M2 due to the enlargement on the outlet pipe immediately downstream the final manhole of the system, where the diameter of the pipe increases to 100 mm.

For manholes M1 and M3, K values are slightly higher than expected. This may be explained by the 135 degree pipe bends immediately upstream of the manholes which may cause irregular flow patterns inside the manhole inlet pipe, influencing the flow patterns inside the manhole, and increasing the energy losses. The same justification has been given to justify the non-perfect linear trend obtained by the values recorded, even if trend lines acquired show good agreement for manhole M1 (R^2=0.985) and M3 (R^2=0.992). The experiments conducted demonstrate the high variability of K values and the sensitivity to upstream and downstream pipe and flow conditions.

Another significant difference with previous studies is the presence of several manholes in series. All previous studies have reported results for a single manhole. For example, the energy losses generated by the configuration reported in Marsalek (1985) are caused only by the main body of the stream crossing the single manhole. For the experimental facility reported here each manhole is followed by another manhole and this could lead to additional turbulence and associated energy losses. Some variability between observed values and those found in the literature may also be explained by the presence of ‘still’ water in the pipe network during test when only one upstream valve is open.

4.5 Energy Losses Through Manholes with Multiple inlets

Predictions for the energy loss coefficients have been made by applying the framework described in section 2.5 (Zhao et al., 2006 and Pfister et al., (2014) and have been compared with experimental data collected from the facility. Energy loss values presented here are defined as those detailed in equations 9 and 10.

Relationships presented in section 2.4 have been applied to different flow combinations through the experimental facility. Water was running through the pipes which were full (i.e. pressurized flow).

Energy loss coefficients comparisons have been made between predictions and experimental data for manhole 4 which is most hydraulically similar (if considered separated from the entire system) to hydraulic models previously used. Comparisons were not completed for manhole 5 because this junction is affected both by upstream and downstream conditions, which are different from inlet and outlet conditions used by Zhao et al., (2006) and Pfister et al., (2014). K_{12}, K_{13} and Total K values as a function of relative flow in the inflow pipes are presented in figure 75, alongside predictions made using the relationship defined by Zhao (2006), i.e. equation 9-10.

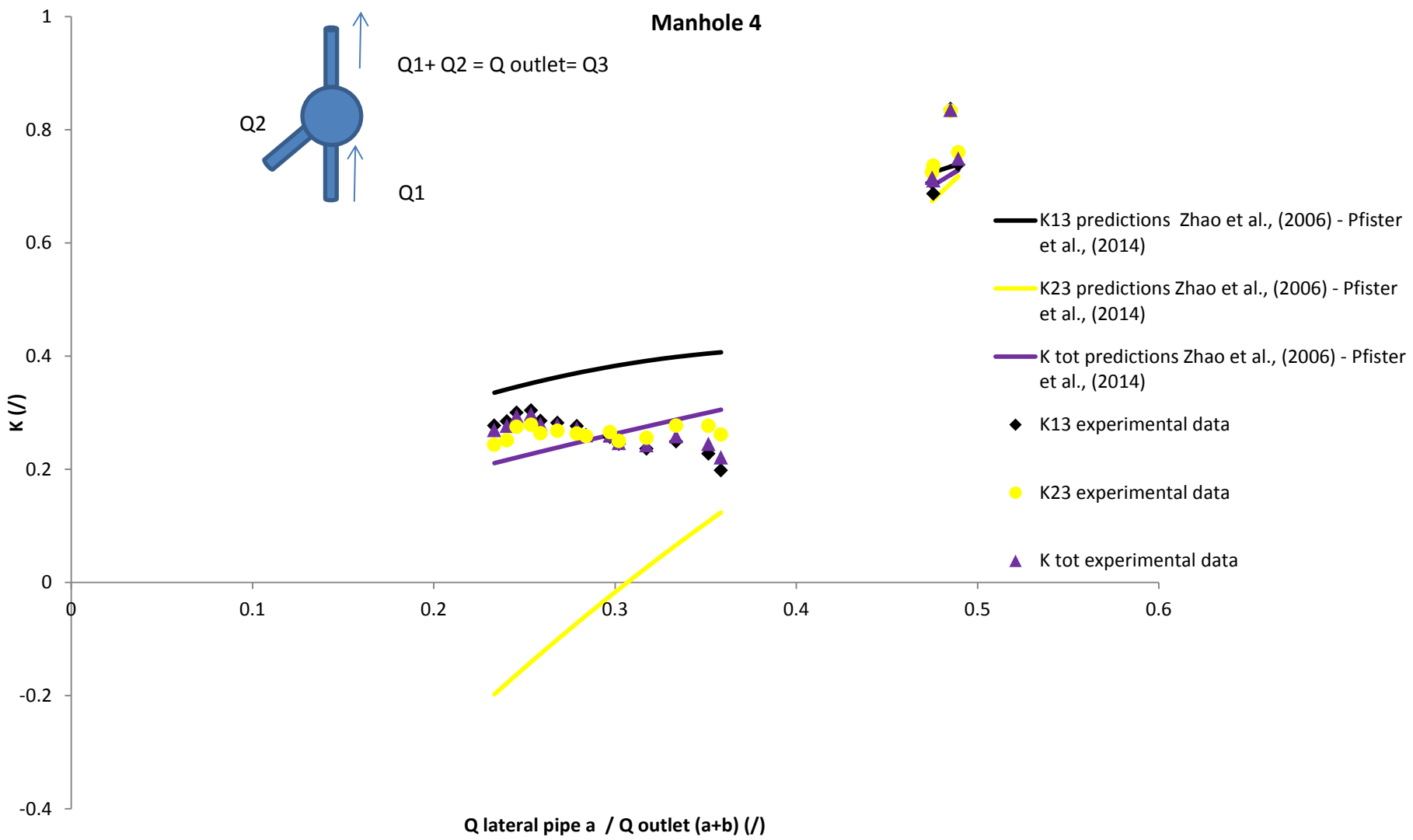

Figure 75 – Manhole 4, comparison between energy loss relationship [Zhao et al., (2006) and Pfister et al., (2014)] and experimental data.

It should be noted that, previous research (sections 2.3, 2.4, 2.5), has not used directly comparable geometries to that in the current facility, hence it is difficult to identify if these findings are in direct agreement with previous work, Zhao et al., (2006) and Pfister et al., (2014).

Despite this, the results show interesting similarities between experimental data and energy losses coefficients defined by equation 9-10 for $Q_{lateral}/Q_{outlet}$ = 0.5. For $Q_{lateral}/Q_{outlet}$ = 0.22-0.36 comparisons have shown the predictions obtained using the model of Zhao et al., 2006, overestimate the energy loss coefficients K_{23} and underestimate the energy loss coefficients K_{13}. However overall, this means that the predictions for the total K are reasonably accurate (with 6.8%). Discrepancies in terms of predicted trends using equation 9-10 are also evident. These comparisons have highlighted the significance of flow streamlines created inside the manholes under different flow combinations on energy losses coefficients. Having more complex flow patterns generates more effects on energy losses due to retardation, acceleration, rotation in different planes and flow interference.

4.6 Quantification of hydraulic capacity of the sewer system

The number of times the flow breached a defined level in the manholes during all the steady tests was also recorded. The threshold level was selected as 430 mm, dependent on the number of valve opening and on the magnitude of flow rate, therefore primary decision of the controller to stop the simulation during the tests.

The results are presented in figure 76:

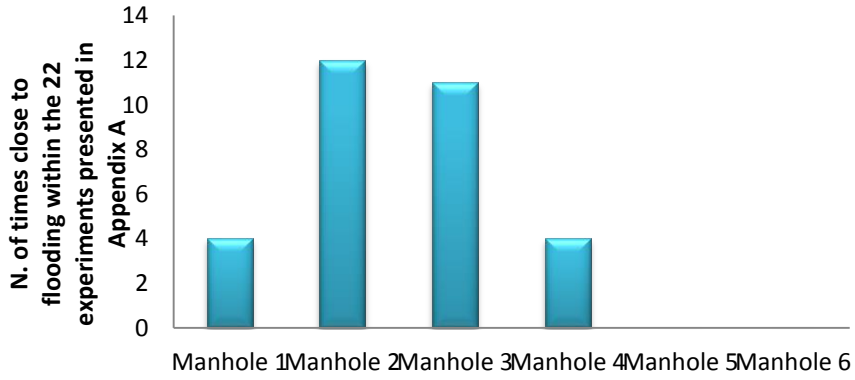

Figure 76– Flooding times.

It is possible to notice that the bigger risk of flooding comes from the manhole 2, followed by manhole 3 and then 1 and 4.

For each simulation the maximum flow contained by the system has been calculated and figure 76 displays the overall values.

The maximum flow reached through branch A was 6.072 l/s.

The maximum flow reached in the branch B was 6.975 l/s.

The maximum flow achieved in branch C corresponds to 6.564 l/s.

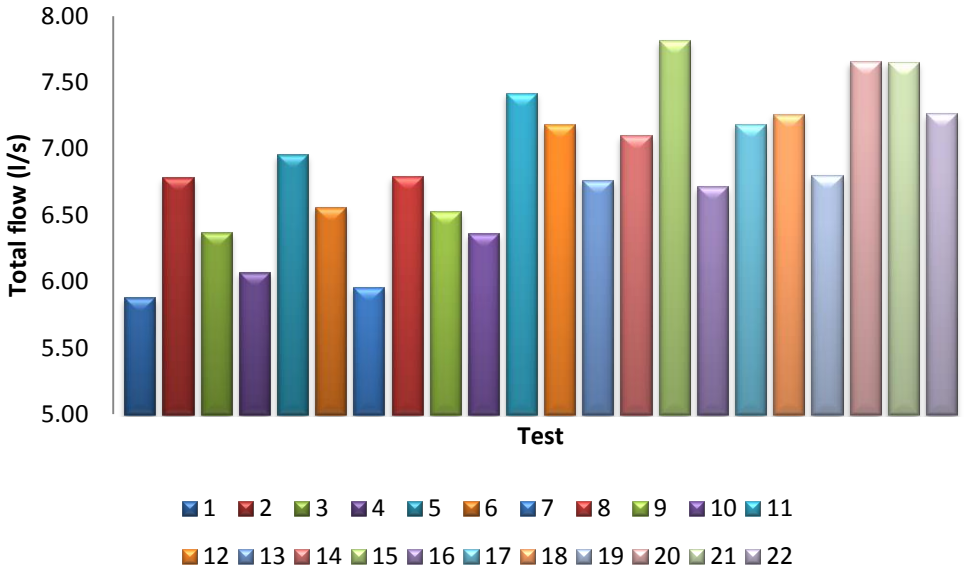

Figure 77 - Total flow for each simulation.

4.7 Scaled Rainfall Event Simulations

Having characterized the steady state system, a number of unsteady flow events were conducted. The flow hydrographs tested were based on real storm events measured in an urban catchment in the north of England, scaled to the experimental facility. The overall aim of these tests was to provide datasets that could be used to calibrate and validate sewer flow models including the commercial model Infoworks as well as the SIPSON model provided by collaborators at the University of Coimbra, as well as identify the significance of local head losses (research objective 2). However initial tests conducted were focused on identifying if the scaled physical model could reproduce hydraulic phenomena as observed in a full scale system.

For these initial tests, unsteady flow input hydrographs were based on rainfall events measured by using a rain gauge from a site. The data was provided by Yorkshire Water Services, and converted into sewer inflow hydrographs using empirical rainfall-runoff relationships as utilised within commercial Infoworks software. These hydrographs

were then scaled and replicated into the physical model by applying the similitude of Froude as explained in section 3.1.

The real site used in this study is a section of an urban drainage system situated in the upstream suburbs of a city in the North of England, UK. The configuration of the real site closely matches that of the physical model. The area of interest has a population of around 2,500 and a contributing area of 67 Ha. Rainfall data has been collected in the catchment as part of a long term monitoring study using a tipping bucket rain gauge. A map of the site is presented in figure 78.

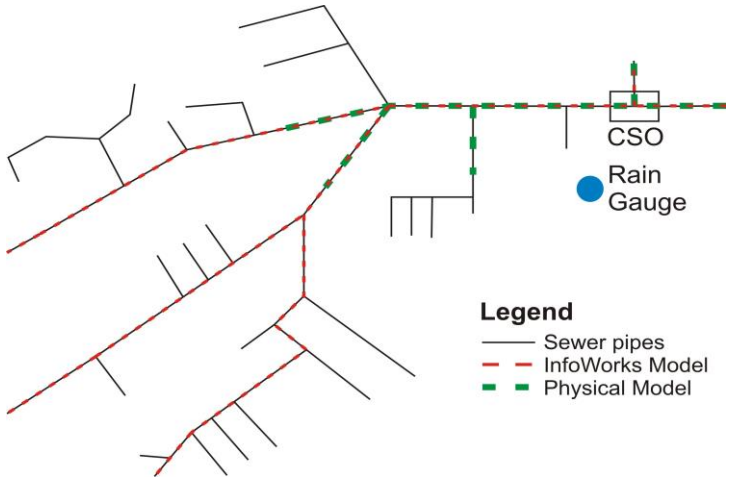

Figure 78- Map of the site in InfoWorks. © Crown Copyright/Digimap 2011. An Ordnance Survey/EDINA supplied service.

The industry standard InfoWorks software incorporates a hydrology model and a hydraulic model which is utilised in the work presented here (hereinafter referred to as 'the hydraulic model').

The calibrated hydraulic model was supplied by the water and sewerage company for use in this project. The 'Code of Practice for the Hydraulic Modelling of Sewer Systems' (WaPUG, 2002) has been used for the model developed by Yorkshire water. The model has been built predominantly as a 'drainage area planning' model, thus it does not include all pipes in the system, but is simplified to around 20 nodes per 1,000 population. 45 pipes are modelled with a total length of 3000 m and pipe diameters between 225 and 600 mm.

The model has been calibrated based on the results of a short term sewer flow survey; these types of survey are described in WRc (1987).

Essentially the survey consists of monitoring rainfall and sewer flows at key locations in the network with a 2 minute logging interval. The flow survey will therefore have

recorded 2 dry weather flow days and 3 rainfall events which meet criteria including minimum flow depths, rainfall intensity, duration and limits on spatial variability.

The model available covers the entire city, but only a very small section relating to the area of interest is described here because the aim was to find a site with similar characteristics of the experimental model.

Considering that the physical model includes three inlet pipes with the addition of two junctions, a specific analysis of the existing real model has been completed to find a similar geometrical combination to use for a comparison between experimental and physical results.

The area identified for the analysis is presented in figure 78 and includes three pipes plus a CSO.

Input flow hydrographs for the physical and numerical models were based on rainfall data (depth, intensity and duration) measured in the catchment using the rain gauge over the period April 2008 - June 2009.

The events selected for the simulations (listed in table 12) were those recorded within the catchment with durations of 15 ± 1, 30 ±2, 45 ±1 and 60 ± 2 minutes.

This period represents the typical range used for planning sewer systems. The rainfall events were converted into runoff using the "new UK runoff equation" and the equation for the time of entry as utilized in Infoworks. The Infoworks hydraulics were also used to simulate sewer network flows upstream of the simulated area.

To determine hydrographs for each drained section of the catchment, Infoworks creates a volume model to establish the volume generated from the rainfall event. Successively, it produces a routine model calculating the flow generated within each subcatchment which then can be used for simulations in the physical model.

A description of the simulation process using Infoworks has been omitted for brevity but the interested reader is referred to WAPUG (Code of practice, 2002).

Table 12 - Rainfall events selected.

N° of event	Duration of the rainfall event (min)	Date (day/month/year)	Average Intensity (mm/h)	Rainfall Depth (mm)	UCWI (-)
1	15	5 August 2008	2.25	0.6	135
2	15	29 June 2008	4.5	1.2	158
3	15	17 Nov 2008	2	0.6	135
4	15	17 Jan 2009	2	0.6	153
5	15	11 Feb 2009	3	0.8	147
6	30	31 August 2008	0.7	1	140
7	30	29 Sept 2008	0.5	0.8	132
8	30	12 Dec 2008	1.8	1	134
9	30	9 Feb 2009	1.2	0.6	159
10	30	4 May 2009	1.2	0.6	109
11	45	4 May 2008	2	1.6	145
12	45	14 August 2008	4	3.2	180
13	45	2 Nov 2008	1.8	1.4	134
14	45	8 March 2009	3.4	2.6	164
15	45	26 March 2009	2.9	2.2	155
16	60	11 April 2008	2.6	2.6	137
17	60	28 May 2008	4	4	107
18	60	3 June 2008	2	2	164
19	60	8 Nov 2008	1.6	1.6	139
20	60	10 March 2009	2.5	2.6	170

4.8 Scaling procedures for physical models

Results in this section have been previously presented at the 10th International Conference on Hydroinformatics, Hamburg, Germany, 14 July 2012 - 18 July 2012 (Rubinato et al. 2012).

Infoworks had been used to generate the inflow hydrographs (Figure 79) to the real system.

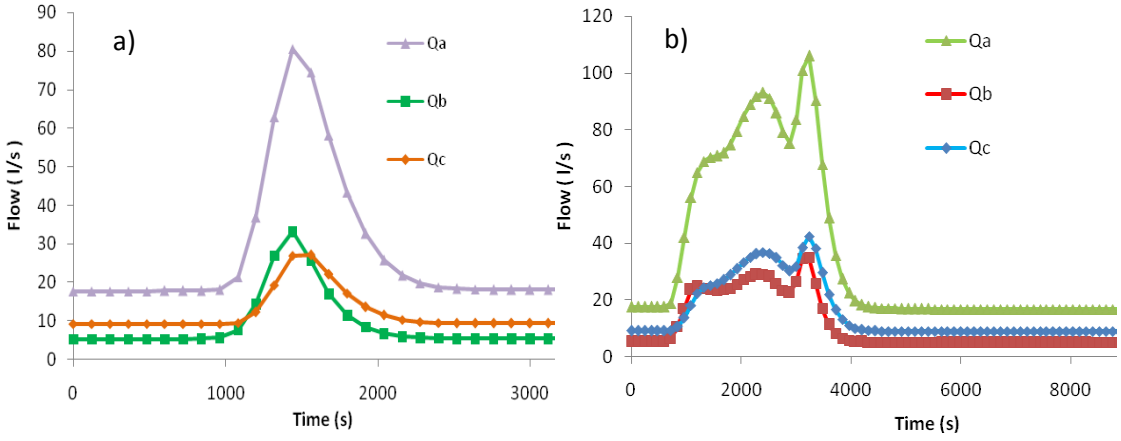

Figure 79– [a) Event 3 of 15 minutes, b) - Event 11 of 45 minutes] generated with Infoworks

The hydrographs were then scaled for reproduction on the physical model. To do this, scaling procedures are required for the reproduction of flow according with similitude of Froude No previously described in section 3.1. Based on these scaling laws the principal physical dimensions of the physical model study were based on the ratios presented in table 13.

Table 13 - Scale factors for satisfaction of Froude Similitude.

Relationship	Scale
Length λ	1 : 6
Velocity $\lambda^{0.5}$	1 : 2.45
Volume Flow $\lambda^{2.5}$	1 : 88.2
Time $\lambda^{0.5}$	1 : 2.45

Figure 80 displays two examples of the scaled flow hydrographs reproduced within the physical model.

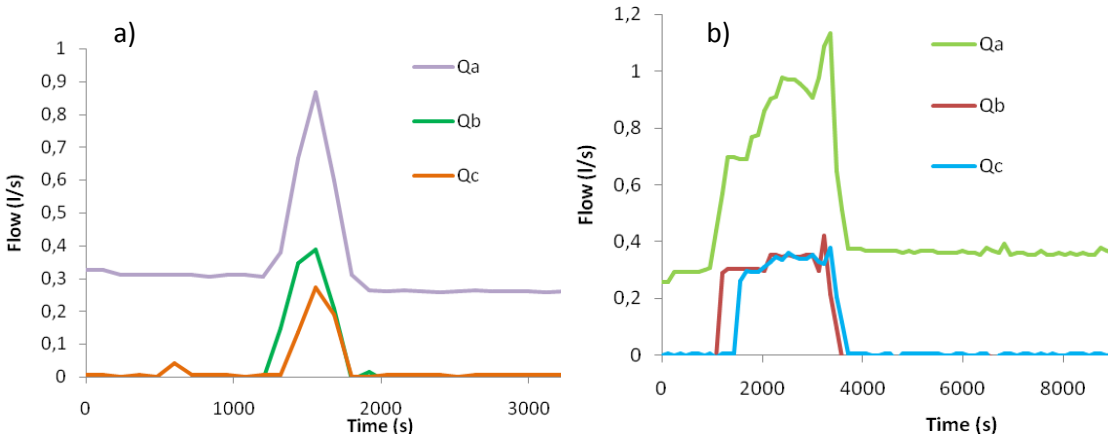

Figure 80 – [a) Event 3 of 15 minutes, b) - Event 11 of 45 minutes] reproduced in the physical model.

At this stage of the research, the main focus was the peak of flow. Therefore 'full scale' and modelled values obtained have been compared by calculating the relationship between the peak scaled measured flow and the peak Infoworks scaled flow for each simulation at the inlet of each pipe.

$$x = \frac{Q_m}{Q_i} * 100 \qquad \text{Equation 55}$$

Table 14 highlights the results for two events selected.

Table 14 - Values of peak flow for each channel for the two events 3 and 11.

	Peak Flow Infoworks (l/s) Q_i	Peak Flow Physical model (l/s) Q_m	Percentage of reproduction (%)
Event 3			
Qa	0.913	0.866	94.8
Qb	0.378	0.388	102.6
Qc	0.308	0.273	88.6
Event 11			
Qa	1.203	1.1348	94.3
Qb	0.435	0.4192	96.3
Qc	0.481	0.3770	78.4

These results suggest that the physical model is accurately reproducing the peak of flow in the real system.

4.9 Comparison between computer modelling results in Infoworks and the physical model results for flow

Results in this section have been presented in a journal paper (**Rubinato M.**, Shucksmith J., Saul A.J. ***"Comparison between Infoworks results and a physical model of an urban drainage system",*** Water Science and Technology, Vol. 68, No 2, pp. 372–379*)*

Once the scaled flow hydrographs had been run through the physical model, a direct comparison was produced between measured hydraulic parameters (velocity) from the physical simulations and those from the calibrated hydraulic Infoworks models of the real site. Infoworks has been used to define inflow hydrographs for the physical model.
The physical model has been run for the 15 input events described in table 12. Figures 81-84 display 8 example-events reproduced which compare the measured results (physical model) and simulated results (hydraulic model) in terms of *velocity/velocity*$_{Max}$ measured at the three inlet pipes. In the legend, "CM" is referring to Computer Model (Inforwoks) results, while PM is related to Physical Model results. In all cases U_{max} is defined as the maximum velocity over each Infoworks simulation. In all conditions, free surface flows were maintained in the pipes (no surcharging).

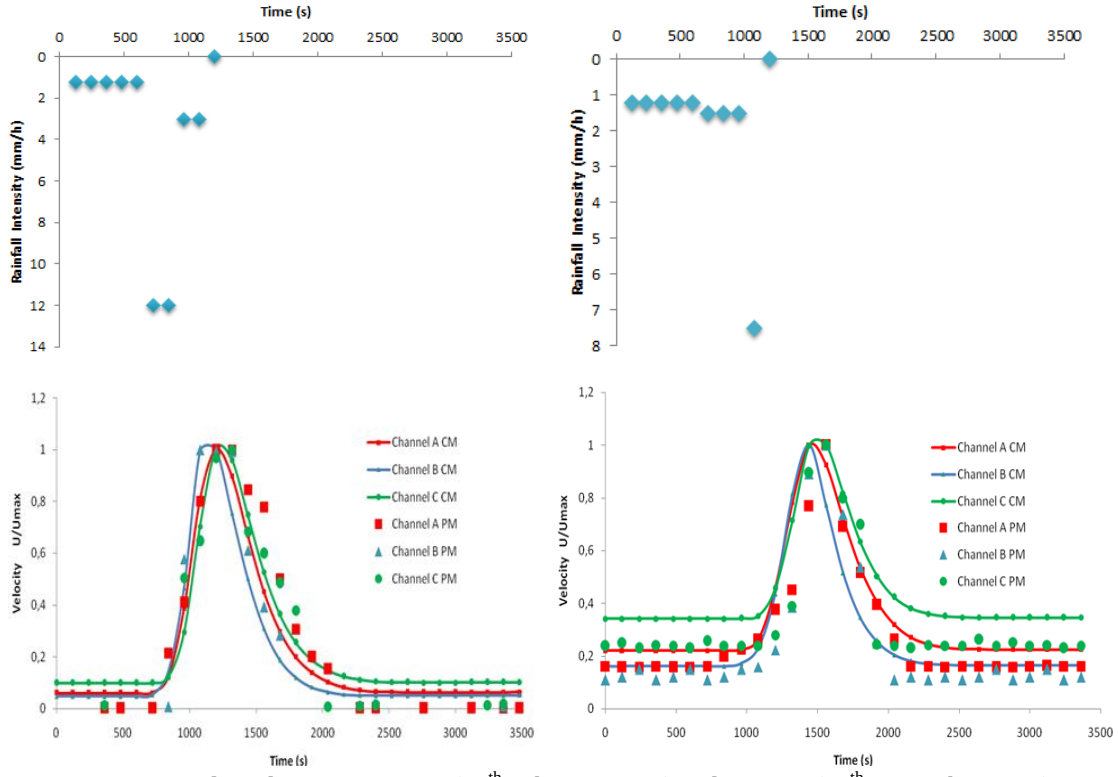

Figure 81- Two selected events, Event 5 (11th February 2009) and Event 3 (17th November 2008), are displayed. Both rainfall events are of 15 minutes duration.

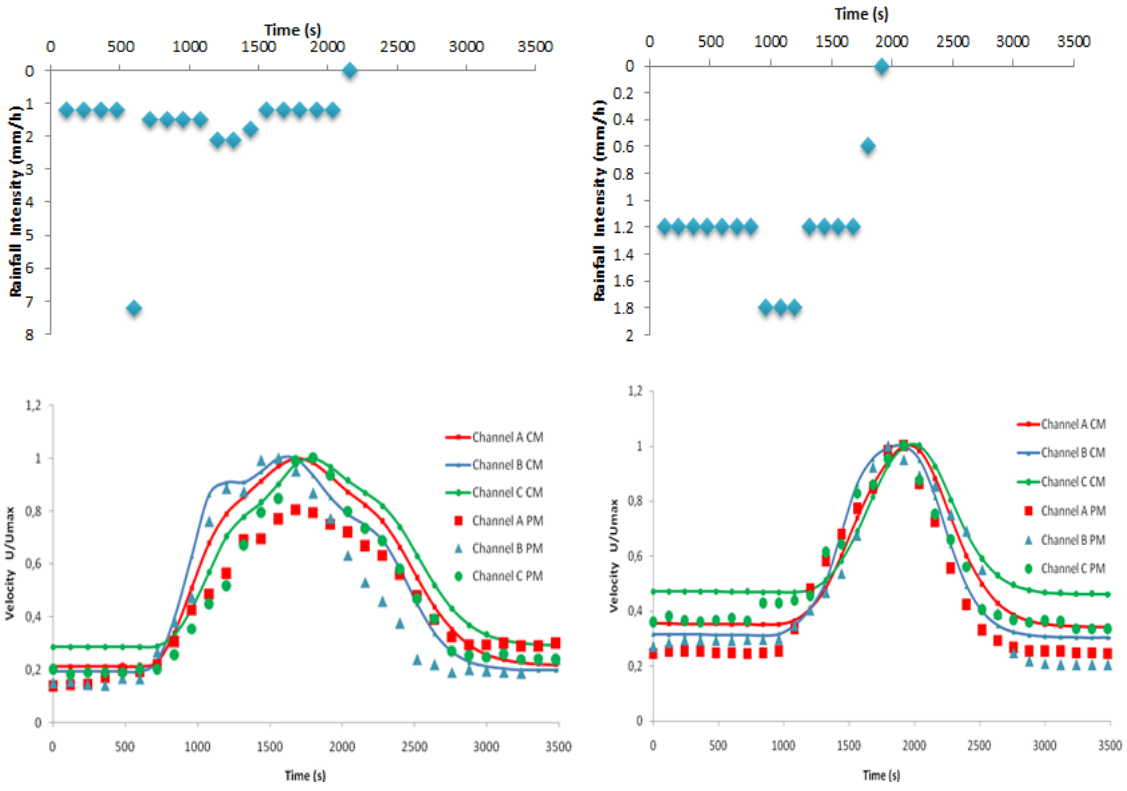

Figure 82 - Two selected events, Event 10 (4th May 2009) and Event 9 (9th February 2009), are displayed. Both rainfall events are of 30 minutes duration.

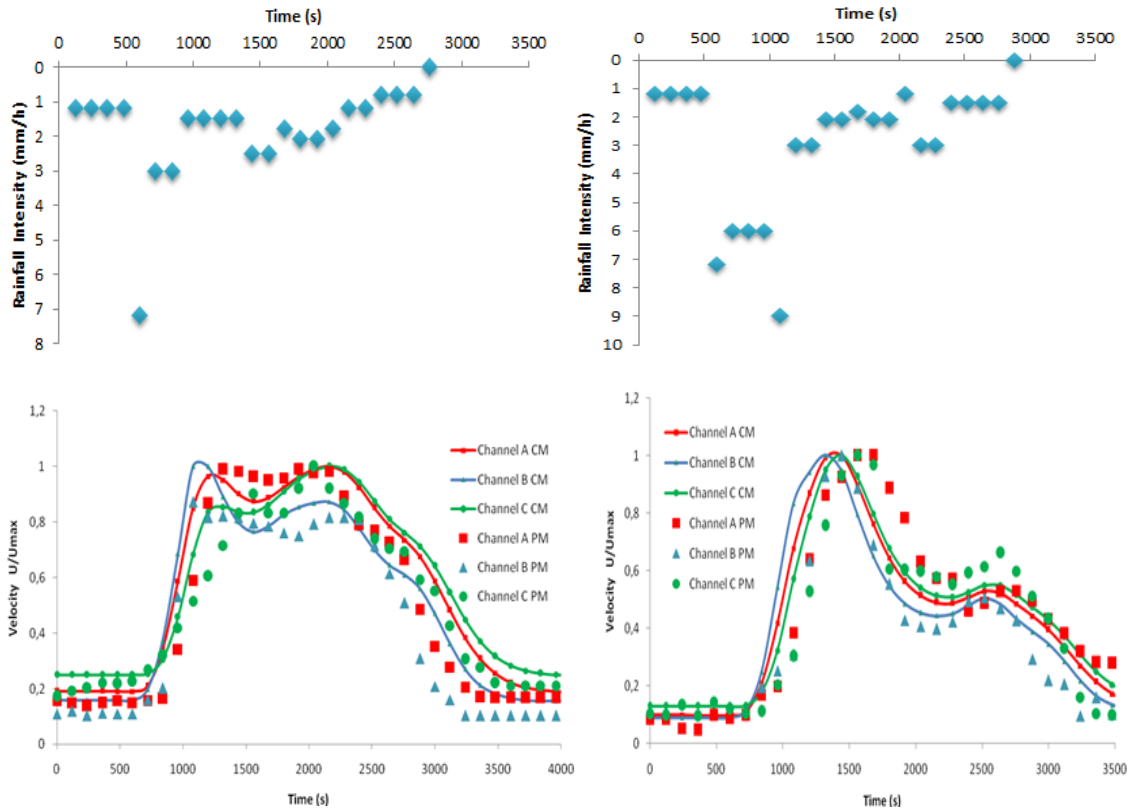

Figure 83- Two selected events, Event 13 (2nd November 2008) and Event 15 (26th March 2009), are displayed. Both rainfall events are of 45 minutes duration.

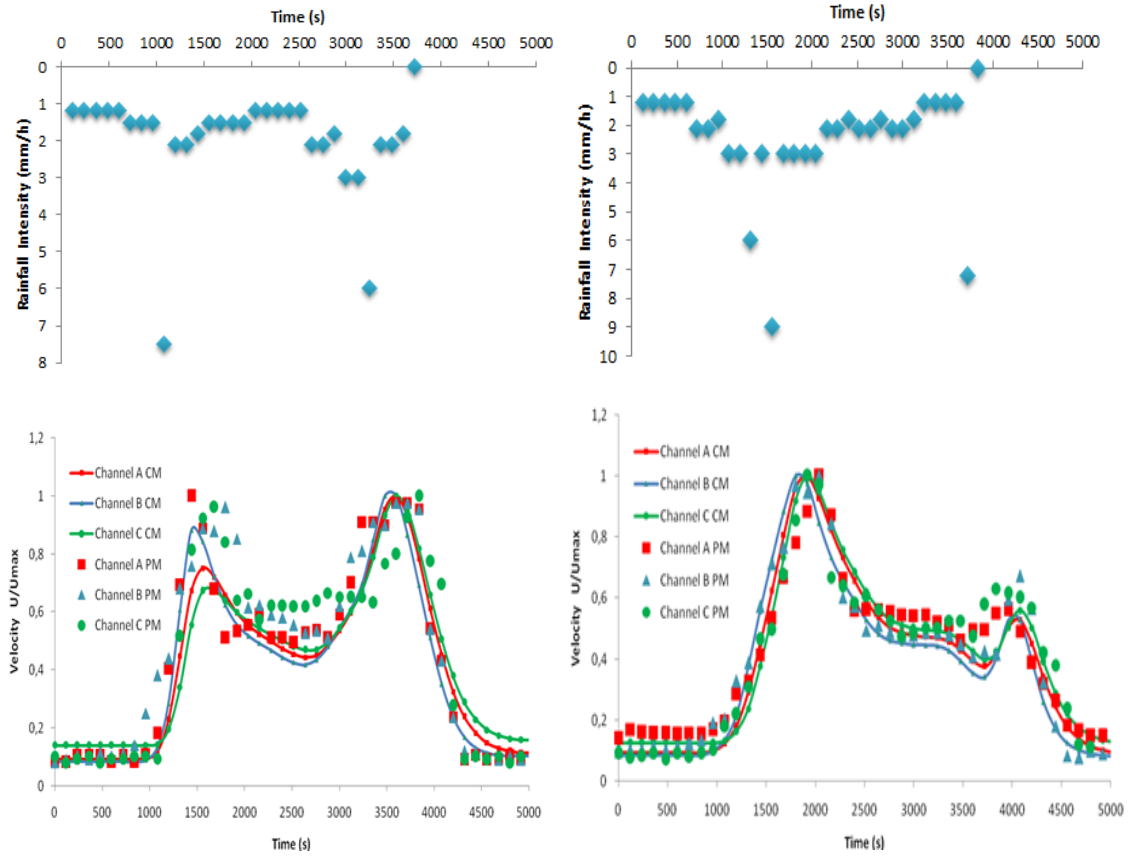

Figure 84 - Two selected events, Event 18 (3rdJune 2008) and Event 16 (11thApril 2008), are displayed. Both rainfall events are of 60 minutes duration.

To determine an overall accuracy of this data, a multiple correlation coefficient R^2 has been calculated for each event using the formula described in Young et al. (1980) to measure how well the variables could have been predicted using a linear function of a set of other variables.

This parameter is defined as (Young et al., 1980) "a normalized measure of the degree to which the model explains the data and if R_t^2 = 1.0 then the data are explained perfectly by the model while if R_t^2 = 0.0 the model has failed to represent any of the data".

$$R^2{}_t = 1 - \left[\frac{\sum_{t=1,n}(m_t - p_t)^2}{\sum_{t=1,n} m_t{}^2}\right] \qquad \text{Equation 56}$$

Table 15 - Values of R^2 for each test in each channel.

N. of Event	R^2 Pipe A	R^2 Pipe B	R^2 Pipe C
15 Minutes			
2	0.952	0.963	0.949
3	0.863	0.923	0.889
4	0.838	0.927	0.981
5	0.827	0.792	0.810
30 Minutes			
8	0.942	0.877	0.859
9	0.932	0.966	0.947
10	0.966	0.936	0.937
45 Minutes			
11	0.977	0.975	0.987
13	0.965	0.946	0.972
14	0.983	0.954	0.952
15	0.944	0.925	0.945
60 Minutes			
16	0.955	0.957	0.969
18	0.965	0.941	0.942
19	0.948	0.894	0.959
20	0.964	0.979	0.971

Analysing R^2 coefficients and visually comparing the trend of the simulation, it is possible to conclude that the physical and computer model were in close agreement, this provides confidence that the physical model can reproduce full scale systems.

The time scaling ratio (as defined in section 3.1) has not been considered for these simulations because the principal aim of these tests was to demonstrate that the model could run unsteady flow events by scaling a real hydrograph using the indirect

interpolation between valve openings and flow rates by subsequently applying the time ratio scale.

Table 16 displays the duration of the tested storm events scaled by using the similitude of Froude (1:6).

Table 16 – Time scales to satisfy the similitude of Froude within the physical model.

Time (min) Real System	Time (min) Prototype – Physical Model
15	6.12
30	12.25
45	18.37
60	24.49

The consideration of time scaling may be important for future studies as the turbulence and the streamlines created inside the manhole may be different if flow rise or fall at different rates, which may affect local energy losses. Therefore the time scaling ratio will be considered for future studies. Based on Froude similitude, replicating real events of 15, 30, 45 and 60 minutes will correspond to 6, 12, 18 and 24 minutes events in the physical model. This is an important aspect to consider when designing Particle Image Velocimetry (PIV) systems because the duration of the event simulated has to be related with the time acquisitions of the cameras and the capacity of the hardware (Weitbrecht et al., 2001 – Weitbrecht et al., 2002).

4.10 Flow conditions at network junctions

Results in this section have been previously presented at the 9th International Conference on Urban Drainage Modelling, Belgrade, Serbia, 3-8 September 2012 and are under review for publication. The experimental part of this work and the associated data presented has been collected and analysed by the author. The numerical analysis and sewer network modelling described in this section has been conducted by collaborators at the University of Coimbra, in particular by PhD student Nuno Melo.

The aim of this work was to compare the observed flow in a scale model of an urban drainage system, with the results obtained using two one-dimensional (1D) numerical models, SIPSON and SWMM, in order to validate the internal boundary conditions. The calibration of the models was completed using the experimental data of the two storm events occurred on 12th December 2008 and 17th January 2009 (data measured by a rain

gauge installed in the basin), thus validating the internal boundary conditions. Infoworks was not used for this comparison because this model (i.e. the one developed and made available by Yorkshire Water) was not an exact replica of the experimental facility. In particular, the manhole angles and location in the infoworks model and the physical model were not identical. In order to provide a more robust comparison between computational and physical models it was necessary to build a model which represented the physical model exactly. For this work two one-dimensional models, SIPSON and SWMM were used.

SIPSON is a 1D/1D integrated hydraulic model developed by Djordjevic (2001) at the University of Belgrade. The acronym SIPSON stands for "Simulation of Interaction between Pipe flow and Overland flow in Networks". SIPSON, besides being a hydraulic model, also incorporates a hydrologic model (rainfall runoff), called BEMUS, which is used for calculating the surface runoff input to the hydraulic model. A GIS interface, named 3DNet, works as the platform for management and editing of data and visualization of the SIPSON results. The hydraulic model solves simultaneously the continuity equations for network nodes, the complete St. Venant equations for the 1D network and the links equations (Djordjevic et al., 2005). The modelling of the manhole head losses was done by considering local losses (ΔH) for both the inlet and the outlet of the manholes quantified through equations of the type $\Delta H=K(V^2/2g)$ in which V is the average velocity in the upstream pipe, and K is the head loss coefficient (which is to be calibrated). Storm Water Management Model (SWMM) is a dynamic rainfall-runoff model. The component of runoff operates on a collection of sub-catchment areas that receive precipitation and generate runoff. The routing of the SWMM runoff is done through the system of channels, pipes and devices. The flow routing in this case is calculated, using the complete one-dimensional Saint Venant flow equations (Dynamic Wave Routing) (Rossman, 2010). This routing method can account for channel storage, backwater, entrance/exit losses, flow reversal, and pressurized flow (Rossman, 2010). As in SIPSON, the head losses in the manholes are considered by introducing local loss coefficients at entry and exit of each pipe.

In order to obtain consistent modelling results with SIPSON and SWMM, a calibration process was applied. The selected calibration parameters included roughness of the pipe and the local head losses at manholes. The computational model parameters where adjusted such that the best possible fit was obtained between the computational and physical model results for all the unsteady simulations tests (i.e. one set of calibration

parameters for all tests). Calibration is achieved through an iterative process, in the first stage the frictional losses are calibrated without the local head losses taken in consideration at the manholes, with pipe roughness values ranging between 0.008-0.014. In a second stage the energy losses coefficients (K) are calibrated whilst keeping constant the roughness obtained in the previous step. The energy losses values at the inlet vary from 0.05 to 1 (full sudden enlargement) and the outlet energy losses coefficients vary from 0 to 0.5 (full sudden contraction).

Both SIPSON and SWMM models have the option to be run both including and neglecting local head losses. A direct comparison of the results from the computational models (with and without the consideration of local losses) and the observations from physical model allows the quantification of the importance of local head losses within urban drainage models.

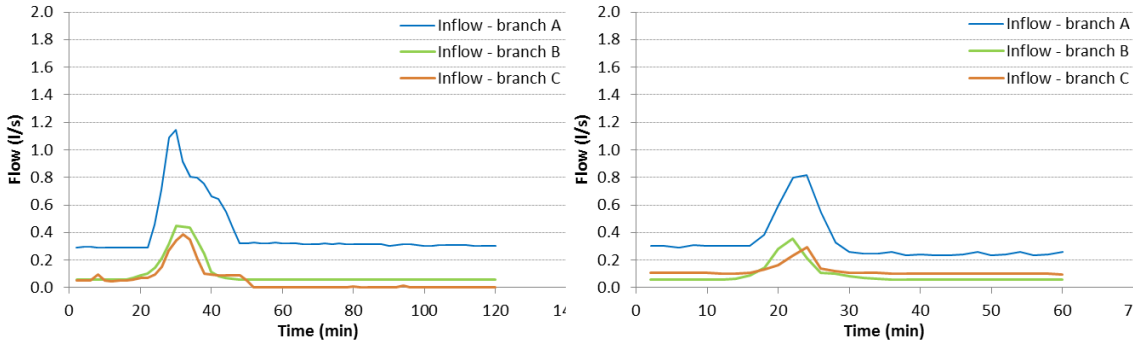

a) b)

Figure 85- Inflow hydrographs at each inlet pipes of the system, a) event of 12th December 2008 and b) event of 17th January 2009.

4.11 Results and Discussion

Figures 86 to 91 show the variations of the water depth in the manholes over the simulated events. In each graph the results obtained experimentally in the scale model and the results obtained by the SIPSON and SWMM models are compared. Two computational cases are analysed in both SIPSON and SWMM. The first case considers only the continuous head losses (neglecting local losses) and the second case considers the continuous head losses and the local head losses at the manholes.

The flow Froude number is always less than 1 irrespectively of the event (and regardless of local head losses at the manholes), indicating the presence of subcritical flow. The SIPSON model best reproduced the water depths observed in manholes 1, 2

and 3 for the event of 12th December 2008, if the local head losses are neglected. This includes better reproduction of the maximum peak depths recorded in the manholes. It was observed that SWMM suffered from over dampening the flow peaks. The results obtained by both models when including local head losses were very similar. For the event of the 17th of January 2009, the conclusions are approximately the same. However in this case both SIPSON and SWMM over predict the time of peak when compared with the experimental data. In manhole 4 there was a significant difference between the all the computationally simulated and experimentally recorded depths. This could be due to the more complex flow structure in this junction manhole. A significant proportion (>33%) of the flow enters the manhole at an angle of 45° causing a higher turbulence and a consequent increase in the water level, a situation that is not reproduced by the models. In manhole 5 the flow depths resulting from SIPSON fit relatively well with the experimental data. Although this is also a junction manhole the incoming lateral flow (at 45°) is smaller than 25% of the flow in the main flow direction, and hence has less of an effect.

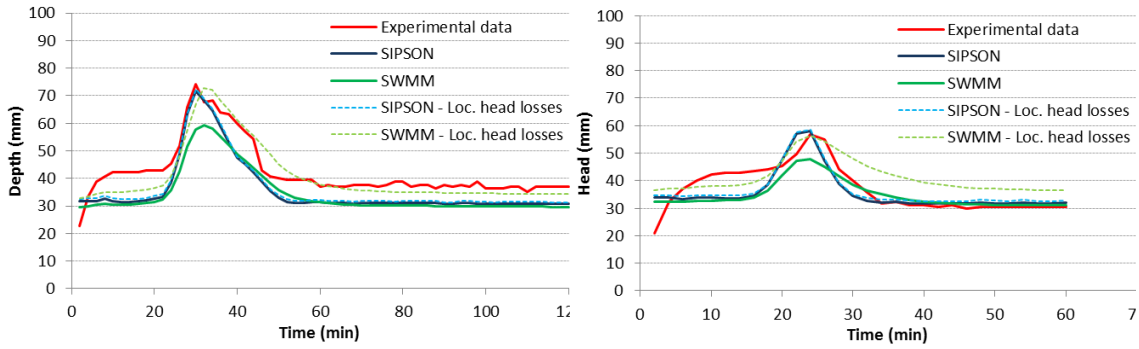

a) b)

Figure 86. Variation of water depth at manhole 1, a) event of 12th December 2008 and b) event of 17th January 2009 (Potential error included ±2 mm).

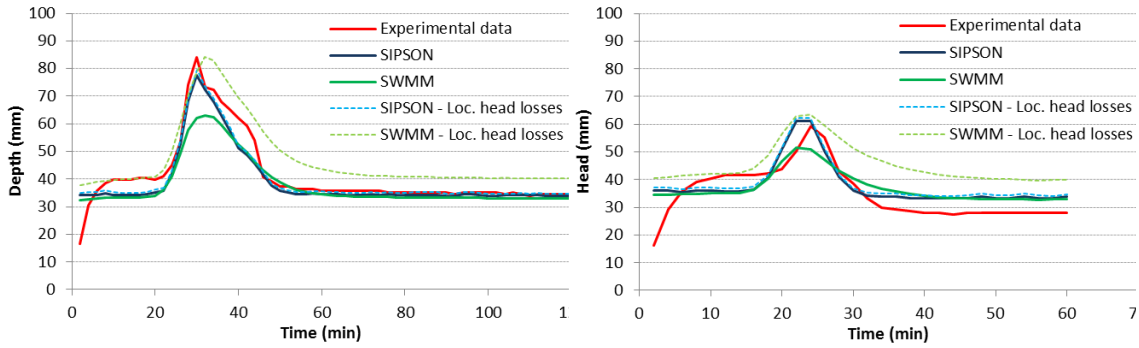

a) b)

Figure 87. Variation of water depth at manhole 2, a) event of 12th December 2008 and b) event of 17th January 2009. (Potential error included ±2 mm).

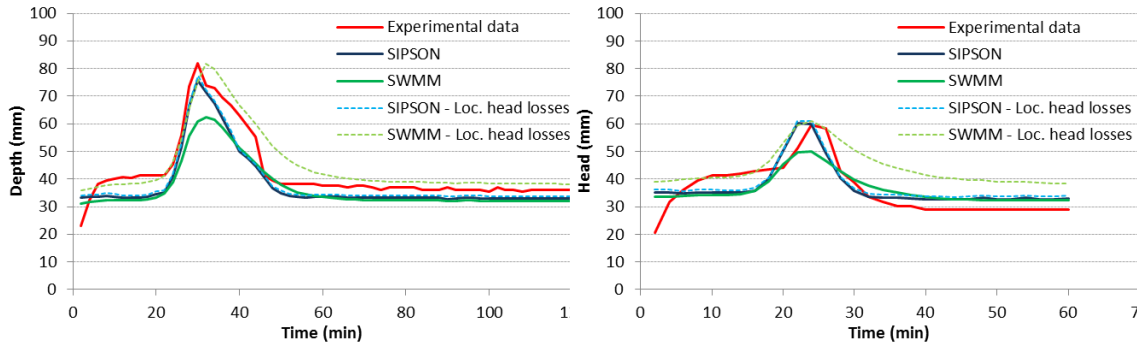

a) b)

Figure 88. Variation of water depth at manhole 3, a) event of 12th December 2008 and b) event of 17th January 2009. (Potential error included ±2 mm).

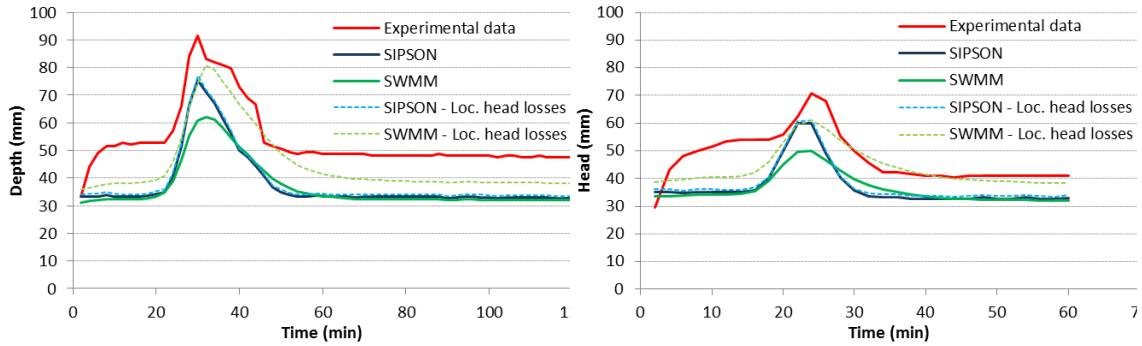

a) b)

Figure 89. Variation of water depth at manhole 4, a) event of 12th December 2008 and b) event of 17th January 2009. (Potential error included ±2 mm).

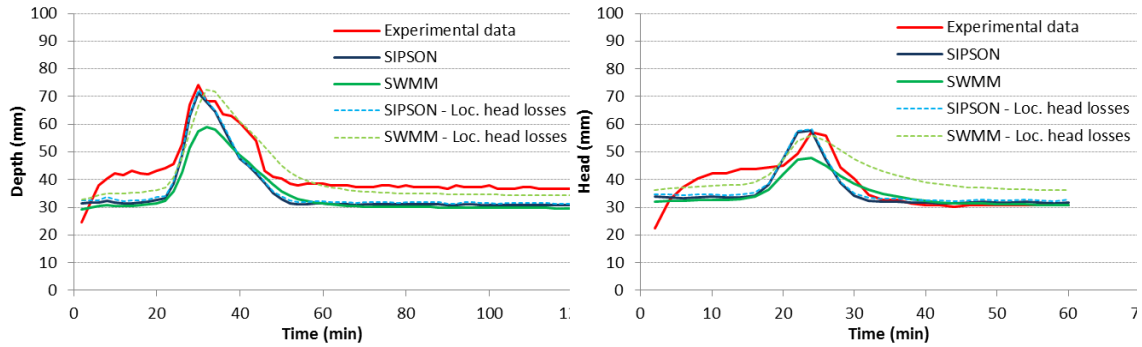

a) b)

Figure 90. Variation of water depth at manhole 5, a) event of 12th December 2008 and b) event of 17th January 2009. (Potential error included ±2 mm).

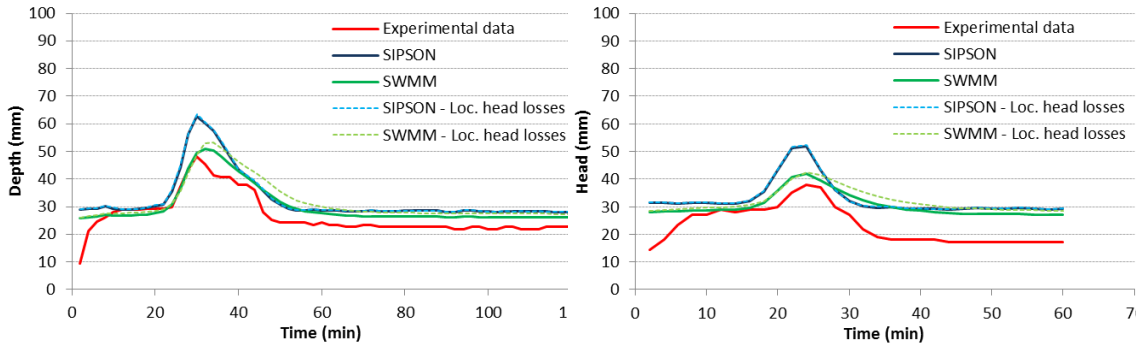

a) b)

Figure 91. Variation of water depth at manhole 6, a) event of 12th December 2008 and b) event of 17th January 2009. (Potential error included ±2 mm).

In the case of manhole 6 (Figure 91), for both simulated events, the water depths obtained by the numerical models are higher than the ones observed in the experimental facility. One possible reason is the position of the pressure sensor that is next to the downstream pipe. This is the only manhole for which the downstream pipe has a larger diameter than ø 75 mm, i.e. ø 100 mm. When including both friction and local head losses, SIPSON is the model that best reproduces the experimental data for manhole 1, 2, 3, 4, 5 in event 1 and 2 while SWMM better represents experimental data observed in manhole 6 for both events. In Figures 92 to 95 the flow rate at the different manholes obtained using the models SIPSON and SWMM for the different simulation conditions are presented (with and without head losses in manholes). Comparing the flow rates obtained from both rainfall events, the flow rates obtained from the modelling with SIPSON are larger than those obtained by SWMM. Comparing the flow rates with and without inclusion of the head losses in manholes, the results obtained from SIPSON are relatively insensitive to the inclusion of local energy losses.

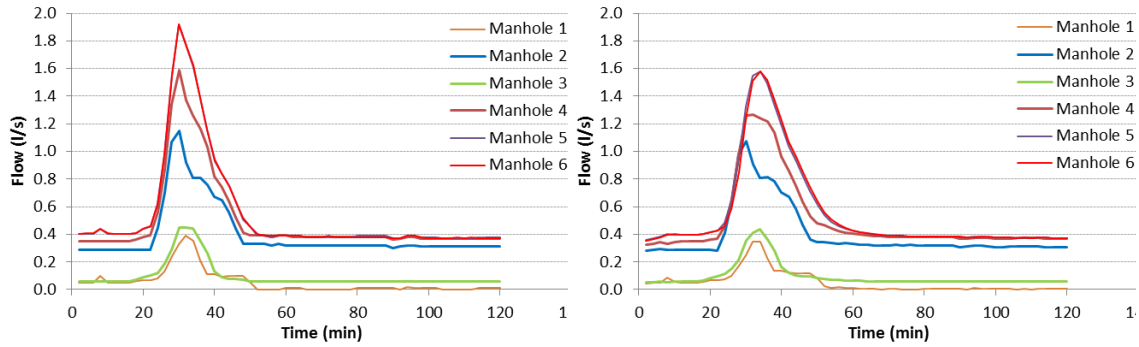

a) b)

Figure 92. Variation of flow rate at manholes, for the situation without considering head losses in manholes for the event of 12th December 2008, a) SIPSON results and b) SWMM results.

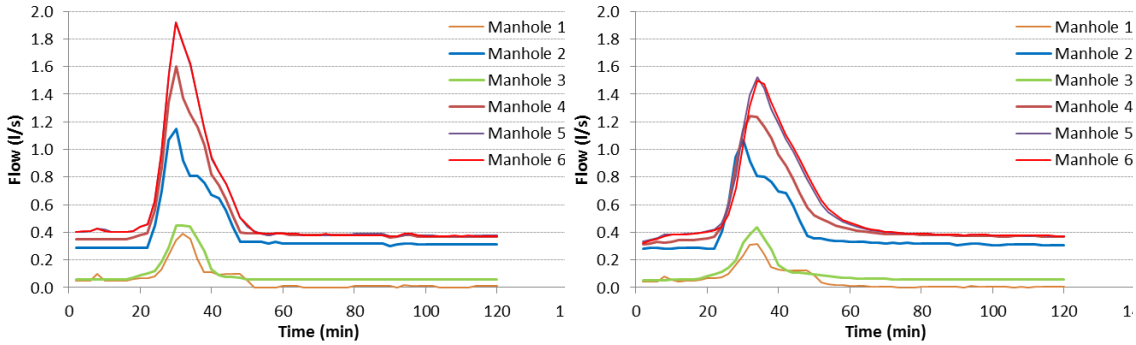

a) b)

Figure 93. Variation of flow rate at manholes, for the situation considering head losses in manholes for the event of 12th December 2008, a) SIPSON results and b) SWMM results.

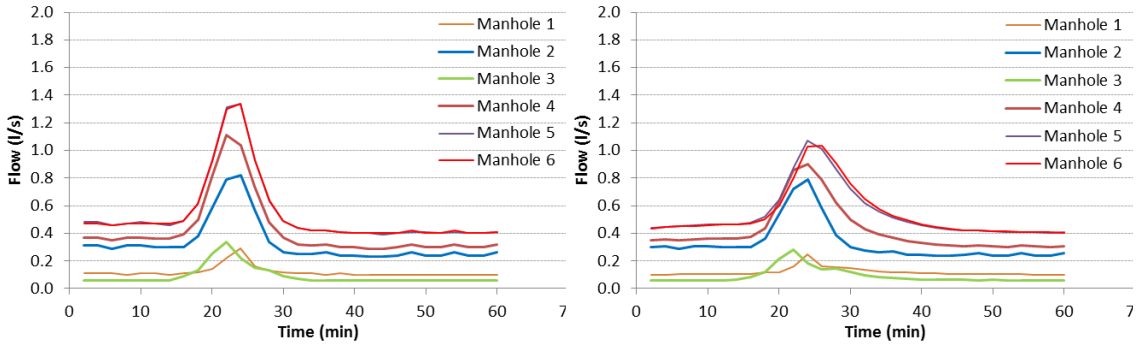

a) b)

Figure 94. Variation of flow rate at manholes, for the situation without considering head losses in manholes for the event of 17th January 2009, a) SIPSON results and b) SWMM results.

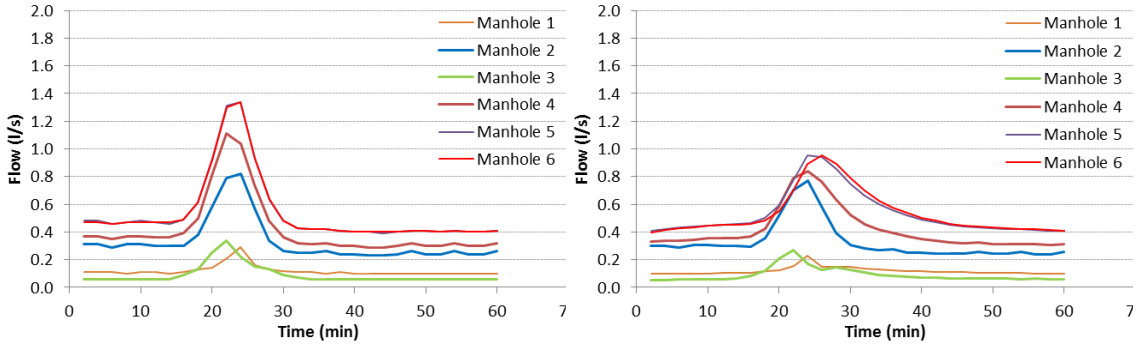

a) b)

Figure 95. Variation of flow rate at manholes, for the situation considering head losses in manholes for the event of 17th January 2009, a) SIPSON results and b) SWMM results.

In SWMM is not possible to define the size of the junctions (i.e. manhole diameter), hence this does not allow the effects of storage to be taken into account unless junctions are switched to reservoirs.

This could explain the differences found in the calibrated roughness parameter obtained for the different models: after the calibration the value of roughness in SWMM are slightly higher than in SIPSON in order to compensate for the damping of the peak flows.

In summary, tests have shown that:

- SWMM shows a higher peak damping than SIPSON;
- For the first event, SWMM overshoots the time to peak when compared with experimental data.
- After calibration, the inclusion of head losses did not significantly improve the overall performance of the computer models over the events tested.

Finally, it should also be mentioned that both models did not reproduce the start-up time seen in the experimental facility. This could also be obtained in SWMM and SIPSON but it would require a further calibration for a gradual input-curve that could simulate the start-up time.

In conclusion hydraulic datasets obtained by the experimental facility have been utilized to verify the accuracy of SWMM and SIPSON. When modelling the experimental facility it was found that SIPSON reproduces fairly well the water depths in the manholes of the drainage system when considering the friction head losses and the local losses at the manholes.

5 Results of above/below ground physical model

This chapter presents the results obtained in the second phase of this research, with the experimental apparatus as described in section 3. This includes the simulation of different pluvial flooding scenarios in the experimental facility after the construction of an urban surface on the top of the pipe network.

The aim of this phase of the research is to investigate flow exchange from sewer to surface flows in flood events and investigate the applicability of weir and orifice linking equations utilized in hydraulic flood models.

A subset of the results in this section has been previously presented at the 11th HIC, International Conference on Hydroinformatics, New York, USA, 17 August 2014- 21 August 2014.

5.1 Exchange below/above ground urban floods: steady flow conditions

Within the physical model during flow events, flow exchange can be quantified via mass balance equations using measured flow data at the facility inlets and outlets as follows:

$$Q_e = Q_1 - Q_3 = -Q_2 + Q_4 \qquad \text{Equation 57}$$

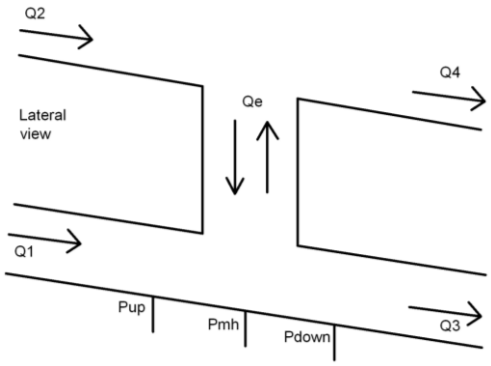

Figure 96- Scheme of flow exchange.

Three different scenarios have been tested and investigated using the physical model:

1. Water running on the urban surface with no flow running into the pipes, to quantify the flow exchange from the above system to the below system;
2. Water running through the pipes and surcharging onto the urban surface, with no additional surface flow (i.e. Q_2=0). To determine the flow exchange from the below system to the above system with no surface water;
3. Water running through the pipes surcharging onto the urban surface, with additional flow (i.e. Q_2>0). To determine the flow exchange from the below system to the above system in the presence of shallow surface flow.

As previously explained in section 2.7, according to the framework proposed by Djordjevic and Chen, 2010, flow exchange is dependent on the relative head between sewer and surface flow and is commonly modelled using weir and/or orifice equations.

Within the experimental model, pressure head within the below ground system can be measured directly by the use of three pressure transducers, located respectively upstream, downstream and inside the manhole. Pressure (depth) on the surface can be measured using six pressure transducers: one located upstream the manhole, one downstream with additional two on the right and two on the left to cover the entire area, as displayed in figure 38.

Within this system datum is defined as the free surface bed level, 478 mm above the pipe invert. Velocity at each point in the system can be calculated using mass conservation principles and knowledge of inlet and outlet flows, pipe geometries and free surface depths.

5.1.1 Scenario 1

Five tests have been conducted to replicate surface to sewer transfer with no pipe flow. For each test, different parameters have been quantified as follows:

Head in pipe upstream of the manhole

$$Hup,p = \frac{P_{up,p}}{\rho g} + \frac{{V_{up,p}}^2}{2g} \qquad \text{Equation 58}$$

Head in pipe downstream of the manhole

$$Hdown,p = \frac{P_{down,p}}{\rho g} + \frac{{V_{down,p}}^2}{2g}$$ Equation 59

Head in surface upstream of the manhole (interface)

$$Hup,s = \frac{P_{up,s}}{\rho g} + \frac{{V_{up,s}}^2}{2g} + z$$ Equation 60

Head in surface downstream of the manhole (interface)

$$Hdown,s = \frac{P_{down,s}}{\rho g} + \frac{{V_{down,s}}^2}{2g} + z$$ Equation 61

Total Head Losses, H_t (m)

$$(Hup,p + Hup,s) - (Hdown,p + Hdown,s)$$ Equation 62

For determining kinetic energy in equation 58 and 59, the velocity is calculated using the measured flow rate at the facility sewer inlet or outlet (respectively) and pipe cross-section.

For determining kinetic energy in equation 60 and 61, the velocity is calculated using the measured flow rate at the facility surface inlet or outlet (respectively) and open channel cross-sectional area. Due to the width of the flume and the relatively low exchange rates, the differences in the kinetic energy of the surface flow upstream and downstream of the manhole were negligible in all cases (< 0.001m).

Table 17 presents the experimental hydraulic results obtained for each simulation.

Table 17 – Exchange flow-rate, pressure components and hydraulic head upstream, downstream and on the manhole and hydraulic conditions inside the manhole and on the urban surface obtained simulating the free weir scenario.

Test N.	Q_e (l/s)	Q in Surf. (l/s)	Hup,p (m)	$Hdown,p$ (m)	Hup,s (m)	$Hdown,s$ (m)	US Surface Water depth (m)	Total Head Losses H_t (m)
1	1.10	6.61	0.081	0.075	0.489	0.489	0.009	0.007
2	1.28	7.36	0.063	0.059	0.490	0.489	0.010	0.005
3	1.38	8.05	0.075	0.069	0.491	0.490	0.011	0.006
4	1.53	9.44	0.108	0.101	0.492	0.491	0.012	0.007
5	1.71	10.17	0.084	0.078	0.493	0.492	0.013	0.006

Figure 97– An example of surface to sewer exchange reproduced within the experimental facility.

A linear relationship exists between water depth on the surface and flow exchange. This can be expressed in the form of the weir equation (figure 98).

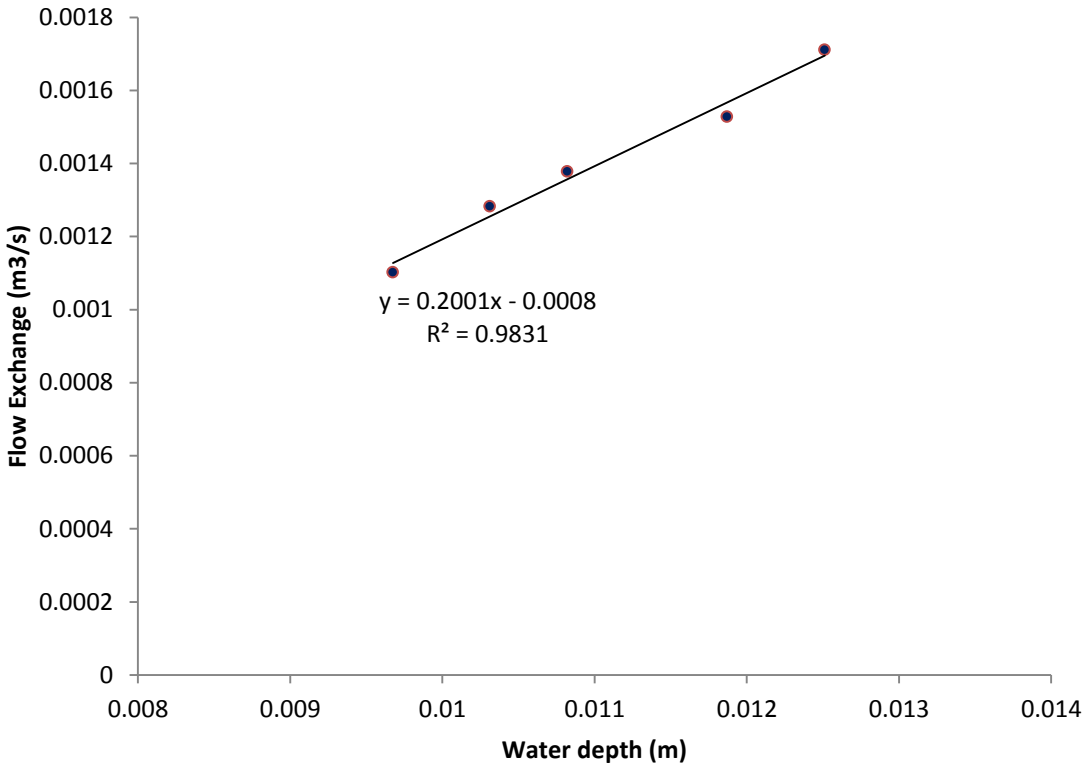

Figure 98– Flow exchange vs water depth urban surface.

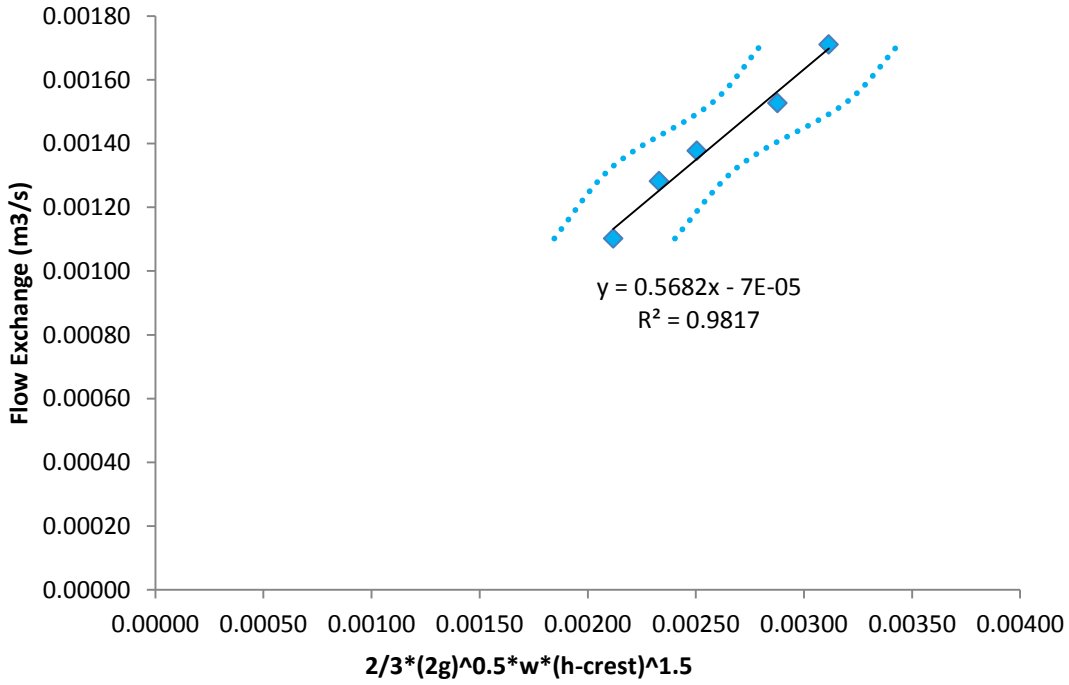

Figure 99– Observed flow exchange vs weir equation Error bars represents expected measurement error within the flow and pressure instrumentation (see section 3.6.3).

This relationship has confirmed then that in steady conditions the manhole can be considered as a weir and the discharge coefficient can be approximated as 0.568, with a good correlation of R^2=0.98.

5.1.2 Scenario 2: Outflow with urban surface flow

Five tests have been completed for scenario 2 with flow exchange ranging between 0.6-4.68 l/s. Surface flow was subcritical in all conditions.

Table 18 presents experimental values obtained for the five tests using equations in section 5.1.1.

Table 18 –Exchange flow-rate, pressure components and hydraulic head upstream, downstream and on the manhole and hydraulic conditions inside the manhole and on the urban surface obtained simulating the orifice scenario with no interaction of shallow water into the urban surface.

N.	Q ex. (l/s)	Q in Sew. (l/s)	Hup,p (m)	$Hdown,p$ (m)	Hup,s (m)	$Hdown,s$ (m)	US Surface Water depth (m)
1	0.63	5.55	0.580	0.519	0.482	0.482	0.0038
2	1.16	6.16	0.609	0.527	0.482	0.482	0.0043
3	1.65	6.72	0.636	0.544	0.483	0.483	0.0046
4	2.91	7.88	0.700	0.581	0.483	0.484	0.005
5	4.68	9.13	0.778	0.622	0.484	0.486	0.006

Total losses between upstream and downstream of the manhole are displayed in Figure 100.

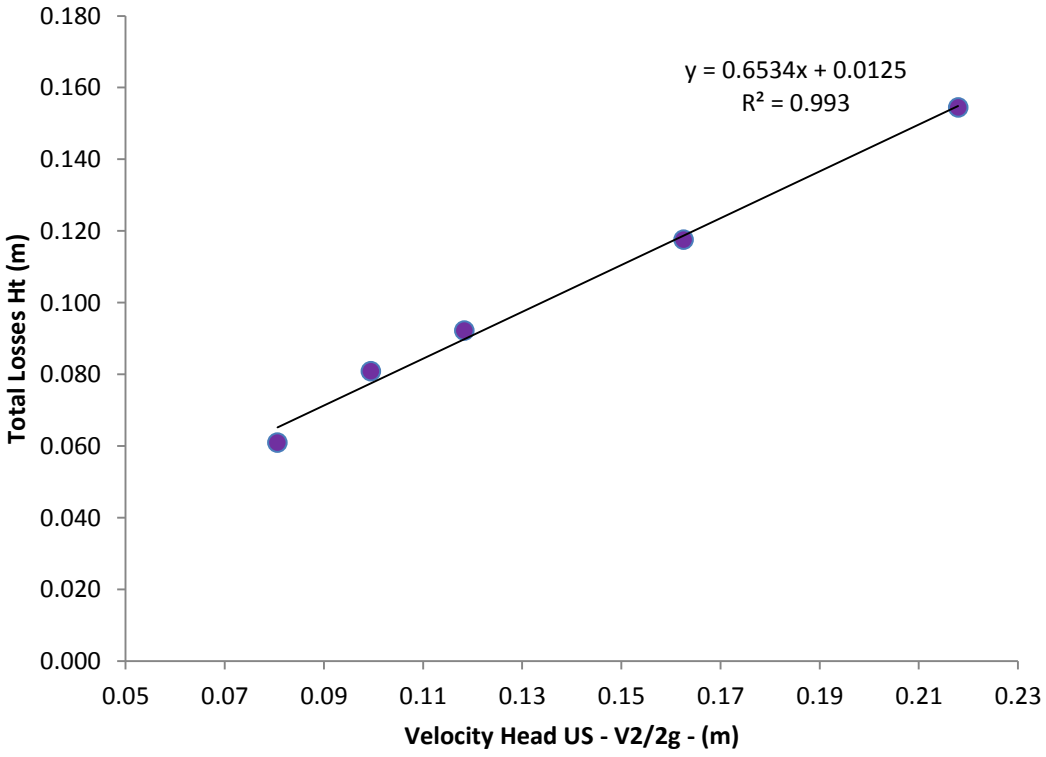

Figure 100 - Total energy losses in the manhole vs velocity head upstream the manhole.

A linear relationship exists between hydraulic head in the pipe and flow exchange. This can be expressed in the form of the orifice equation (Figure 101).

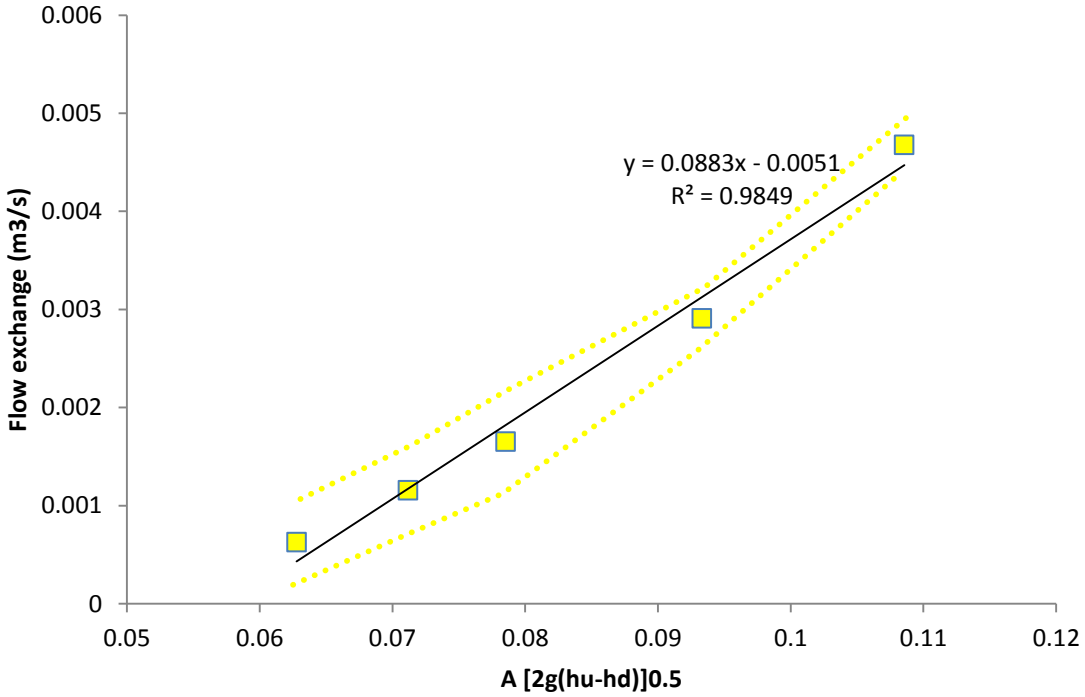

Figure 101– Observed flow exchange vs orifice equation Error bars represents expected measurement error within the flow and pressure instrumentation (see section 3.6.3).

This relationship has confirmed then that in steady conditions the manhole can be considered as a orifice and the discharge coefficient can be approximated as 0.0883, with a good correlation of R^2=0.98.

5.1.3 Scenario 3: Outflow with interaction of shallow water in the urban surface

This final scenario replicates the water exceeding the manhole and reaching the urban surface where there is also a component of shallow surface flow running from the inlet tank to the outlet tank (Q_2>0).

Figure 102- Examples of sewer to surface exchange simulated with the experimental facility.

The hydraulic parameters for each of the 6 tests are displayed in table 19.

Table 19 - Exchange flow-rate, pressure components and hydraulic head upstream, downstream and on the manhole and hydraulic conditions inside the manhole and on the urban surface obtained simulating the orifice scenario with interaction of shallow water into the urban surface.

Test N.	$Q_{ex.}$ (l/s)	Q in Sew. (l/s)	Hup,p (m)	$Hdown,p$ (m)	Hup,s (m)	$Hdown,s$ (m)	US Surface Water depth (m)	Total Head Losses H_t (m)	Re_m (/)
1	1.26	5.52	0.584	0.520	0.539	0.565	0.011	0.0376	93665
2	2.46	6.71	0.638	0.549	0.530	0.578	0.012	0.0399	113894
3	3.57	7.87	0.701	0.585	0.525	0.597	0.013	0.0441	133485
4	4.39	8.77	0.757	0.614	0.523	0.611	0.0135	0.0542	148810
5	5.05	9.43	0.799	0.637	0.521	0.625	0.014	0.0586	159924
6	5.51	9.90	0.833	0.654	0.521	0.638	0.0141	0.0618	167857

Where Re_p= Reynolds through the pipe and Fr_s = Froude on urban surface.

Based on scaling factors, as discussed in section 3.1 the tests conducted here represent a "full scale" flow velocity range of 0.21-0.38 m/s within the pipes and 0.19-0.25 m/s on the urban surface. Figure 103 presents the relationship between the total energy losses within the system and velocity head of the inlet flow.

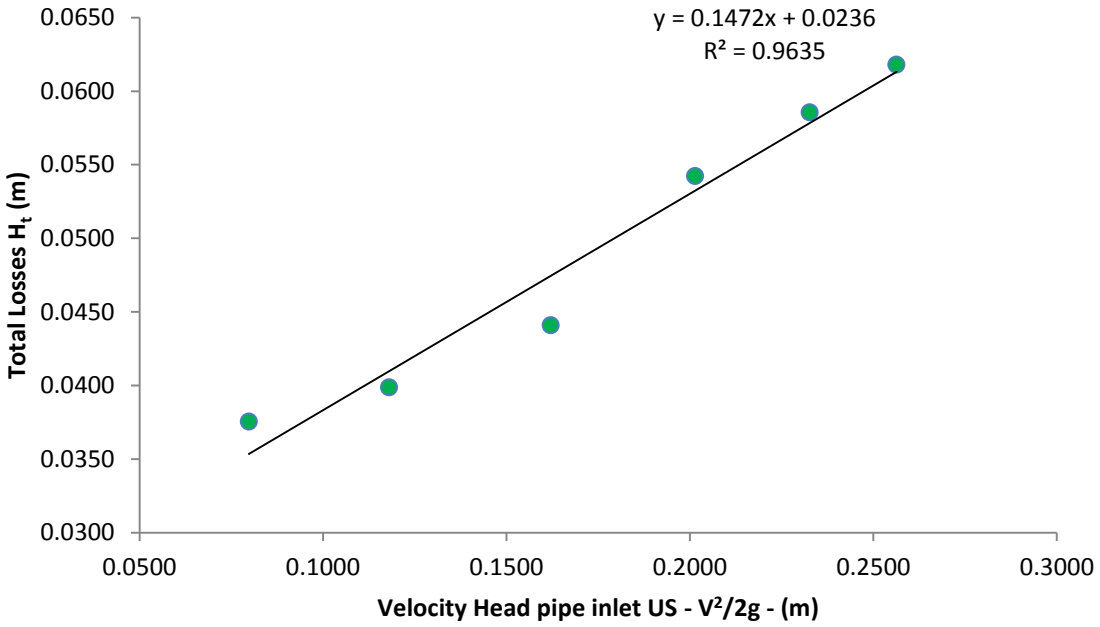

Figure 103- Total energy losses within the system and velocity head of the inlet flow.

A linear relationship exists between the hydraulic head difference between pipe, surface flow and flow exchange. This can be expressed in the form of the orifice equation (Figure 104).

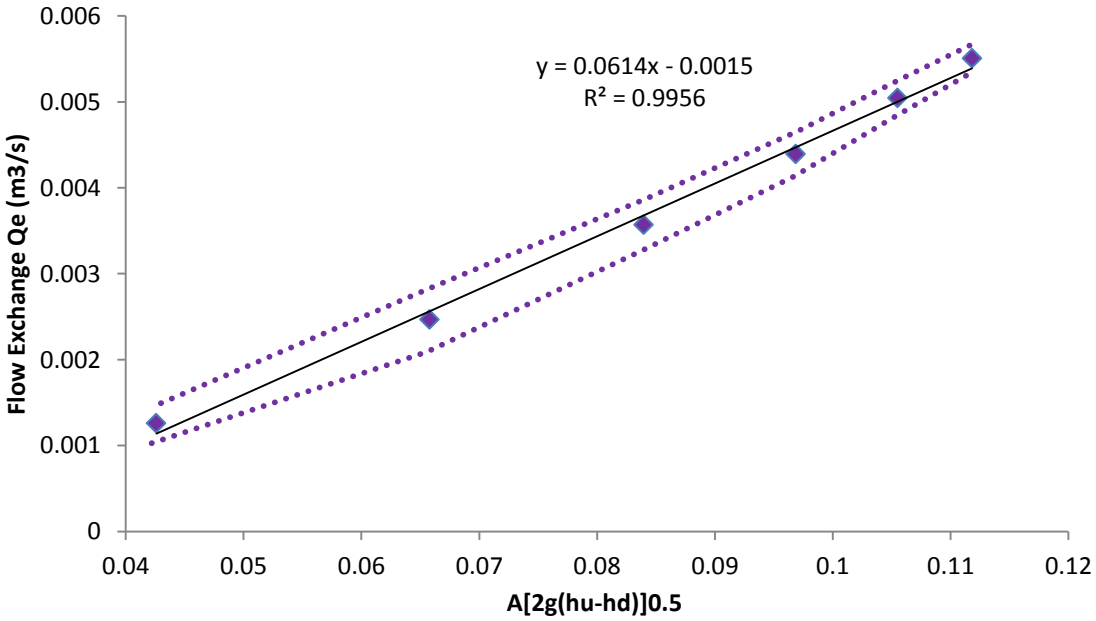

Figure 104 - Flow exchange as a function of head difference measured immediately upstream of the manhole. Error bars represents expected measurement error within the flow and pressure instrumentation (see section 3.6.3).

This relationship has confirmed then that in steady conditions the manhole can be considered as a orifice and the discharge coefficient can be approximated as 0.061, with a good correlation of R^2=0.99.

6 Conclusions

The aim of this thesis was to use a physical model to improve understanding of flood risk in the urban environment. Four specific research objectives were identified, requiring two distinct physical model setups to be designed, constructed and tested. The first experimental setup was based on an existing laboratory model at the University of Sheffield, tests were conducted to identify local head losses through manholes under a range of inlet conditions and flow rates, as well as test and verify the performance of numerical models (SIPSON and SWMM) during scaled unsteady storm flow events. This work required modification of the existing physical model inlet conditions in order to achieve the flow rates and Reynolds numbers required. The main findings of this phase of work are that the energy loss coefficient found for manholes with a "in line" configuration fit within the range of existing values found in literature. The work has presented new head loss values for manholes characterized by multiple inlets, with a lateral inflow orientated at 45 degrees to the main flow direction. These are significantly higher than those for in line manholes, this is most likely due to more complex flow patterns which cause effects of acceleration and retardation and flow interference. K values are sensitive to upstream and downstream pipe flow conditions. K_{ij} values for junction manholes have been compared to existing theoretical frameworks; however differences in trends predicted using the frameworks and experimental observations are observed. Overall hydraulic computer models replicating the physical system reproduce the hydraulic characteristics well. Considering friction losses SIPSON is the model that best reproduces the experimental data for manhole 1, 2, 3, 4, 5 of event 1 and 2 presented while SWMM better represents experimental data related to manhole 6 (downstream in the system) for both events. Tests have shown that by including local head losses, SWMM improves its performance. The analysis has demonstrated that neglecting local energy losses reduces their performance. This confirms the need to provide more experimental data to improve the accuracy and efficiency of computer models.

The second phase of the research involved the construction of a novel above/below ground flow interaction model. This model was designed to provide datasets concerning one of the most significant current uncertainties in urban flood modelling, regarding energy losses and flow interaction at the interface between pipe network and surface

flow at manhole junctions. The aim of this phase of the research was to quantify the suitability of weir and orifice equations to describe the interaction between above and below ground system, and determine a suitable range of coefficients of these equations. The main findings of this phase of the work were the confirmation that weir and orifice equations can be used to quantify flow exchange between a sewer system linked to an urban surface through a single manhole under steady flow conditions. This has been verified under different pluvial conditions replicated within the facility. Additionally, for each specific scenario a range of discharge coefficients has been calculated. For a typical weir scenario, with water running onto the urban surface reaching the sewer system, 0.57 is the best fit value. Regarding the orifice scenario, for simulations that have been characterized by water escaping the manhole reaching the urban surface the best fit coefficient is 0.0883. Finally, when there is a complex interaction between water running into the surface and water escaping the sewer from the manhole the best fit discharge coefficient is 0.061.

The experimentally derived discharge coefficient in the orifice flow regime was unable to be directly compared to other studies due to the lack of C_o prediction at low head in the available literature and similar experimental studies completed.

The limitations of the present study should be noted. The current model considers an open manhole which discharges directly into the surface; this does not include the effects of any manhole lid on the flow interaction. In addition, unsteady events have not yet been considered, further research should consider how energy losses are effected by rapidly changing flow rates which are common in urban flooding situations.

7 Further work

This model considers an open manhole which discharges directly into the surface. Despite the fact that in some countries this aspect is something normal during urban flooding events (in Portugal for example the Civil Protection has to remove all the gates to avoid blockages as showed in figure 105a and 105b), manholes are covered by gridlines which influence the discharge of the flow.

Figure 105– a) Viana do Castelo, urban inundation (Source ARMENIO BELO/LUSA, accessed the 06/06/2014 http://www.tvi24.iol.pt/sociedade/mau-tempo-lisboa-cheias-inundacoes-meteorologia-tvi24/1203790-4071.html) b) Another example, urban inundation and gate removal. (Photo LUIS PARDAL/GLOBAL IMAGENS, accessed the 06/06/2014 (Right)http://www.jn.pt/PaginaInicial/Sociedade/Interior.aspx?content_id=2862575)

Hence future work will focus on designing a "lid" above the manhole to make the system more realistic and provide more datasets with different configurations.

As described, computer models are inherently problematic to verify due to the difficultly of acquiring reliable data during the flood event and most models are calibrated using only an estimated measure of the extent of flooding. Similarly, existing models do not currently attempt to quantify the transport and fate of sewer derived pollutants and hence it is difficult to assess the risk of exposure and the potential impact of flood waters on health. Manholes are interaction points where there is a critical transfer of flow and pollution and this process is difficult to quantify due to the complex and time varying nature. Understanding such behaviour is essential to accurately evaluate urban flood risk by hydraulic models.

Modelling the transport of harmful contaminants/pollutants from sewer interface points is a relevant step to increase the accuracy of computer models and it has only recently been attempted (Pathirana, 2011). Coupled with studies of health risk from exposure to flood water (Fewtrell et al, 2011) such models could be used to predict both areas most at risk from contamination and the potential health impacts of flood events. The large

number of uncertainties involved (e.g. impact of urban topographies on hydraulic profiles, storage zones and dispersion) means that such modelling is at an early stage, and is extremely prone to inexact calibration and verification.

The next feasible outputs from this experimental facility will provide the first data sets for such advanced calibration and verification, thereby providing enhanced opportunities for the prediction of accurate combination between flood flow and contaminant movement during flood events. The results will subsequently be used to improve the accuracy of commercial modelling software with significant benefits in the evaluation of flood risk and the prioritisation of asset investment.

Future work will utilise this unique surface/subsurface together with numerical and computational advances in the solution of the hydraulic and pollutant transport equations. The main challenge will consider the experimentally investigation of the transport of soluble material from sewers to surface flows via manholes and determine the transport and mixing characteristics in typical overland shallow flow flooding conditions.

Pollutant transport through the system will be quantified in both steady and time varying flow conditions. In time varying tests, dye will be injected into the pipe immediately prior to a manhole surcharge event to simulate contaminates being flushed through the system and quantify the total transfer of mass to surface flow via an individual manhole. Different surface topographical setups (Figure 106) will be tested to determine how features influence mass transport in surface flow via the creation of turbulent structures, local velocity shear and trapping zones (characterised with PIV measurements, using the equipment designed and tested during the final part of this research). Three test surface topographies will be installed and tested which are designed to simulate the effect of typical street features. The geometry of surface features will be based on the sewer scaling.

1. **Featureless bed** – Initial tests to characterise mixing over a range of flow conditions.
2. **Road and pavement** – At low flows, pavements will promote transverse velocity gradients and shear. At higher flows, flow will overtop pavements, potentially creating turbulent mixing layers and considerable extra velocity shear.

3. **Trapping zones** - A range of street features may act as trapping zones and affect the transport of pollutants. Such zones will be simulated by constructing gaps in the pavement profile.

Dimensionless mixing coefficients (i.e. normalised by flow depths and shear velocities) within the surface flow will be determined. Characterisation of the velocity fields via PIV developed during this research will be determined. Mixing coefficients will be initially quantified for the featureless bed in steady uniform flow conditions via both analytical and numerical solutions. By achieving that, a unique data set that will be made available to other researchers and software developers.

Once these results will be provided, considering that hydraulic models are increasingly being used to plan significant asset investment and form the basis of flood awareness/warning schemes, there will be significant benefits in terms of more efficient drainage design/investment and increased resilience to flood events.

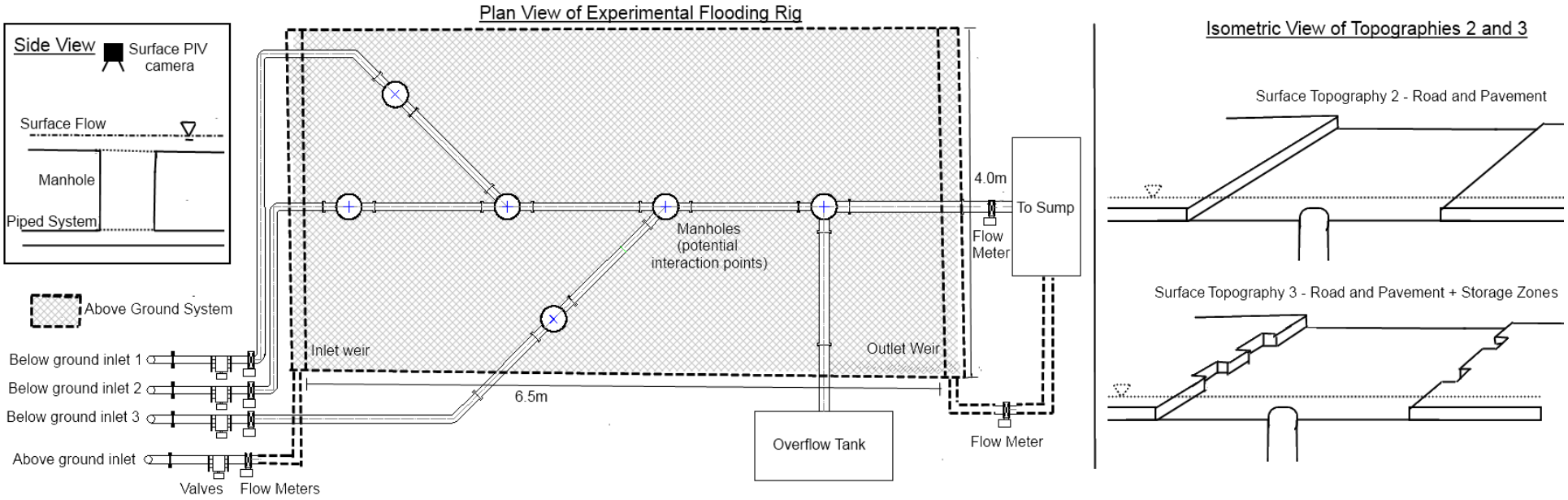

Figure 106- Picture of surface profile facility and diagram of testing setup (adapted from Melo et al. 2012)

8 References

Ackers P. (1959) An investigation of head losses at sewer manholes. *Civil Engineering and Public Work Review*, 54, 637, 882-884 and 1033-1036.

Archer B., Bettes F., Colyer P.J. (1978) Head losses and air entrainment at surcharged manholes. Report No IT 185, Hydraulic Research Station, Wallingford, England.

Arao, S., Kusuda T., Moriyama K., Hiratsuka S., Asada J., Hirose N. (2012) Energy losses at three-way circular drop manholes under surcharged conditions. *Water Science and Technology*, 66, **1**.

Ashley, R.M., Balmforth, D.J., Saul, A.J., Blanskby, J.D. (2005) Flooding in the future - Predicting climate change, risks and responses in urban areas. *Water Science and Technology*, 52, **5**, 265-273.

Asztely M. (1995) Literature Review of energy losses in manholes. The Universiy of Goteborg, Department of Hydraulics.

Bamford T.B., Digman C.J., Balmforth D.J., Waller S., Hunter N. (2008) Modelling flood risk – an evaluation of different methods. WaPUG Autumn Conference, Blackpool.

Bazin P.H., Nakagawa H., Kawaike K., paquier A., Mignot E. (2014) Modeling Flow Exchanges between a Street and an Underground Drainage Pipe during Urban Floods. *Journal of Hydraulic Engineering*, 140, **10**.

Biron P., Best J.L., Roy A.G. (1996) Effects of bed discordance on flow dynamics at open channel confluences. *Journal of Hydraulic Engineering*, 122, **12**, 676-682.

Carpenter G. & Company, LLC, Guy Carpenter & Company Ltd. or Guy Carpenter & Company, S.A.S. (2013) Floods in Eastern Australia.

Chanson Hubert, (1999) Hydraulics of Open Channel Flow: An Introduction - Basic principles, Sediment Motion, Hydraulic Modeling, Design of Hydraulic Structures, *Elsevier*.

Chen A., Djordjievic S., Leandro J., Savic D. (2007) The urban inundation model with bidirectional flow interaction between 2D overland surface and 1D sewer networks. Workshop, *Novatech 2007*, 25-28 June, Lyon, France.

City and County of San Francisco 2030 Sewer System Master Plan (2011) Task 500, Technical Memorandum No.506, Collection System Rehabilitation Program. Climate Change Report.

Cohen B., (2006) Urbanization in developing countries: Current trends, future projections, and key challenges for sustainability. *Technology in Society*, **28**, 63–80.

Defra. The appraisal of human related intangible impacts of flooding. Defra, Flood management division, R&D Technical Report FD2005/TR, London, UK. 2004.

Del Giudice G., Gisonni C. and Hager W. H. (2000). Supercritical flow in bend manhole. *Journal of Irrigation and Drainage Engineering*, 126, 48-56.

Del Giudice G., Hager W.H. (2001) Supercritical flow in bend manhole. *Journal of Irrigation and Drainage Engineering*, ASCE, 126, **1**, 48-56.

Djordjevic S., Prodanovic D., Maksimovic C. (1999) An approach to simulation of dual drainage, *Water Science and Technology*, 39, **9**, 95-103.

Djordjevic S., Prodanovic D., Maksimovic C., Ivetic M. and Savic D. (2005). SIPSON - simulation of interaction between pipe flow and surface overland flow in networks. *Water Science and Technology*, 52, **5**, 275-283.

Djordjevic S., Saul A.J., Tabor G.R., Blanksby J., Galambos I, Sabtu N. and Sailor G. (2013). Experimental and numerical investigation of interactions between above and below ground drainage systems. *Water Science and Technology*, Vol. 67, **3**, 535-42.

Dottori F., Todini E. (2013) Testing a simple 2D hydraulic model in an urban flood experiment. *Hydrological Processes*, 27, **9**, 1301-1320.

Environment Agency (2010) The costs of the 2007 summer floods in England.

Environmental Engineering Dictionary, Mehdi Ahmadi, http://www.ecologydictionary.org/URBAN_FLOODING (accessed the 06/06/2014).

Fewtrell L. & Kay D. An attempt to quantify the health impacts of flooding in the UK using an urban case study. *Public Health* 2008, **122**, 446–451.

Fewtrell L., Kay D., Watkins J., Davies C., Francis C. (2011) *Journal of Flood Risk Management*, **4,** Issue 2, 77-87.

Flood Risk in Brazil, http://www.preventionweb.net/files/20634_floodriskinbrazil1.pdf , (Accessed on the 4th of November 2013).

Gargano R., Hager W.H. (2002) Supercritical across sewer manholes. *Journal of Hydraulic Engineering, ASCE*, 128, **11**, 1014-1017.

Gisonni C, Hager W.H. (2002) Supercritical flow in the junction. *Journal of Irrigation and Drainage Engineering*, 126, 1, 48-56.

Gurram S.K., Karki K.S. (2000) Subcritical open-channel junction flow. *Journal of Hydraulic Engineering, ASCE*, 126, **1**, 87-91.

Hager W.H. (1989) Transitional flow in channel junctions. *Journal of Hydraulic Engineering*, ASCE, 115, **2**, 243-259.

Hare C.M. (1983) Magnitude of hydraulic losses at junctions in piped drainage systems. Civil engineering transactions, Institute of Civil Engineers, 71-77.

Howarth D.A., Saul A.J. (1984) Energy loss coefficient at manholes. *Proceedings of the 3rd International Conference on Urban Storm Drainage*, June 4-8, 127-136, Gothenburg, Sweden.

Hsu C.C., Wu F.S., Lee W.J. (1998) Flow at equal width open channel junction. *Journal of Hydraulic Engineering, ASCE*, 124, **2**, 186-191.

Hunter, N. M., Bates, P. D., Neelz, S., Pender, G., Villanueva, I., Wright, N. G., Liang, D., Falconer, R. A., Lin, B., Waller, S., Crossley, A. J. & Mason, D. C. (2008) Benchmarking 2D hydraulic models for urban flooding. *Water Management*, 161 (WM1), 13–30.

Hunter NM, Bates PD, Horritt MS, Wilson MD. (2007). Simple spatially distributed models for predicting flood inundation: a review. Geomorphology 90: 208–225.

IPCC (2014) Summary for policymakers. *Climate Change 2014: Impacts, Adaptation and Vulnerability*.

Jha A.K., Bloch R., Lamond J. (2012) Cities and Flooding. A guide to integrated urban flood risk management for the 21st century. © 2012 International Bank for Reconstruction and Development/ International Development Association.

Johnston A.J., Volker R.E. (1990) Head losses at junction boxes. *Journal of Hydraulic Engineering*, 116, 326-341.

Kerr Wood Leidal Associates LTD, Consulting Engineers (2008). Vulnerability of Vancouver Sewerage Area Infrastructure to Climate Change, Final Report. METRO Vancouver, KWL File No. 251.219.

Liebmann H (1970) Der Einfluss von Einsteigschachten auf den Abflussvorgang in Abwasserkanalen. Wasser und Abwasser in Forschung und Praxis. Erich Schmidt Verlag (in German).

Lindvall G. (1984) Head losses at surcharged manholes with a main pipe and a 90 degrees lateral. *Proceedings of the 3rd International Conference on Urban Storm Drainage*, June 4-8, 137-146, Gothenburg, Sweden.

Lindvall G. (1987) Head losses at surcharged manholes. *Proceedings of the AIRH- XXII congress* – IAHR and the Fourth International Conference on Urban Storm Drainage, 140-141, Lausanne, Switzerland.

Lopes P. , Lenadro J., Carvalho R.F., Pascoa P., Martins R. (2013). Numerical and experimental investigation of a gully under surcharge conditions. *Urban Water Journal*, 10.1080/1573062X.2013.831916.

Mark O. (1989) En matematisk model for energitab I broønde. Thesis presented at the Institute of Hydrodynamics and Hydraulic Engineering, Technical University of Denmark. Lyngby, Denmark, in partial fulfilment of the requirements for the degree of Master Science.

Mark O., Weesakul S., Apirumanekul C., Boonya Aronnet S., Djordjevic S. (2004) Potential and limitations of 1D modeling of urban flooding. *Journal of Hydrology*, **299**, 284-299.

Marsalek J. (1981) Energy losses at straight-flow through sewer junctions. Research report No 111. Research program for the abatement of municipal pollution under provisions of the Canada-Ontario agreement on the Great Lakes Water Quality. Training and Technology Transfer Division, Environmental Protection Service, Environment Canada, Ottawa, Ontario, KIA, 1C8.

Marsalek J., (1984) Head losses at sewer junction manholes. *Journal of Hydraulics Engineering, ASCE,* 110, **8**, 1150–1154.

Marsalek J., (1985) Head losses at selected sewer manholes. Unpublished report, National Water Research Institute, Burlington, Ontario.

Marsalek J. (1987) Head losses at junction of two opposing lateral sewers. *Proceedings of the AIRH- XXII congress* – IAHR and the Fourth International Conference on Urban Storm Drainage, 140-141, Lausanne, Switzerland.

Marsalek, J., and Greck, B. J. (1988) Head losses at manholes at 90°bend. Canadian Journal of Civil Engineering, 15, 851–858.

Massey B.S., Ward Smith J. (1998) Mechanics of Fluids, Seventh Edition, Volume 1.

Melo N., Leandro J., Shucksmith J., Rubinato M., Djordjevic S., Saul A.J., Ramos H., L.M.P.de Lima J. (2012) Modelling Internal Boundary Conditions of a Sewer Network. *9th International Conference on Urban Drainage Modelling*, Belgrade, Serbia.

Met Office report, Missler C., Eastman M.D. The Creator Beyond Time and Space. *The Word for Today*, 12-17.

Mrowiec M. (2007) Head Loss at two-way circular manholes in drainage systems under surcharge conditions. *Environment Protection Engineering*, 33, **2**.

Mugdal B., Pani B.S. (1993) Head Losses in sewer manholes. *Proceedings of the Sixth International Conference on Urban Storm Drainage*, Niagara Falls, Ontario, Canada, 134-139.

Neal J.C., Bates P.D., Fewtrell T.J., Hunter N.M., Wilson M.D., Horritt M.S. (2009) Distributed whole city water level measurements from the Carlisle 2005 urban flood event and comparison with hydraulic model simulations. *Journal of Hydrology*, 368, **1-4**, 42-55.

Notaro V., Fontanazza C.M., Freni G., La Loggia G. (2010). Uncertainty connected with design rainfall for urban flood risk evaluation. Novatech, Lyon, France.

Ohl C. & Tapsell S. Flooding and human health. *Br Med J* 2000, **321**, 1167–1168.

Phang X., O'Loughlin G. (2011) Pressure change at stormwater pits with part full flows. *12th International Conference on Urban Drainage*, Porto Alegre, Brazil, 10-15 September.

Parkin G. (2010) The September 2008 Morpeth flood: information gathering for dynamic flood reconstruction. *Summary Report* 31 May 2010.

Pathirana A., Mahen D., Brdjanovic D. 12th International Conference on Urban Drainage Modelling, Porto Alegre, Brazil, September 2011.

Pedersen F.B. and Mark O. (1990) Head losses in storm sewer manholes: submerged jet theory. *Journal of Hydraulic Engineering, ASCE*, 116, **11**, 1317-1328.

Pfister M., Ginsonni C. (2014) Head Losses in Junction Manholes for free Surface Flows in circular Conduits. Technical Note, *Journal of Jydraulic Engineering*, 140, **9**.

Photo Another example, urban inundation and gate removal. (Photo LUIS PARDAL/GLOBAL IMAGENS, accessed the 06/06/2014 http://www.jn.pt/PaginaInicial/Sociedade/Interior.aspx?content_id=2862575)

Photo Viana do Castelo, urban inundation (Source ARMENIO BELO/LUSA, accessed the 06/06/2014 http://www.tvi24.iol.pt/sociedade/mau-tempo-lisboa-cheias-inundacoes-meteorologia-tvi24/1203790-4071.html)

Prodanović D., Djordjević S., Maksimović Č. (1998) GIS assisted model for dual drainage simulation. *Hydroinformatics*, '98, 1, V.Babovic and L.C. Larsen (Eds). Balkema, Rotterdam, 535-542.

Ramamurthy A.S., Zhu W. (1997) Combining flows in 90 º junctions of rectangular closed conduits. *Journal of Hydraulic Engineering*, 123, 1012-1019.

Rouse, H., (1950) Engineering Hydraulics. *Proceedings of the Fourth Hydraulics Conference*, Iowa Institute of Hydraulic Research, John Wiley and Sons, Inc., New York.

Saldarriaga J., Bermúdez N., Rubio D.P. (2012) Hydraulic behaviour of junction manholes under supercritical flow conditions, *Journal of Hydraulic Research*, 50**, 6**, 631-636.

Sangster W.M., Wood H.W., Smerdon E.T., Bossy H.S., (1958) Pressure changes at storm drain junctions. Bulletin No. 41, Engineering Experiment Station, University of Missouri.

Schmidt R. (2011) Urban Flood Risk in Dakar, Senegal. *The World Bank, Africa Disaster Risk Management*.

Serre M., Odgaard A.J., Elder R.A. (1994) Energy loss at combining pipe junction. *Journal of Hydraulic Engineering*, 120, **7**, 808-830.

Seyoum S., Vojinovic Z., Price K.R., Weesakul S. (2012) Coupled 1D and Noninertia 2D flood inundation model for simulation of urban flooding. *Journal of Hydraulic Engineering*, 138, 23-34.

Singh R., Social Vulnerability and Wastewater Related Risks: A case Study of Delhi. Project "*Vulnerability in Mega Cities: New approaches to analyse urban water system in Delhi*".

Stovin V., Bennett P., Guymer I. (2013) Absence of a hydraulic threshold in small-diameter surcharged manholes. *Journal of Hydraulic Engineering*, 139, **9**, 984-994.

Taylor E.H. (1944) Flow characteristics at rectangular open channel junctions. *Trans. ASCE*, 109, 893-912.

ten Veldhuis J.A.E. (2011) How the choice of flood damage metrics influences urban flood risk assessment. *Journal of Flood Risk Management*, 4, Issue 4.

The Pitt Review (2008) An Update of the Foresight Future Flooding 2004 qualitative risk analysis.

Tominaga A. (2007) Lesson learned from Tokai heavy rainfall. *Journal of Disaster Research*, **2**, No.1.

United Nations, Department of Economic and Social Affairs, Population Division: *World Urbanization Prospects, the 2011 Revision*. New York, 2012.

Unwin D.M. (2008) Development of control algorithms: to describe flow discharge reduction and energy loss at a manhole junction. Thesis (Ph.D.) - University of Sheffield, Department of Civil and Structural Engineering.

Wang K. H., Cleveland T. G., Towsley C. and Umrigar D. (1998) Head loss at manholes in surcharged sewer systems. *Journal of the American Water Resources Association*, 34, **6**, 1391-1400.

WaPUG. Code of practice for the hydraulic modelling of sewer systems. 2002. Available from: http://www.ciwem.org/media/44426/Modelling_COP_Ver_03.pdf. (Accessed 16th August 2011).

Water and wastewater services in Columbo to be improved with ABD funding. (Accessed on 06/06/2014, http://www.waterworld.com/articles/2012/10/water-and-wastewater-services-in-columbo-restored-by-adb-300m-funding.html).

Weitbrecht V., Jirka G.H. (2001) Flow patterns and exchange processes in dead zones rivers. *Proceedings of the IAHR Congress 2001*, Beijing.

Weitbrecht V., Kuhn G., Jirka G.H. (2002) Large scale PIV-measurements at the surface of shallow water flows. *Journal of Flow Measurement and Instrumentation*, 13, 237-245.

WRc, 1987. A Guide to Short-Term Flow Surveys of Sewer Systems. Swindon: Water Research Centre.

Wu, S. and Rajaratnam, N. (1996). Submerged Flow Regimes of Rectangular Sharp-Crested Weirs. *Journal of Hydraulic Engineering*, 122, **7**, 412–414.

Yevjevich V., Barnes A.H., (1970) Flood routing through storm drains. Part 1-4, Hydrology Papers 43-46, Colorado State University, Fort Collins, Colorado, USA.

Young P.C., Jakeman A.J., McMurtrie R. (1980) An instrumental variable method for model order identification. *Automatica*, 16, 281-294.

Zhao C.H., Zhu D. Z., Rajaratnam N. (2004) Supercritical sewer flows at combining junction: a case study of Edworthy Trunk Junction, Calgary, Alberta. *Journal of Environmental Engineering Science*, NRC, 3, **5**, 343-353.

Zhao C.H., Zhu D. Z., Rajaratnam N. (2006) "Experimental Study of Surcharged Flow at Combining Sewer Junctions". *Journal of Hydraulic Engineering*, 132, **12**, 1259-1271.

Zhao C.H., Zhu D. Z., Rajaratnam N. (2008) "Computational and Experimental Study of Surcharged Flow at a 90° Combining Sewer Junction". *Journal of Hydraulic Engineering*, **134**(6), 688–700.

9 Appendix A

Table 20 – Hydraulic parameters for test 1.

Test number	*Flow Channel A (l/s)*	*Flow Channel B (l/s)*	*Flow Channel C (l/s)*	*M1 water level (mm)*	*M2 water level (mm)*	*M3 water level (mm)*	*M4 water level (mm)*	*M5 water level (mm)*	*M6 water level (mm)*
1a	0	2.265	0	77.54	104.45	124.48	105.97	79.23	48.16
1b	0	2.689	0	90.65	126.03	155.84	131.98	92.27	53.46
1c	0	3.114	0	102.79	153.42	190.80	160.15	104.74	56.62
1d	0	3.536	0	111.37	178.63	220.52	183.12	113.97	52.31
1e	0	4.146	0	128.85	219.95	278.42	223.91	131.80	51.58
1f	0	4.533	0	146.20	251.65	303.31	259.41	150.46	51.60
1g	0	5.023	0	165.61	288.73	350.85	298.69	169.10	51.55
1h	0	5.384	0	182.18	321.40	392.48	334.50	186.44	52.65

Table 21 – Hydraulic parameters for test 2.

Test number	*Flow Channel A (l/s)*	*Flow Channel B (l/s)*	*Flow Channel C (l/s)*	*M1 water level (mm)*	*M2 water level (mm)*	*M3 water level (mm)*	*M4 water level (mm)*	*M5 water level (mm)*	*M6 water level (mm)*
2a	2.177	0	0	75.93	103.449	90.57	92.32	77.99	46.75
2b	2.598	0	0	89.08	122.848	106.49	108.08	90.84	52.56
2c	3.046	0	0	101.12	146.658	123.82	125.22	103.61	56.38
2d	3.484	0	0	109.70	168.745	138.09	139.19	112.03	52.20
2e	3.902	0	0	121.24	192.385	154.99	155.49	124.07	51.76
2f	4.337	0	0	132.51	230.842	177.04	178.55	135.74	51.99
2g	4.753	0	0	146.80	266.567	198.62	200.43	150.55	51.89
2h	5.134	0	0	164.12	297.792	225.58	228.45	168.88	52.37
2i	5.560	0	0	182.39	325.682	252.11	254.91	187.31	53.17
2l	5.911	0	0	199.27	353.963	276.55	278.56	205.26	53.63

Table 22 – Hydraulic parameters for test 3.

Test number	*Flow Channel A* (l/s)	*Flow Channel B* (l/s)	*Flow Channel C* (l/s)	M1 water level (mm)	M2 water level (mm)	M3 water level (mm)	M4 water level (mm)	M5 water level (mm)	M6 water level (mm)
3a	0	0	2.101	97.487	82.26	84.69	87.01	83.23	45.91
3b	0	0	2.529	122.620	100.05	102.40	104.64	97.29	51.51
3c	0	0	2.964	146.570	117.87	120.04	122.12	121.57	55.91
3d	0	0	3.476	181.742	138.53	140.51	142.54	145.69	51.13
3e	0	0	3.984	222.181	171.83	174.34	175.83	179.73	50.84
3f	0	0	4.432	259.651	202.55	205.15	206.23	205.10	52.21
3g	0	0	4.771	282.776	225.18	227.91	229.15	229.15	52.64
3h	0	0	5.266	318.022	256.58	259.30	260.23	268.24	53.39
3i	0	0	6.625	348.007	280.70	283.62	284.25	293.98	53.21

Table 23 – Hydraulic parameters for test 4.

Test number	*Flow Channel A* (l/s)	*Flow Channel B* (l/s)	*Flow Channel C* (l/s)	M1 water level (mm)	M2 water level (mm)	M3 water level (mm)	M4 water level (mm)	M5 water level (mm)	M6 water level (mm)
4a	0	0.297	0	28.88	27.74	31.20	32.80	29.40	18.45
4b	0	0.294	0	28.84	27.71	31.12	32.89	29.32	18.31
4c	0	0.390	0	31.11	30.52	33.84	35.56	31.52	20.42
4d	0	0.467	0	34.03	33.90	37.40	39.35	34.48	22.93
4e	0	0.604	0	38.44	39.09	42.13	43.87	38.64	26.92
4f	0	0.668	0	41.00	42.07	44.98	46.78	41.44	29.37
4g	0	0.807	0	44.06	46.03	49.78	50.72	44.52	31.65
4h	0	0.952	0	47.69	50.65	54.98	55.24	48.11	35.42
4i	0	1.007	0	49.05	52.21	56.61	57.03	49.57	36.85
4j	0	1.114	0	51.45	56.28	61.23	60.53	53.18	38.46
4k	0	1.242	0	54.98	60.55	65.93	64.86	55.42	39.77
4l	0	1.437	0	58.41	65.59	71.27	69.76	59.09	39.82
4m	0	1.591	0	62.86	71.61	77.80	75.78	63.39	39.74
4n	0	1.658	0	64.71	74.18	81.27	78.07	65.28	40.21
4o	0	1.836	0	68.29	81.26	91.92	84.93	69.61	41.51
4p	0	2.006	0	71.97	88.71	101.72	90.87	73.43	44.50
4q	0	2.108	0	74.11	93.51	106.98	95.09	75.45	45.73
4r	0	2.263	0	79.23	105.80	119.59	108.87	80.06	46.03
4s	0	2.383	0	82.25	108.13	126.73	115.40	82.73	48.10
4t	0	2.550	0	86.18	115.81	136.60	122.76	86.60	50.07
4u	0	2.669	0	90.32	122.81	145.24	129.27	91.05	51.76
4v	0	2.857	0	96.81	136.17	162.50	142.60	97.80	53.60
4w	0	3.055	0	102.24	149.18	177.81	155.53	103.36	55.30
4x	0	3.260	0	106.67	161.61	192.62	167.94	108.44	55.26
4y	0	3.333	0	107.73	165.19	196.10	170.71	109.37	55.00
4z	0	3.521	0	112.76	177.30	211.46	181.59	114.57	50.34
4aa	0	3.610	0	113.75	182.16	218.48	186.27	115.70	49.48
4ab	0	3.791	0	120.23	195.52	236.04	197.87	122.20	49.62
4ac	0	3.964	0	124.89	206.13	250.48	210.18	127.08	50.54
4ad	0	4.052	0	126.67	211.21	257.17	215.55	128.56	50.30
4ae	0	4.227	0	132.69	224.73	272.59	229.54	134.80	49.93

4af	0	4.317	0	137.72	234.49	283.66	239.65	140.14	49.70
4ag	0	4.485	0	143.95	246.25	295.95	251.53	146.36	49.67
4ah	0	4.565	0	147.85	253.24	301.39	260.70	150.55	49.48
4ai	0	4.713	0	153.98	264.28	310.50	273.93	156.82	49.37
4aj	0	4.901	0	161.38	278.62	326.64	290.21	164.03	49.77
4ak	0	5.078	0	168.40	292.69	343.90	304.47	170.65	50.48
4al	0	5.171	0	172.24	299.84	353.55	312.51	174.21	50.64
4am	0	5.310	0	178.79	313.21	370.45	327.12	182.23	51.18
4an	0	5.418	0	184.34	323.84	382.84	339.55	187.96	51.50
4ao	0	5.556	0	193.88	338.08	400.26	355.08	196.56	51.32
4ap	0	5.711	0	202.67	354.26	420.26	373.96	205.25	51.47
4aq	0	5.802	0	207.75	363.94	432.04	381.97	210.00	51.68
4ar	0	5.943	0	212.97	375.05	445.27	393.34	215.32	51.40
4as	0	6.072	0	218.57	388.03	461.59	409.57	220.75	51.37

Table 24 – Hydraulic parameters for test 5.

Test number	*Flow Channel A (l/s)*	*Flow Channel B (l/s)*	*Flow Channel C (l/s)*	M1 water level (mm)	M2 water level (mm)	M3 water level (mm)	M4 water level (mm)	M5 water level (mm)	M6 water level (mm)
5a	0.301	0	0	28.65	28.01	30.09	32.60	29.28	18.65
5b	0.331	0	0	29.72	29.43	31.32	33.71	30.43	20.12
5c	0.455	0	0	33.02	33.30	35.08	37.76	33.67	23.19
5d	0.515	0	0	35.62	36.12	37.94	40.72	36.36	25.41
5e	0.622	0	0	38.69	40.13	41.11	43.90	39.59	28.63
5f	0.802	0	0	43.19	45.90	46.29	48.76	44.19	32.27
5g	0.935	0	0	46.98	50.45	51.15	52.88	47.95	36.02
5h	0.994	0	0	48.96	52.65	53.31	55.07	49.90	37.47
5i	1.177	0	0	52.74	57.95	57.46	59.72	53.45	38.81
5j	1.237	0	0	54.63	60.58	59.93	62.14	55.64	39.60
5k	1.388	0	0	57.70	64.43	63.60	65.47	58.73	39.26
5l	1.564	0	0	61.62	71.72	69.02	70.53	62.95	39.66
5m	1.654	0	0	64.14	76.66	72.70	74.77	65.53	40.61
5n	1.828	0	0	68.34	84.96	78.49	79.75	70.15	42.50
5o	1.983	0	0	71.68	93.83	83.32	84.70	73.56	45.21
5p	2.106	0	0	74.56	99.81	87.86	89.39	76.53	45.88
5q	2.282	0	0	79.34	108.36	94.38	96.06	80.49	47.23
5r	2.378	0	0	81.21	111.30	96.81	98.57	82.15	48.79
5s	2.552	0	0	87.90	120.72	104.56	106.17	88.91	51.25
5t	2.748	0	0	94.43	131.49	113.50	115.47	95.87	53.52
5u	2.919	0	0	99.48	141.54	121.17	122.69	100.93	54.90
5v	3.001	0	0	100.59	144.79	122.89	124.53	102.22	55.00
5w	3.150	0	0	103.87	152.65	128.37	129.35	106.02	55.12

5x	3.267	0	0	106.43	157.52	131.78	132.78	108.75	52.03
5y	3.423	0	0	108.91	165.02	136.35	137.35	111.21	50.31
5z	3.606	0	0	113.95	176.04	144.35	145.00	116.82	51.12
5aa	3.708	0	0	117.62	181.71	149.36	149.81	120.54	51.52
5ab	3.867	0	0	121.59	191.39	155.55	156.32	123.87	51.27
5ac	3.969	0	0	124.22	196.10	158.51	158.68	126.08	51.71
5ad	4.127	0	0	128.40	208.50	166.53	167.29	130.42	51.57
5ae	4.273	0	0	132.17	217.91	171.74	172.72	134.45	51.99
5af	4.394	0	0	136.02	236.04	180.24	181.44	138.71	51.62
5ag	4.540	0	0	141.86	253.05	190.99	192.71	144.33	51.73
5ah	4.706	0	0	147.40	267.94	200.80	202.92	149.78	51.45
5ai	4.815	0	0	151.35	275.38	205.40	207.46	153.77	51.73
5aj	4.966	0	0	159.59	284.09	215.66	216.83	162.46	51.99
5ak	5.148	0	0	168.97	301.62	230.15	233.14	171.61	52.53
5al	5.226	0	0	172.03	308.01	233.74	236.67	174.53	52.77
5am	5.368	0	0	177.80	316.53	240.83	242.80	180.09	53.27
5an	5.543	0	0	186.46	328.15	253.77	256.30	189.01	52.98
5ao	5.650	0	0	190.31	333.26	261.96	264.88	193.23	52.98
5ap	5.761	0	0	194.50	342.15	267.90	270.50	197.77	52.95
5aq	5.878	0	0	201.09	353.47	276.81	278.79	204.46	53.19
5ar	6.002	0	0	205.55	362.56	283.48	284.53	208.99	53.43
5as	6.114	0	0	211.49	373.20	290.93	290.96	215.11	53.12
5at	6.233	0	0	217.63	381.07	296.68	296.50	220.97	52.31
5au	6.374	0	0	225.34	391.04	303.85	302.52	228.15	52.98
5av	6.510	0	0	230.41	398.12	306.02	303.26	232.96	51.62
5aw	6.604	0	0	234.91	405.93	312.57	309.10	237.48	51.19
5ax	6.695	0	0	239.63	415.55	319.28	316.46	242.71	50.70
5ay	6.794	0	0	250.11	432.11	331.88	328.44	252.24	51.12
5az	6.865	0	0	265.86	450.84	348.63	345.38	266.62	50.77

Table 25 – Hydraulic parameters for test 6.

Test number	*Flow Channel A (l/s)*	*Flow Channel B (l/s)*	*Flow Channel C (l/s)*	*M1 water level (mm)*	*M2 water level (mm)*	*M3 water level (mm)*	*M4 water level (mm)*	*M5 water level (mm)*	*M6 water level (mm)*
6a	0	0	0.22	30.60	25.87	27.49	31.50	29.05	15.68
6b	0	0	0.35	33.10	28.24	30.55	33.90	31.29	17.75
6c	0	0	0.48	37.65	32.45	34.80	38.52	35.47	21.57
6d	0	0	0.53	40.82	35.19	37.57	41.40	38.20	23.86
6e	0	0	0.67	45.17	39.86	41.57	45.44	42.79	27.72
6f	0	0	0.80	49.36	43.75	45.51	49.25	46.49	30.74
6g	0	0	0.87	52.08	46.44	48.62	51.85	49.20	32.54
6h	0	0	1.05	56.67	50.30	52.79	56.06	53.00	36.22
6i	0	0	1.210	61.70	55.34	57.77	61.26	58.17	39.29
6j	0	0	1.288	64.24	58.20	60.23	63.61	60.89	39.97
6k	0	0	1.444	68.55	61.82	64.12	67.01	64.34	39.57
6l	0	0	1.594	74.20	66.39	68.83	71.84	69.05	39.36
6m	0	0	1.664	78.50	68.80	70.92	74.20	71.31	40.04
6n	0	0	1.865	86.87	74.18	76.39	79.43	76.10	41.59
6o	0	0	1.957	91.33	77.23	78.92	82.42	79.04	42.92
5p	0	0	2.134	102.24	83.64	85.40	89.38	84.58	43.81
5q	0	0	2.300	111.19	90.42	91.62	95.62	90.09	46.06
5r	0	0	2.410	119.05	95.30	96.58	100.47	94.37	47.46
5s	0	0	2.534	125.49	101.27	102.99	106.71	99.64	48.86
5t	0	0	2.671	134.13	111.05	112.86	116.62	111.62	50.84

6u	0	0	2.833	145.00	107.66	109.57	113.06	107.70	50.56
6v	0	0	3.077	156.00	122.66	124.37	127.82	127.77	52.28
6w	0	0	3.310	171.18	130.32	132.07	135.62	137.28	50.38
6x	0	0	3.501	186.17	139.99	141.37	144.96	147.97	47.16
6z	0	0	3.622	194.23	146.83	148.47	151.91	154.27	47.34
6aa	0	0	3.795	207.97	156.95	158.80	162.03	166.07	47.82
6ab	0	0	3.962	225.51	172.11	173.86	176.75	180.34	48.28
6ac	0	0	4.085	236.35	182.88	184.87	187.63	187.39	48.86
6ad	0	0	4.235	248.64	191.70	193.62	196.26	195.39	49.05
6ae	0	0	4.414	262.35	201.68	203.48	206.15	203.78	49.76
6af	0	0	4.530	272.67	209.17	211.48	213.89	212.36	49.63
6ag	0	0	4.677	282.21	218.54	220.64	223.13	221.86	49.98
6ah	0	0	4.785	285.53	227.49	229.90	232.03	231.90	50.13
6ai	0	0	4.927	295.93	236.02	238.34	240.66	241.91	49.98
6aj	0	0	5.120	310.43	248.26	250.31	252.62	256.09	51.09
6ak	0	0	5.232	318.28	255.46	257.61	259.70	265.45	50.60
6al	0	0	5.353	326.65	262.70	264.79	266.53	277.50	50.87
6am	0	0	5.542	341.18	274.28	276.02	277.98	289.11	50.40
6an	0	0	5.656	352.83	282.22	284.13	286.36	296.59	50.66
6ao	0	0	5.758	361.42	288.84	291.07	292.85	303.93	50.05
6ap	0	0	5.935	378.70	300.89	303.24	304.77	317.54	48.94
6aq	0	0	6.071	393.15	311.00	313.39	314.76	327.19	48.60
6ar	0	0	6.187	403.46	318.98	321.49	322.44	338.91	47.20
6as	0	0	6.321	419.84	331.12	333.14	334.91	352.65	47.48

6at	0	0	6.445	431.57	339.94	342.76	343.46	362.84	46.23
6au	0	0	6.564	445.27	349.88	352.18	352.95	372.30	45.59

Table 26 – Hydraulic parameters for test 7.

Test number	***Flow Channel A*** **(l/s)**	***Flow Channel B*** **(l/s)**	***Flow Channel C*** **(l/s)**	**M1 water level (mm)**	**M2 water level (mm)**	**M3 water level (mm)**	**M4 water level (mm)**	**M5 water level (mm)**	**M6 water level (mm)**
7a	0	0.737	0	42.94	45.02	47.87	49.83	43.76	30.00
7b	0	0.913	0	45.95	49.65	53.12	54.02	46.91	33.75
7c	0	1.215	0	51.66	57.30	60.70	62.02	52.57	37.56
7d	0	1.453	0	58.32	66.39	70.69	70.55	59.45	38.48
7e	0	1.686	0	63.89	74.98	80.89	78.76	65.02	39.69
7f	0	1.940	0	69.82	86.29	98.86	89.39	71.71	43.01
7g	0	2.219	0	76.38	101.19	115.01	102.74	78.09	45.11
7h	0	2.599	0	87.87	119.82	139.24	125.99	89.11	50.54
7i	0	2.836	0	95.94	135.75	160.89	142.15	97.63	53.55
7j	0	3.245	0	105.23	160.07	190.67	166.85	107.20	55.16
7k	0	3.528	0	111.42	178.03	211.61	182.31	113.71	50.77
7l	0	3.789	0	118.98	195.57	234.76	198.59	121.59	49.78
7m	0	4.066	0	126.65	212.99	256.53	215.61	129.11	50.32
7n	0	4.323	0	137.22	234.64	282.34	238.59	140.17	49.65
7o	0	4.569	0	148.10	254.73	297.80	262.86	151.92	49.47
7p	0	4.874	0	160.53	277.68	324.95	286.68	163.87	49.69
7q	0	5.161	0	171.52	300.29	354.35	312.83	175.24	50.19
7r	0	5.409	0	182.82	322.62	381.50	337.14	187.38	50.66
7s	0	5.696	0	198.14	349.99	415.03	367.06	202.17	50.79
7t	0	5.959	0	213.10	377.49	448.88	398.33	216.46	51.18

Table 27 – Hydraulic parameters for test 8.

Test number	*Flow Channel A* (l/s)	*Flow Channel B* (l/s)	*Flow Channel C* (l/s)	M1 water level (mm)	M2 water level (mm)	M3 water level (mm)	M4 water level (mm)	M5 water level (mm)	M6 water level (mm)
8a	0.859	0	0	45.33	49.02	49.74	51.76	46.69	34.32
8b	1.022	0	0	48.47	53.31	53.41	55.27	49.76	37.27
8c	1.302	0	0	54.43	61.80	60.48	62.65	55.80	38.92
8d	1.612	0	0	61.91	73.24	69.80	71.56	63.39	39.67
8e	1.866	0	0	68.79	89.07	79.61	81.21	70.89	42.73
8f	2.163	0	0	75.41	102.32	89.52	90.87	77.54	45.14
8g	2.450	0	0	82.79	114.00	99.72	100.82	84.14	49.10
8h	2.799	0	0	94.34	133.11	114.75	115.65	96.38	53.75
8i	3.072	0	0	101.39	147.68	124.80	125.85	103.76	55.42
8j	3.289	0	0	104.97	157.97	131.39	132.06	108.01	55.73
8k	3.672	0	0	114.89	179.24	146.18	146.96	118.66	50.73
8l	3.920	0	0	121.25	193.12	155.28	155.51	124.32	50.54
8m	4.179	0	0	128.35	210.91	167.49	167.33	131.25	50.54
8n	4.433	0	0	135.86	242.23	183.24	182.74	139.17	50.67
8o	4.766	0	0	147.59	268.55	200.91	200.41	151.28	50.91
8p	5.016	0	0	161.37	287.79	219.07	218.42	165.31	50.86
8q	5.267	0	0	172.66	309.74	234.98	233.73	175.38	51.64
8r	5.494	0	0	182.17	321.23	248.47	247.04	185.42	51.72
8s	5.826	0	0	195.23	345.49	269.63	267.91	199.58	52.08
8t	6.063	0	0	207.50	368.28	286.20	283.46	212.01	52.02
8u	6.284	0	0	218.93	386.05	298.65	295.98	222.95	52.04
8w	6.534	0	0	230.06	401.87	309.57	306.83	234.01	51.77
8x	6.795	0	0	248.10	429.01	329.82	326.85	250.83	50.73

Table 28 – Hydraulic parameters for test 9.

Test number	*Flow Channel A* (l/s)	*Flow Channel B* (l/s)	*Flow Channel C* (l/s)	M1 water level (mm)	M2 water level (mm)	M3 water level (mm)	M4 water level (mm)	M5 water level (mm)	M6 water level (mm)
9a	0	0	0.891	51.16	48.02	50.20	52.18	49.59	35.20
9b	0	0	1.054	55.15	51.40	53.62	55.88	53.10	38.25
9c	0	0	1.307	62.16	58.59	60.36	62.95	60.34	41.26
9d	0	0	1.618	72.09	67.29	69.17	71.46	68.74	41.29
9e	0	0	1.906	85.40	75.68	77.95	79.95	76.88	43.64
9f	0	0	2.180	102.91	85.85	88.14	90.35	85.71	46.37
9g	0	0	2.441	117.62	95.97	98.29	99.97	93.99	49.43
9h	0	0	2.716	134.77	111.19	113.67	115.72	111.72	53.02
9i	0	0	3.070	153.62	119.68	121.78	123.78	125.10	55.79
9j	0	0	3.345	172.63	132.33	134.70	136.71	138.76	54.96
9k	0	0	3.605	193.36	146.23	148.48	150.26	154.28	50.93
9l	0	0	4.012	225.78	175.07	177.60	179.15	181.18	49.87
9m	0	0	4.275	249.59	194.40	196.56	197.95	196.69	51.04
9n	0	0	4.541	270.23	210.14	212.77	213.86	213.33	51.33
9o	0	0	4.776	284.23	225.57	228.43	229.57	229.27	51.30
9p	0	0	5.165	310.67	249.96	252.66	253.36	258.01	52.07
9q	0	0	5.420	329.29	266.97	269.49	270.28	279.35	52.55
9r	0	0	5.670	350.28	282.09	284.79	285.57	296.60	52.62
9s	0	0	5.964	378.09	301.59	304.45	304.54	318.63	50.61
9t	0	0	6.238	406.86	323.16	325.71	325.91	341.53	48.96
9u	0	0	6.481	433.49	341.82	344.40	344.78	361.31	47.66
9v	0	0	6.528	439.67	347.52	349.79	349.33	372.51	46.25

Table 29 – Hydraulic parameters for test 10.

Test number	*Flow Channel A* (l/s)	*Flow Channel B* (l/s)	*Flow Channel C* (l/s)	M1 water level (mm)	M2 water level (mm)	M3 water level (mm)	M4 water level (mm)	M5 water level (mm)	M6 water level (mm)
10a	0.867	0.698	0.507	82.55	95.31	96.72	97.11	84.10	44.63
10b	1.283	1.164	0.503	102.71	137.01	138.32	136.47	104.78	54.74
10c	1.847	1.671	0.502	131.98	194.82	195.14	187.33	134.55	52.66
10d	2.368	2.269	0.500	173.69	277.71	275.70	263.35	176.23	51.69
10e	3.020	2.846	0.494	230.37	392.90	391.53	372.10	233.20	52.17

Table 30 – Hydraulic parameters for test 11.

Test number	*Flow Channel A* (l/s)	*Flow Channel B* (l/s)	*Flow Channel C* (l/s)	M1 water level (mm)	M2 water level (mm)	M3 water level (mm)	M4 water level (mm)	M5 water level (mm)	M6 water level (mm)
11a	0.844	0.412	0.840	84.96	92.58	92.86	94.65	85.88	44.67
11b	1.292	0.411	1.295	122.28	134.31	132.24	133.69	120.75	55.08
11c	1.884	0.405	1.868	179.01	195.58	188.94	189.40	170.85	51.51
11d	2.398	0.402	2.418	241.39	260.27	248.26	248.54	223.63	52.91
11e	2.974	0.402	3.019	329.71	357.45	339.06	338.90	308.37	54.07
11f	3.519	0.399	3.504	415.52	449.35	424.49	423.39	387.74	50.90

Table 31 – Hydraulic parameters for test 12.

Test number	*Flow Channel A* (l/s)	*Flow Channel B* (l/s)	*Flow Channel C* (l/s)	M1 water level (mm)	M2 water level (mm)	M3 water level (mm)	M4 water level (mm)	M5 water level (mm)	M6 water level (mm)
12a	0.491	0.672	0.858	81.47	86.49	89.66	90.65	82.33	46.68
12b	0.485	1.180	1.313	118.78	130.30	135.69	133.64	117.90	55.33
12c	0.481	1.670	1.833	172.29	188.63	197.75	190.25	164.50	50.71
12d	0.477	2.279	2.427	236.39	255.40	267.58	257.27	218.43	53.13
12e	0.471	2.778	3.039	322.11	350.40	368.14	362.97	297.93	54.32
12f	0.467	3.307	3.409	375.67	410.11	434.20	416.32	348.76	51.11

Table 32 – Hydraulic parameters for test 13.

Test number	*Flow Channel A* (l/s)	*Flow Channel B* (l/s)	*Flow Channel C* (l/s)	M1 water level (mm)	M2 water level (mm)	M3 water level (mm)	M4 water level (mm)	M5 water level (mm)	M6 water level (mm)
13a	1.475	1.319	1.498	177.02	208.33	209.96	205.86	171.19	48.08
13b	1.473	1.414	1.500	179.01	213.15	215.94	211.12	173.42	48.24
13c	1.469	1.576	1.497	183.69	222.73	226.91	220.03	178.12	48.23
13d	1.469	1.641	1.498	185.36	226.85	232.28	223.86	179.83	48.16
13e	1.466	1.836	1.496	193.44	240.04	245.60	237.21	188.05	48.50
13f	1.462	1.959	1.491	198.70	249.66	256.89	246.25	193.86	48.82
13g	1.460	2.079	1.485	204.20	259.39	267.10	255.46	199.37	49.49
13h	1.460	2.161	1.487	208.12	263.88	270.87	260.62	203.11	49.74
13i	1.458	2.347	1.484	215.72	276.96	286.51	273.13	211.22	49.76
13j	1.455	2.527	1.485	223.67	289.52	299.31	286.31	219.99	50.61
13k	1.453	2.624	1.481	227.92	296.87	306.41	293.33	223.97	50.36
13l	1.445	2.793	1.481	235.03	315.79	328.20	310.07	231.08	50.31
13m	1.438	2.978	1.473	244.81	332.61	346.25	326.89	241.60	50.74
13n	1.432	3.181	1.474	256.22	358.11	374.32	352.07	253.06	50.60
13o	1.430	3.254	1.470	262.70	372.06	388.43	365.15	259.56	50.23
13p	1.426	3.419	1.471	270.77	387.92	405.89	380.39	267.12	49.56
13q	1.425	3.519	1.470	277.07	399.59	418.71	391.73	273.30	50.39
13r	1.421	3.675	1.466	286.50	416.93	437.15	409.10	282.22	50.36
13s	1.415	3.847	1.461	298.69	438.97	461.17	430.47	294.33	49.91
13t	1.414	3.895	1.456	297.28	440.82	464.81	432.68	294.37	52.04

Table 33 – Hydraulic parameters for test 14.

Test number	*Flow Channel A* (l/s)	*Flow Channel B* (l/s)	*Flow Channel C* (l/s)	M1 water level (mm)	M2 water level (mm)	M3 water level (mm)	M4 water level (mm)	M5 water level (mm)	M6 water level (mm)
14a	1.421	1.259	1.456	171.60	200.90	202.69	199.19	166.93	49.90
14b	1.526	1.261	1.454	173.35	205.64	206.64	203.34	168.84	50.48
14c	1.606	1.260	1.457	175.81	210.09	210.57	207.17	171.47	50.28
14d	1.794	1.259	1.450	179.64	221.38	220.94	217.49	175.66	50.31
14e	1.976	1.252	1.450	186.22	235.67	233.62	229.83	182.16	50.30
14f	2.048	1.253	1.446	189.91	241.76	239.11	234.54	185.96	50.12
14g	2.238	1.251	1.446	197.64	256.48	249.06	245.40	194.15	50.80
14h	2.306	1.250	1.442	200.97	261.68	252.95	249.34	197.35	50.79
14i	2.489	1.247	1.440	209.27	276.60	264.92	261.22	205.07	50.88
14j	2.678	1.246	1.441	218.66	290.31	277.47	273.74	214.82	51.75
14k	2.870	1.243	1.442	226.89	303.73	289.60	285.82	223.49	51.60
14l	2.937	1.242	1.438	229.55	308.90	294.22	290.48	226.65	51.46
14m	3.119	1.238	1.438	237.68	322.20	305.99	302.41	234.83	51.92
14n	3.200	1.238	1.435	241.69	328.84	312.57	309.06	239.12	51.86
14o	3.366	1.234	1.432	250.03	344.18	324.80	320.71	247.16	51.95
14p	3.528	1.233	1.435	258.79	359.10	338.32	334.36	256.27	51.93
14q	3.626	1.233	1.426	263.96	369.37	346.28	341.60	261.43	51.57
14r	3.773	1.230	1.422	271.92	382.76	357.71	353.85	269.16	51.26
14s	3.881	1.228	1.421	278.48	394.33	367.06	363.38	275.59	51.39
14t	4.029	1.227	1.418	290.21	411.32	381.30	376.96	286.41	50.61
14u	4.187	1.223	1.413	300.69	428.47	396.04	391.72	297.21	50.91
14v	4.280	1.221	1.414	300.78	434.47	399.54	395.36	299.62	49.99
14w	4.427	1.220	1.412	308.59	448.67	411.41	406.88	308.26	50.63
14y	4.476	1.223	1.403	311.99	455.42	416.74	413.17	311.03	48.21

Table 34 – Hydraulic parameters for test 15.

Test number	*Flow Channel A* (l/s)	*Flow Channel B* (l/s)	*Flow Channel C* (l/s)	M1 water level (mm)	M2 water level (mm)	M3 water level (mm)	M4 water level (mm)	M5 water level (mm)	M6 water level (mm)
15a	1.399	1.283	1.426	158.14	185.85	186.87	185.02	152.70	64.42
15b	1.397	1.284	1.537	164.04	190.26	191.04	189.35	157.25	64.57
15c	1.396	1.282	1.638	168.97	193.86	194.71	192.82	160.33	64.01
15d	1.396	1.280	1.752	173.67	197.96	198.26	196.81	163.63	63.46
15e	1.396	1.281	1.880	179.93	203.10	203.39	201.94	168.20	62.76
15f	1.394	1.278	2.045	186.49	208.10	208.68	206.89	173.15	61.10
15g	1.394	1.279	2.198	188.80	208.83	209.63	207.80	173.38	60.69
15h	1.391	1.277	2.303	192.81	210.77	211.81	210.28	174.82	61.46
14i	1.388	1.275	2.482	207.40	220.15	220.53	218.94	184.01	62.33
15j	1.389	1.275	2.558	215.50	226.20	227.16	225.37	190.19	62.78
15k	1.388	1.273	2.752	231.70	237.90	239.33	237.87	203.07	63.72
15l	1.386	1.270	2.911	242.49	247.25	247.82	246.50	211.14	64.19
15m	1.384	1.267	3.162	260.93	260.30	260.97	259.58	223.63	64.83
15n	1.381	1.268	3.262	269.29	267.10	267.17	265.72	230.25	65.63
15o	1.381	1.262	3.468	278.48	277.73	277.96	276.61	240.73	66.22
15p	1.379	1.261	3.572	283.10	284.08	284.39	282.90	247.35	67.07
15q	1.377	1.256	3.768	294.04	294.98	295.71	294.30	258.30	66.51
15r	1.374	1.256	3.947	306.84	306.63	307.57	305.93	269.49	66.94
15s	1.375	1.258	3.994	310.57	308.25	309.35	307.85	272.11	67.32
15t	1.371	1.255	4.140	320.91	317.78	319.27	317.43	281.87	66.92
15u	1.368	1.252	4.369	339.98	333.84	335.16	333.47	297.84	66.95
15v	1.366	1.250	4.484	349.79	343.54	344.67	343.19	304.87	67.49
15w	1.363	1.249	4.631	362.22	353.11	354.55	352.62	314.91	67.32
15x	1.361	1.247	4.721	374.26	364.10	365.62	363.55	323.55	67.20
15y	1.360	1.246	4.893	392.50	379.70	380.84	379.09	338.04	66.74
15z	1.355	1.240	5.046	414.42	398.50	399.57	397.52	354.16	66.60
15aa	1.351	1.239	5.152	434.58	418.10	419.60	416.86	372.04	65.52
15ab	1.351	1.239	5.230	442.64	423.83	425.55	422.91	379.11	65.81

Table 35 – Hydraulic parameters for test 16.

Test number	*Flow Channel A* (l/s)	*Flow Channel B* (l/s)	*Flow Channel C* (l/s)	M1 water level (mm)	M2 water level (mm)	M3 water level (mm)	M4 water level (mm)	M5 water level (mm)	M6 water level (mm)
16a	1.419	1.282	1.481	173.49	203.32	204.38	201.29	168.50	48.56
16b	1.413	1.663	1.478	182.21	223.22	227.39	220.80	177.63	49.00
16c	1.406	2.080	1.469	198.91	251.75	258.91	248.21	194.74	49.58
16d	1.401	2.524	1.461	219.28	283.73	294.44	281.00	215.53	50.98
16e	1.393	2.967	1.459	239.57	321.68	336.48	317.01	236.92	50.77
16f	1.381	3.441	1.454	264.95	378.78	397.83	371.70	261.31	50.50
16g	1.372	3.864	1.450	290.19	428.37	451.65	420.72	286.82	49.80
16h	1.368	3.898	1.454	293.58	435.45	458.58	429.95	290.96	49.85

Table 36 – Hydraulic parameters for test 17.

Test number	*Flow Channel A* (l/s)	*Flow Channel B* (l/s)	*Flow Channel C* (l/s)	M1 water level (mm)	M2 water level (mm)	M3 water level (mm)	M4 water level (mm)	M5 water level (mm)	M6 water level (mm)
17a	1.388	1.271	1.446	170.37	199.38	200.60	197.37	165.54	48.61
17b	1.826	1.263	1.439	180.75	222.03	219.64	216.83	176.41	49.41
17c	2.278	1.255	1.436	199.04	257.91	248.02	244.48	195.40	50.39
17d	2.720	1.251	1.433	219.52	291.35	278.05	273.80	215.61	50.98
17e	3.143	1.244	1.424	237.88	323.63	306.99	302.93	234.83	51.23
17f	3.569	1.238	1.425	258.38	360.30	337.89	334.01	255.47	50.56
17g	3.886	1.233	1.418	278.14	393.83	366.00	362.02	275.07	50.81
17h	4.292	1.227	1.413	302.54	435.19	400.45	396.36	300.30	50.17
17i	4.541	1.222	1.426	310.83	453.58	412.96	408.68	309.31	49.60

Table 37 – Hydraulic parameters for test 18.

Test number	*Flow Channel A* (l/s)	*Flow Channel B* (l/s)	*Flow Channel C* (l/s)	M1 water level (mm)	M2 water level (mm)	M3 water level (mm)	M4 water level (mm)	M5 water level (mm)	M6 water level (mm)
18a	1.422	1.245	1.452	171.38	200.30	202.12	198.54	166.72	48.72
18b	1.418	1.241	1.865	191.61	217.11	218.95	215.17	181.82	49.81
18c	1.413	1.232	2.287	227.64	244.87	247.08	243.71	211.25	50.69
18d	1.407	1.228	2.662	258.02	268.87	270.56	267.53	234.63	52.61
18e	1.401	1.223	3.174	292.97	298.93	300.56	297.69	266.70	51.93
18f	1.395	1.218	3.568	319.87	323.92	325.92	322.54	291.71	51.30
18g	1.389	1.211	4.003	360.61	362.97	365.44	361.62	326.90	52.08
18h	1.380	1.202	4.428	416.79	412.49	414.51	410.61	373.24	50.49
18i	1.375	1.202	4.686	449.44	438.00	440.26	436.63	399.33	49.30

Table 38 – Hydraulic parameters for test 19.

Test number	*Flow Channel A* (l/s)	*Flow Channel B* (l/s)	*Flow Channel C* (l/s)	M1 water level (mm)	M2 water level (mm)	M3 water level (mm)	M4 water level (mm)	M5 water level (mm)	M6 water level (mm)
19a	1.399	1.268	0.806	129.79	168.84	171.04	167.67	130.13	48.41
19b	1.530	1.388	0.801	134.44	179.65	182.25	177.28	134.92	49.68
19c	1.622	1.545	0.805	141.63	189.65	192.70	185.62	141.99	50.67
19d	1.788	1.628	0.797	149.68	205.01	207.21	199.30	149.81	50.77
19e	1.931	1.799	0.797	159.80	227.30	228.99	220.15	160.59	50.72
19f	2.159	1.922	0.797	173.25	255.39	255.40	243.41	174.29	50.77
19g	2.227	2.027	0.795	181.45	269.68	268.58	258.18	182.42	50.59
19h	2.305	2.191	0.793	193.31	290.23	288.93	277.68	194.75	51.66
19i	2.487	2.261	0.796	205.92	310.45	310.51	299.81	206.55	51.29
19j	2.666	2.468	0.789	223.82	345.42	345.61	331.22	224.45	51.92
19k	2.840	2.646	0.787	241.41	384.76	385.38	367.87	243.10	51.99
19l	2.904	2.737	0.784	250.77	403.60	404.20	384.79	251.81	50.52
19m	3.060	2.928	0.781	271.88	441.59	442.19	421.43	272.87	49.66
19n	3.084	2.952	0.769	278.92	453.69	452.83	431.15	279.20	50.27

Table 39 – Hydraulic parameters for test 20.

Test number	*Flow Channel A* (l/s)	*Flow Channel B* (l/s)	*Flow Channel C* (l/s)	M1 water level (mm)	M2 water level (mm)	M3 water level (mm)	M4 water level (mm)	M5 water level (mm)	M6 water level (mm)
20a	1.414	0.688	1.390	150.64	168.55	168.56	167.62	146.97	47.57
20b	1.536	0.688	1.540	164.39	181.10	180.64	179.78	157.91	47.58
20c	1.616	0.687	1.656	173.25	191.24	189.81	188.75	165.76	47.99
20d	1.794	0.686	1.810	183.09	204.16	201.36	200.38	174.50	49.53
20e	1.981	0.684	1.928	193.96	217.78	213.21	212.26	183.89	49.74
20f	2.053	0.682	2.097	211.83	233.44	227.88	226.82	198.33	50.03
20g	2.224	0.678	2.261	235.43	261.36	252.63	251.44	220.10	50.77
20h	2.320	0.675	2.355	250.71	279.58	268.41	267.24	234.65	51.54
20i	2.475	0.674	2.526	274.39	303.49	292.15	290.39	255.40	53.20
20j	2.651	0.673	2.623	293.07	323.22	312.16	310.34	272.15	53.08
20k	2.835	0.670	2.780	320.70	354.70	342.16	340.26	300.45	53.16
20l	2.909	0.668	2.956	344.01	380.24	366.78	364.39	323.55	51.47
20m	3.134	0.665	3.186	373.66	413.52	396.44	394.47	348.90	53.96
20n	3.434	0.661	3.469	392.18	436.68	415.03	412.23	362.04	63.36
20o	3.506	0.660	3.494	400.41	448.39	425.57	422.69	371.17	63.55

Table 40 – Hydraulic parameters for test 21.

Test number	*Flow Channel A* (l/s)	*Flow Channel B* (l/s)	*Flow Channel C* (l/s)	M1 water level (mm)	M2 water level (mm)	M3 water level (mm)	M4 water level (mm)	M5 water level (mm)	M6 water level (mm)
21a	0.811	1.280	1.459	142.58	158.02	166.24	161.99	137.27	65.45
21b	0.807	1.388	1.596	153.75	171.12	179.73	173.98	146.73	65.72
21c	0.805	1.557	1.673	164.35	185.12	193.94	187.30	156.59	65.49
21d	0.804	1.641	1.832	173.38	194.30	203.02	196.58	163.45	65.16
21e	0.802	1.832	1.937	180.52	205.42	215.42	207.60	169.21	63.63
21f	0.801	1.995	2.116	189.88	216.71	226.82	218.18	175.70	62.20
21g	0.796	2.074	2.271	195.98	222.57	233.22	224.21	179.57	63.17
21h	0.796	2.260	2.356	209.28	237.61	249.51	239.27	190.93	64.61
21i	0.793	2.341	2.508	225.86	251.73	262.56	253.47	203.88	65.50
21j	0.791	2.521	2.599	241.07	271.40	283.58	272.32	217.74	66.32
21k	0.788	2.661	2.756	262.40	294.68	308.25	295.34	236.46	67.03
21l	0.787	2.782	2.904	278.10	316.55	332.52	318.13	252.88	67.80
21m	0.783	2.951	3.069	301.36	346.59	364.24	348.49	274.76	67.64
21n	0.776	3.150	3.163	323.30	378.63	397.22	378.67	297.10	67.30
21o	0.773	3.241	3.344	344.63	403.01	421.72	402.40	317.32	66.73
21p	0.769	3.409	3.436	365.20	428.42	449.26	426.81	334.51	67.07
21q	0.766	3.442	3.446	369.26	435.71	456.62	434.60	339.96	66.23

Table 41 – Hydraulic parameters for test 22.

Test number	*Flow Channel A* (l/s)	*Flow Channel B* (l/s)	*Flow Channel C* (l/s)	M1 water level (mm)	M2 water level (mm)	M3 water level (mm)	M4 water level (mm)	M5 water level (mm)	M6 water level (mm)
22a	0.306	0.280	0.332	50.75	51.10	54.00	56.61	52.60	35.13
22b	0.442	0.392	0.450	59.07	60.50	63.24	65.38	60.37	37.65
22c	0.481	0.456	0.551	65.91	68.48	70.69	73.07	66.88	38.21
22d	0.623	0.586	0.636	74.82	80.56	82.91	85.01	76.42	41.91
22e	0.756	0.646	0.798	88.24	96.12	98.14	99.50	88.81	45.18
22f	0.891	0.796	0.853	99.72	113.21	115.46	116.29	100.01	49.31
22g	0.947	0.948	1.015	114.67	132.12	134.65	134.82	114.52	52.54
22h	1.110	0.980	1.170	132.04	153.33	155.25	154.82	131.09	49.14
22i	1.175	1.153	1.234	148.95	173.77	176.10	174.17	147.60	47.43
22j	1.326	1.221	1.405	164.53	190.73	192.47	189.42	160.78	48.61
22k	1.493	1.375	1.565	180.99	215.33	216.40	212.72	175.62	49.69
22l	1.577	1.542	1.642	194.24	235.61	237.68	231.95	188.01	50.21
22m	1.739	1.623	1.834	220.44	265.64	267.17	261.17	211.63	50.55
22n	1.903	1.793	1.905	244.47	299.22	300.05	294.02	235.93	51.14
22o	2.015	1.939	2.059	272.70	335.64	337.59	329.65	262.60	51.53
22p	2.172	2.028	2.239	300.86	373.85	374.04	365.30	288.90	50.25
22q	2.268	2.197	2.334	328.80	412.62	413.94	403.20	316.56	50.61
22r	2.434	2.280	2.458	362.33	454.51	454.70	443.37	349.24	48.50
22s	2.473	2.293	2.503	373.26	468.29	468.19	456.43	358.94	49.72

List of journal papers published

- **Rubinato M.**, Shucksmith J., Saul A.J. ***"Comparison between Infoworks results and a physical model of an urban drainage system",*** *Water Science and Technology, Vol 68, No 2, pp 372–379.*

List of journal papers under review

- Nuno Melo, Leandro J., Shucksmith J., **Rubinato M.**, Djordjevic S., Saul A.J., Ramos H., João L. M. P. de Lima***, "Evaluation of SIPSON and SWMM models ability to Reproduce Experimental Data of a Sewer Network".*** *Water Science and Technology.*

List of journal papers in progress

- **Rubinato M.**, Shucksmith J., Saul A.J. ***"Quantification of energy losses and flow exchange between above and below ground drainage systems through a manhole".*** *Journal of Hydraulic Engineering.*

List of conference papers published

- **Rubinato M.**, Shucksmith J., Saul A.J. ***"Experimental investigation of flow-interactions between above and below ground drainage systems through a manhole",*** 17 August 2014- 21 August 2014, ***11th HIC*** (International Conference on Hydroinformatics), New York, USA.
- Lopes P., Shucksmith J., Jorge L., Fernandes de Carvalho R., **Rubinato M.** ***"Velocities profiles and air-entrainment characterization in a scaled circular manhole",*** 7 September 2014- 12 September 2014, ***13th ICUD*** (International Conference on the Urban Drainage), Sawarak, MALAYSIA.

- **Rubinato M.**, Shucksmith J., Saul A.J. ***"Comparison between Infoworks results and a physical model of an urban drainage system",*** 3 September 2012- 8 September 2012, ***9th UDM*** (International Conference on Urban Drainage Modelling), Belgrade, SERBIA.
- Nuno Melo, Leandro J., Shucksmith J., **Rubinato M.**, Djordjevic Slobodan, Saul A.J., Ramos H., João L. M. P. de Lima***, "Modelling Internal Boundary Conditions of a Sewer Network "***3 September 2012- 8 September 2012, ***9th UDM*** (International Conference on Urban Drainage Modelling), Belgrade, SERBIA.
- **Rubinato M.**, Shucksmith J., Saul A.J. ***"Procedures for downscaling urban drainage systems for physical modelling studies",*** 14 July 2012- 18 July 2012, ***10th HIC*** (International Conference on Hydroinformatics), Hamburg, GERMANY.
- **Rubinato M.**, Shucksmith J., Saul A.J. "***Hydraulic performance of a scale model facility and optimization through the use of real time sensors***", 11 September 2011-17 September 2011, ***12th ICUD*** (International Conference on Urban Drainage), Porto Alegre, BRAZIL.